2018-01-01

Development and characterization of novel materials for the advancement of additive manufacturing by material extrusion 3D printing

Jose Gilberto Siqueiros
University of Texas at El Paso, gilbertosiq25@gmail.com

DEVELOPMENT AND CHARACTERIZATION OF NOVEL MATERIALS FOR THE ADVANCEMENT OF ADDITIVE MANUFACTURING BY MATERIAL EXTRUSION 3D PRINTING

JOSE GILBERTO SIQUEIROS

Doctoral Program in Materials Science and Engineering

APPROVED:

_____
David Roberson, Ph.D., Chair

_____
Stephen Stafford, Ph.D.

_____
Jorge Lopez, Ph.D.

_____
Yirong Lin, Ph.D.

_____
Charles H. Ambler, Ph.D.
Dean of the Graduate School

DEDICATION

For my parents Veronica and Gilberto.

DEVELOPMENT AND CHARACTERIZATION OF NOVEL MATERIALS FOR THE ADVANCEMENT OF ADDITIVE MANUFACTURING BY MATERIAL EXTRUSION 3D PRINTING

by

JOSE GILBERTO SIQUEIROS, B.S.M.E

DISSERTATION

Presented to the Faculty of the Graduate School of

The University of Texas at El Paso

in Partial Fulfillment

of the Requirements

for the Degree of

DOCTOR OF PHILOSOPHY

Materials Science and Engineering

THE UNIVERISTY OF TEXAS AT EL PASO

August 2018

AKNOWLEDGEMENTS

First of all, I would like to thank Dr. Roberson for his mentorship during my doctoral degree. After coming back to the University of Texas at El Paso to pursue a master's degree in metallurgy Dr. Roberson offered me the opportunity to conduct research with him and encouraged me to pursue a Ph.D. As you can read, I took his advice and changed my degree plan to pursue a doctoral degree in materials science and I could not be happier with that decision. This decision has led me to understand the fascinating world of research and additive manufacturing. Along the way I had the opportunity to make new friends, travel and learn the good and bad about academia. So from my heart, I would like to thank you for the opportunity you presented to me and the years we spend working and cycling together.

I would like to thank the members of my committee for their guidance during the pursue of my Ph.D. and your commitment to help me and other student succeed. I had the opportunity to take one or various courses with you and was inspired by the work you do.

My first year as a graduate student I had the chance to work with a very special colleague, now good friend, Dr. Angel Torrado. I would like to thank Angel for all of his help during the time we worked together and after. Angel was always a call away from giving me advice or troubleshooting research and life related. So thank you Angel for being the best colleague I could ever wished for.

Also I would like to thank Dr. David Espalin for all of his research expertise and advice I received while conducting experiments at the W.M. Keck Center for 3D Innovation. David was always glad to help with any of my inquiries about equipment and experiments. As well as all of the students and friends from the center, specially Kevin Schnittker, Francisco Andrade, Carmen Rocha, Adriana Ramirez, Marcos Vanderlinde Brockveld.

ABSTRACT

The development of additive manufacturing technologies has been under the spotlight from the past decade due to its enormous potential to disrupt current manufacturing processes. Material extrusion 3D printing (ME3DP) is the most common type of additive manufacturing technology as it experienced an exponential growth after the expiration of the fused deposition modeling patent filed in 1989 by Scott Crump. The large interest behind this technology is generated from the capacity to create complex shapes, rapid prototyping, relatively ease of use, low cost, and high accessibility. The gradual evolution of material extrusion 3D printing calls to become a technology ordinarily used for rapid prototyping into a rapid manufacturing technology where ready to market functional products are created in a fully automated fashion.

Materials development is an important aspect for the evolution of ME3DP as the introduction of new materials with a varied array of physical qualities would expand the applicability of this technology into more fields. The goal of this work is to introduce new ME3DP materials with tailored physical qualities along processing parameters and material characterization. The studies covered in this dissertation entail the creation of a polymer blend based on acrylonitrile butadiene styrene and an elastomer, an introduction of a new type of in situ fiber reinforcement for different polymers, and phase characterization of the polymer blend through scanning transmission electron microscope.

TABLE OF CONTENTS

LIST OF TABLES

LIST OF FIGURES

CHAPTER 1: INTRODUCTION

1.1 Statement of the Problem

Additive manufacturing (AM) by fused deposition modeling (FDM) or material extrusion 3D printing (ME3DP) is a technology that employs a hot nozzle to deposit material in a layer by layer manner following a series of raster patterns taken from a computer aided design (CAD) until a 3D object is created. Some of the well-known advantages of AM by ME3DP are 1) the ability to create complex shape objects that are not possible to achieve by other manufacturing mean; 2) rapid prototyping/tooling without recurring to molds, fixtures or cutting tools; 3) ease of product customization; 4) sustainability, with the reduction of material waste; and 5) cost of ME3DP is sometimes lower than other AM technologies.

ME3DP is a disruptive technology that could revolutionize the manufacturing industry. ME3DP has the potential to fabricate products/parts in a fully automated fashion that may possibly change business models by shrinking supply chains, shifting manufacture sites, and labor practices. While there are significant advantages of using ME3DP technologies over common manufacturing methods, there are still limiting factors that impede mass scale adoption. One of the major constrains on ME3DP technologies is the limited amount of materials available. ME3DP mostly relies on the use of thermoplastics like acrylonitrile butadiene styrene (ABS), polylactic acid (PLA) and polycarbonate (PC). These thermoplastics are known to have high molecular weight and experience rapid chain weakening when temperatures close to their glass transition temperatures are applied yielding a viscous phase that can be extruded and solidified upon cooling [1], this material characteristic enables fusion between layers which is fundamental for ME3DP technologies. The dependence on thermoplastics in ME3DP limits the use of this technology to applications where different material properties are needed. Hence creating materials with a wide

range of physical properties is crucial for the development of this technology. An expansion in material availability would help reach a larger spectrum of applications that could be benefited from ME3DP.

The goal of this work is to develop and characterize new materials for ME3DP technologies with diverse physical properties from what is currently available in the market through the creation of novel polymer blends and composites. Characterization of the new blends and composites is of vital importance to interpret and adjust processing parameters to enhance print quality, and provide an estimate value of the final physical properties of the printed part. In an effort to further develop ME3DP through materials development this work will present different novel materials that will expand the material range currently available.

1.2 Literature Review

1.2.1 Additive Manufacturing: Advantages, Goals and its Current Needs

Additive manufacturing (AM) or three-dimensional printing (3D printing) is receiving a great ordeal of attention over the past years. Worldwide revenue of AM expanded from 1.7 billion in 2011 to 5.165 billion in 2016 for all related AM products and services [2]. The research community experienced an exponential growth in the amount of articles published related to AM since 2012 where it went from publishing 1,600 articles in 2011 to 16,000 on 2012 [3]. The interest from the public and private sector on AM is imminent with budget increments for research and development (R&D) aimed at this technology. In 2012 President Obama in his State of the Union address, stated that AM could "revolutionize the way we make almost everything". America Makes is a billion-dollar initiative to strengthen U.S. manufacturing and competitiveness, its mission is to accelerate the development of AM technologies. This initiative is a private and public partnership with organizations ranging from academia, government agencies and private industries

[4]. Most of the current development efforts in AM are focused on design, process variability, reducing build time, improving mechanical properties, increasing the amount of materials available, multi-material printing, one step approach manufacturing, and sustainability.

The process of additive manufacturing consists in a bottom-up creation of an object by depositing material layer upon layer following three dimensional digital models [5]. The reason behind this technology is in the spotlight of pioneering industries like the medical, automotive, and aerospace industries is because it could bring major changes to the current design and manufacturing processes. One of the key advantages of AM is the proficiency to create complex shapes that were impossible to fabricate by current manufacturing methods which expands design capabilities for product development. This could potentially reduce manufacturing costs and improve the quality and efficiency of products. Another desirable quality of AM is rapid prototyping, which reduces product development time by eliminating the creation of molds (for parts with complex shapes) which in some cases are time consuming and expensive. Another advantage of this technology is the ability of customization by being able to modify parts more quickly than with conventional manufacturing methods which enables to move from mass production to mass customization [6]. It has also been considered that AM might change the configuration of global and local supply chains by reducing inventories with the ability to reproduce an infinity of different parts quickly using this technology [6]. These are just some examples on how AM can be more suitable over conventional manufacturing and as the AM development continues new applications will surface.

There are different AM technologies available today that share the same principle of creating an object in a layer by layer manner, some of the most common ones are: stereolithography (SLA) which works by curing a polymer resin with ultraviolet light; binder

jetting as its name indicates works by applying a binder into an either metal, polymer, ceramic or composite powder to bind particles together, in some cases are later followed by another process to remove binding agents or improve mechanical properties (e.g. annealing); powder bed fusion technologies like selective laser sintering (SLS), selective laser melting (SLM), and electron beam melting which share the same principle of fusing metal powders with either a laser or by an electron beam (SLS can also be used with thermoplastics; because its sintering nature); and the subject of this study, material extrusion 3D printing (ME3DP), this type of AM extrudes molten material (usually a thermoplastic) into a bed depositing in different directions to create an object.

ME3DP is the most common type of AM technology because of its highly accessibility as there is a wide variety of printers available in the market, from desktop size/home printers to high end and big area additive manufacturing (BAAM). This type of AM technology is known from building simple items in a household or hobbyist setting to really complex shape objects, rapid tooling/prototyping, and actual parts used in aerospace and other specialized industries [7]. The high accessibility and relatively simple mechanisms of ME3DP devices makes them suitable tools for the development of remote places (e.g. rural areas, spaceships, etc.) where the production of items in an as needed basis can be truly beneficial. As a result of ME3DP being the most widespread type of AM technology, more people can be benefited from its development. In the upcoming chapters an effort to develop this technology will be introduced.

1.2.2 Material Extrusion 3D Printing

ME3DP is an AM technique that was first introduced by Scott Crump in 1989. Crump patented the technology under the name of “Fused Deposition Modeling” (FDM). This AM technique as it names indicates works by selectively extruding molten material into a heated bed following a series of movements that have been previously designated from a digital object. A

schematic representation of the ME3DP process is presented on Figure 1.1. The process starts from a computer aided design (CAD) saved as a stereolithography (.STL) file format which is put through a slicing software that separates the 3D design into a series of raster patterns and printing parameters that can be interpreted by the 3D printer. The sliced file is then sent to the printer in the form of a G-code which is a numerical control programing language that is interpreted by the 3D printer to identify movements, temperature settings, and other processing parameters which leads to the layer by layer creation of a physical object. There was a constant increment on ME3DP development after the FDM patent own by Stratasys Inc. expired in 2009 were many startup companies benefited and made ME3DP printers available to a broader audience by reducing prices of systems and materials.

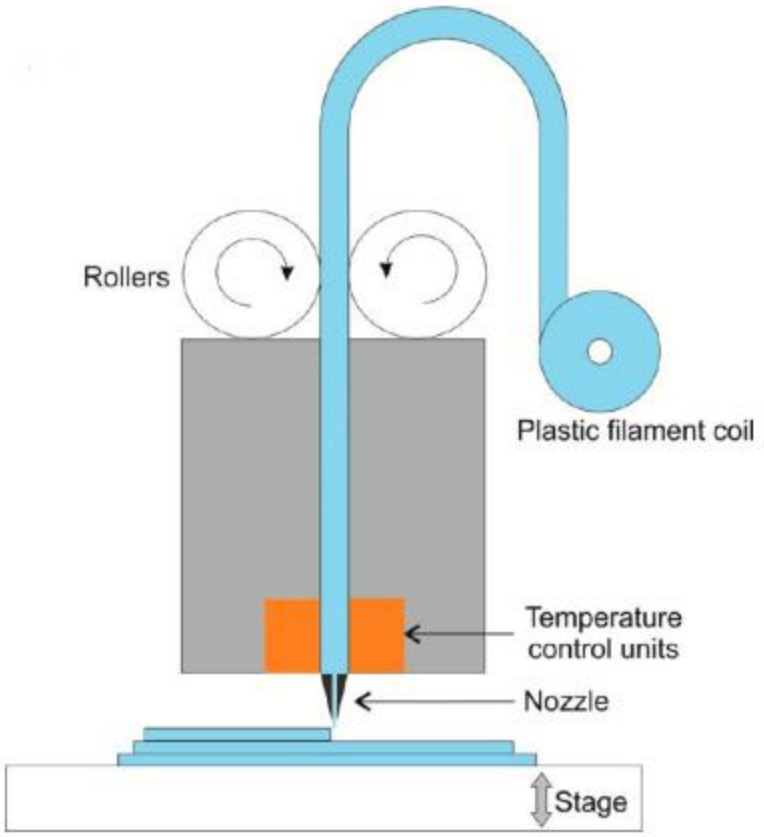

Figure 1. 1 FDM Process [12]

The main material type used in ME3DP are thermoplastics, but other materials like binding ceramics, and particularly the use of waxes is gaining popularity in this field due to the ability to reproduce molds in a short period of time for metal casting [8]. Acrylonitrile butadiene styrene (ABS) and polylactic acid (PLA) are the most common materials used in ME3DP. These thermoplastics have relatively low glass transition temperature (Tg), medium to high melt flow rate (MFR) and a small tendency to shrink upon cooling which are desirable qualities for ME3DP materials. There are other thermoplastics available like polycarbonate (PC), polyamides (NYLON), high temperature resistant polymers like ULTEM and other engineering polymers that are used in more specialized applications. The use of these type of engineering materials in ME3DP

require a higher degree of attention when processing due to their higher Tg and shrink warpage tendencies [9, 10].

At the moment most ME3DP applications rely in rapid prototyping and tooling, but it is progressively being introduced to new applications in a diverse number of fields to produce fully AM goods ready to market [4]. Some of the advantages of ME3DP over other AM technologies are the low maintenance and material cost, compact size units, relatively low temperature of operation, and resolutions of ±0.1 mm tolerance [11]. AM technologies like ME3DP are already reducing costs and facilitating the creation of better products [3, 12, 13], thus further development of this technology would bring major savings and technology advancement. The research community on ME3DP currently works on diminishing some of the common technology drawbacks like surface finish, dimensional accuracy, anisotropy, prolonged build time, material availability and introduction of novel concepts within ME3DP [14-59].

In order for more industries to adopt ME3DP over standard manufacturing methods, quality products must be produced at high production rates with low manufacturing cost and shorter lead times. ME3DP processing conditions affect build time and quality of the printed part, thus identification of crucial processing parameters affecting each quality is important for optimization. Figure 1.2 represents a schematic representation of the process of ME3DP along with parameters that influence quality and build time of the printed part.

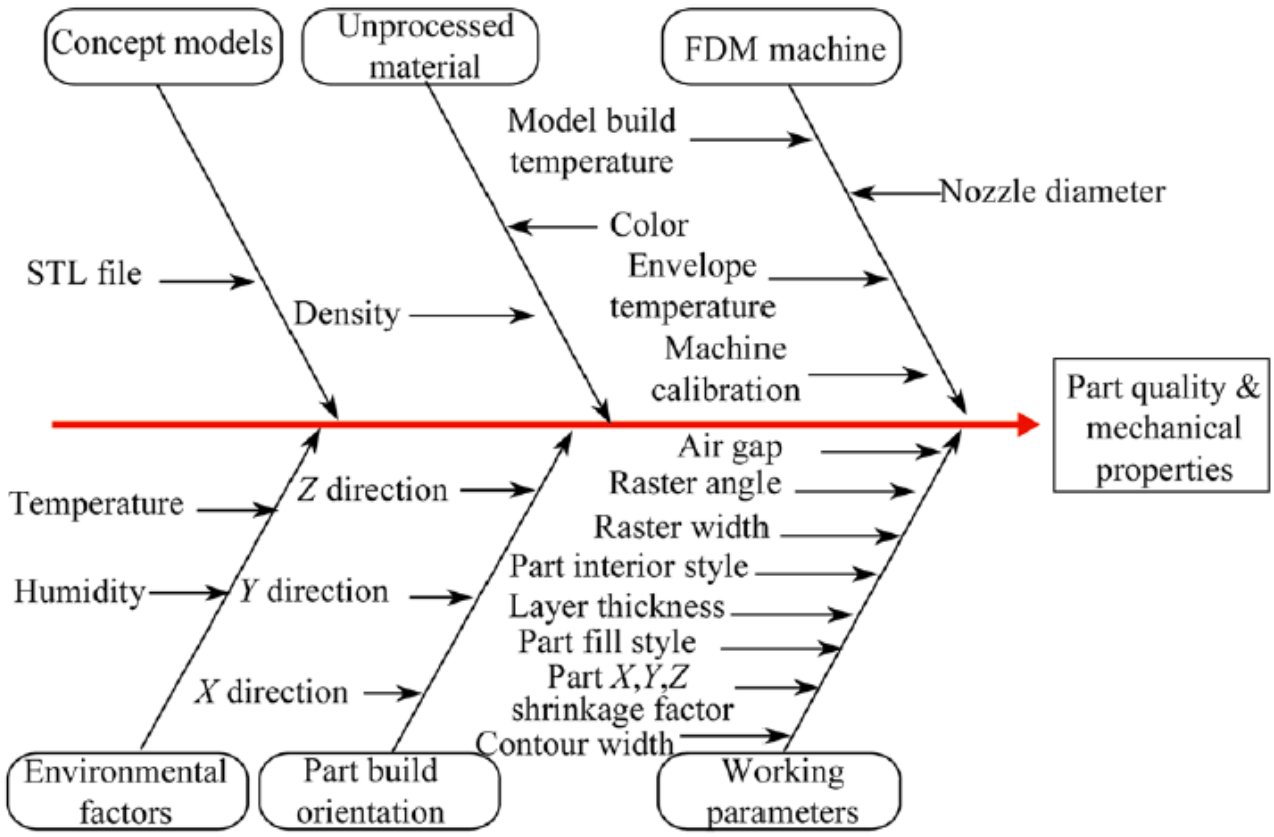

Figure 1.2 Schematic representation of processing parameters for ME3DP [14]

From Figure 1.2 part build orientation relates to the direction at which the object was built which influences the mechanical properties of the ME3DP processed part. Figure 1.3 is a graphical representation of the different build directions that can take place during printing. Other important processing parameters are model build temperature which ensures proper interlayer adhesion between raster pattern and layers; envelope temperature which helps prevent creeping and stress concentration; layer thickness a process parameter that is determined during slicing (software) and is important for surface quality; raster width is determined by the nozzle diameter; air gap refers to the empty space between rasters in a layer as it is graphically represented in Figure 1.4 among other parameters.

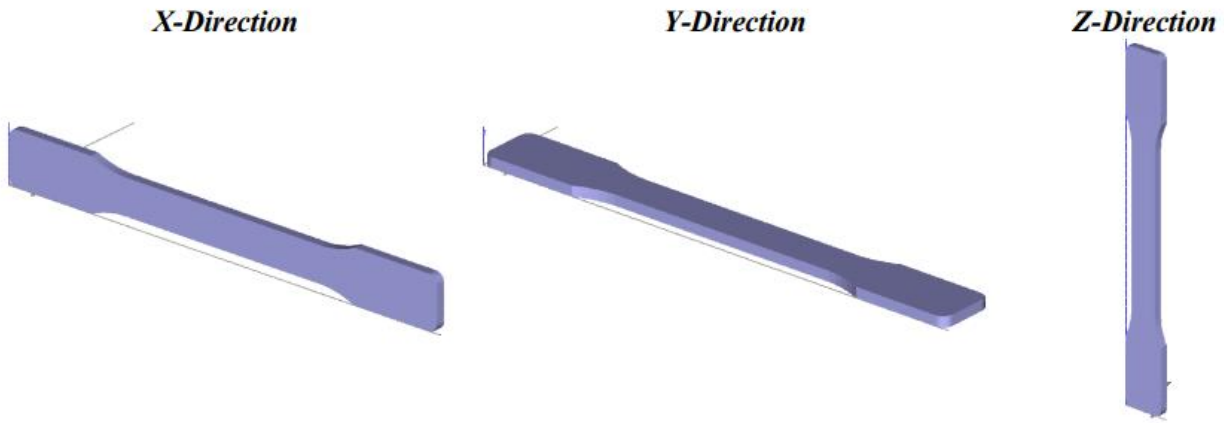

Figure 1. 3 Part build orientation X, Y, and Z [15]

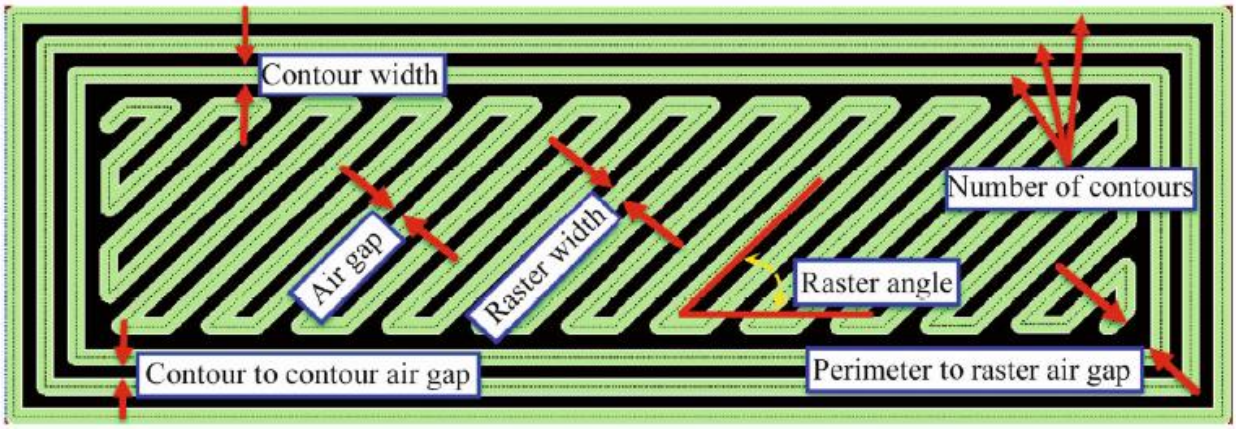

Figure 1. 4 Air gap, contour width, raster width, raster angle [14]

1.3 Drawbacks in ME3DP and current research efforts

In order to expand the applicability of ME3DP through material development it is important to understand common drawbacks within the technology. In this part of the study, common factors that limit main stream adoption of ME3DP will be introduced as well as the efforts from the research community to diminish them.

1.3.1 Surface Roughness

The deposition nature in a layer by layer fashion of ME3DP creates an undesired quality called “staircase effect”, which is represented in Figure 1.5. From a geometrical perspective is apparent that diminishing layer thickness would decrease this effect. Surface roughness main

contributor is layer thickness, but it is not limited to this processing parameter, other parameters like air gaps between rasters, deposition speed, and raster angle also influence surface quality [16]. Lowering layer thickness improves surface quality and at the same time increases the amount of layers needed to complete the 3D object increasing total build time. There are conflicting parameters within ME3DP processes that make optimization a complex subject, this type of dependency is unlikely to be resolved without major technological advancement in the field. There are models and studies available in literature relating the optimization of ME3DP processing parameters for surface finish improvement [14, 16-22]. While some researchers use known optimization methods like the Taguchi or Analysis of Variation (ANOVA) to optimize parameters for better surface resolution [16-17] others focus in optimization methods using 'real coded genetic algorithm' [19-20] and or post processing of the printed part [20 -22].

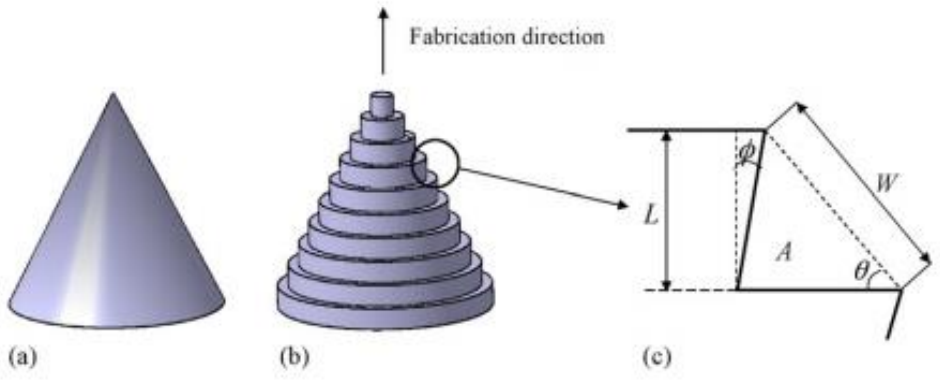

Figure 1. 5 Staircase Effect a) Actual 3D object b) Staircase Effect due to AM c) Geometry of stair-stepping effect by Ahn et al [18]

Anitha et al [16] studied the effects of three processing parameters (layer thickness, road width and speed) in surface quality by using three different methods, the Taguchi technique, signal to noise ratio (S/N) and the ANOVA analysis. Anitha found layer thickness as the main contributor to surface roughness with a 51.7% (to 99%) level of significance and following factors road width and speed of deposition with 15.57 and 15.83% level of significance (to 99%), respectively.

Nancharraiah et al [17] realized a similar study as Anitha, using the Taguchi and ANOVA techniques with different processing parameters: layer thickness, road width, raster angle and air gap. Nancharraiah concluded that surface quality can be improved lowering layer thickness and air gap dimensions. Ahn et al [18] explored surface roughness prediction by using 3 main factors layer thickness, surface angle and profile angle. In this study Ahn formulated Equation 1.1 which can be expressed as an average surface roughness from the geometric relations from Figure 1.5c. Where A,w, and L represent step area, step width and layer thickness, respectively.

Equation 1. 1 [18]

$$R_a = \frac{A}{w} = \frac{L}{2}\left|\frac{\cos(\theta-\phi)}{\cos\phi}\right| \quad (0^\circ < \theta < 180^\circ)$$

Ahn was able to recreate a model that successfully predicted surface roughness from theoretical and experimental data. Figure 1.6 shows the visualized result of a digital object which was formed by twisting at an interval angle of 3 degrees from 0° to 180°. The results of this CAD model validated their predicament with the error of prediction being less than 1 μm [18].

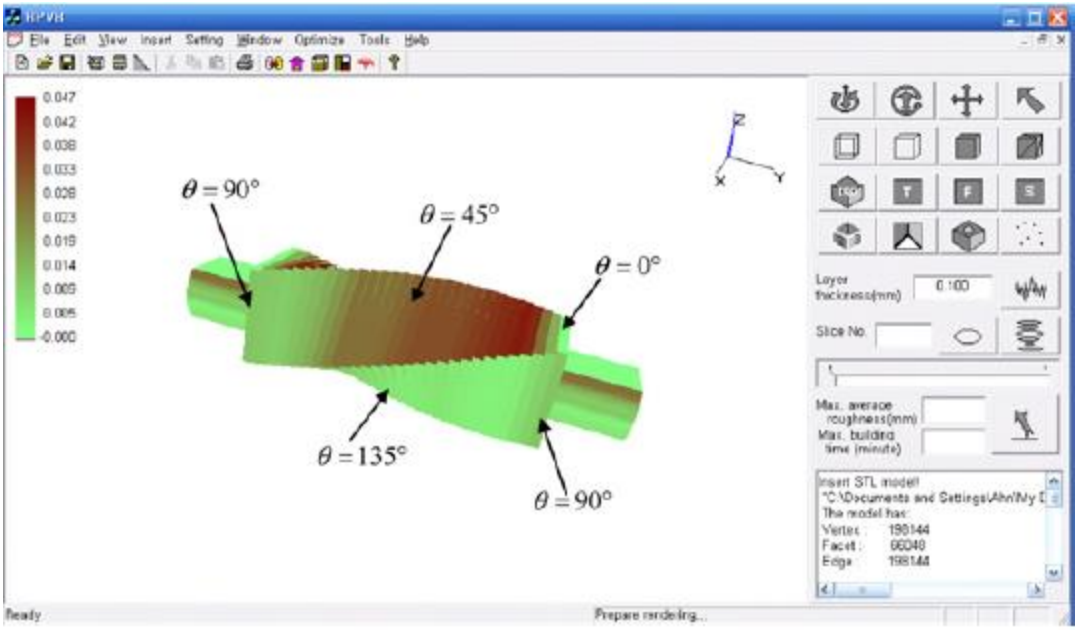

Figure 1. 6 CAD model of Surface Roughness prediction [18]

In an effort to improve surface quality without compromising build time, Thrimurthulu et al [19] used real coded genetic algorithm to create a model that predicted optimum part orientation to improve surface finish. The authors were able to validate their system by using their model simultaneously with an adaptive slicing scheme on two case studies presented in the study, according to the authors any complex geometry can be used in this system.

Post processing methods have also been explored to improve surface quality. Pandey et al [20] introduced a system were a hot cutter machining (HMC) was used to improve surface finish. The HMC is a mechanism that employs a hot cutter with straight edge enhanced the surface finish of a ME3DP part up to 0.5µm R_a value. Pandey et al mentions the future work of this article will be to implement the HMC simultaneously during printing [20], as of now the creation of this device has not been documented but more work on the hybrid system can be found in an article published on 2006 relating to computer models of the ME3DP and HMC hybrid system [21]. Gantucci et al [22] conducted a study were they employed a two phase methodology to improve surface finish. In the first phase they optimized parameters to improve surface finish based on previous studies

controlling nozzle size, raster width and layer thickness. After optimizing parameters, the second phase consisted in a chemical finish where the 3D object was placed on a chemical bath consisting of 90% dimethylketone and 10% water for 300 seconds. The results were very satisfactory, the surface finish after the optimization and chemical bath was greatly improved and it only had a 1% shrinkage from the original prototype after post-processing. Garg et al [23] studied the effect of cold vapor treatment on ABS P430 with parts printed at various orientations (0°, 15°, 30°, 45°, 60°, 75, 90°). The cold vapor used in this experiment consisted of acetone, the best results were obtained on the 90° print orientation were the reduction of surface roughness was as low as 0.02 μm.

1.3.2 Dimensional Accuracy

Between the research goals of ME3DP dimensional accuracy remains among the most important, because it is considered a key factor in quality assessment controls for a wide range of industrial applications [24]. Specialized industries like medical, automotive, and aerospace require higher quality fabricated parts that mandate precise dimensional accuracy. Dimensional accuracy is essential to ensure dimensional stability and repeatability, which are vital concepts in current manufacturing practices [25]. As it is the case with surface roughness, dimensional accuracy depends greatly on the selected processing parameters. Processing parameters influencing dimensional accuracy include layer thickness, build orientation, air gap, raster angle, raster and width. The conflicting parameters in ME3DP and the diverse behavior of different ME3DP materials adds to the complexity of parameter optimization for dimensional accuracy improvement. Mohamed et al [25] unhappy with the limitations of previous studies relating dimensional accuracy, developed a method that can improve dimensional accuracy more effectively and accurate. The model consisted in a methodology based on computer-generated

optimal design using I-optimality criterion. This type of model is able to solve optimization problems involving a large number of ME3DP parameters along levels with constraints (irregular experimentation matrix) [25]. The difference between this study and other studies, is the ability to consider a larger amount of parameters with all possible levels of influence, as well as the consideration of "number of contours" a parameter that was not considered in previous studies [17, 26 – 28]. The major findings in this study were that by increasing raster angle from 0° to 90°, reduced the percentage change in length as the other parameters were increased (layer thickness, air gap, road width, and number of contours). A similar trend was observed in the change of width, were the percentage change in width of the part decreased linearly with the decrease of the before mentioned parameters. Where a decrease in percentage width was experienced after change of raster angle from 0° to 90°. Increasing the number of contours alongside layer thickness, increased the width percentage change but it was reduced by increasing air gap raster angle, built orientation and road width. The overall results obtained from the verification of the experiments show accuracies of +0.02mm in length, +0.004 mm in width and +0.007 in thickness can be obtain using the developed models and that the best parameters settings to achieve the best dimensional accuracy for a Fortus 400 (Stratasys, MN, USA) using PC-ABS is a layer thickness of 0.127 mm; air gap of 0.342 mm; raster angle of 88.918°, build orientation of 89.122°, road width of 0.462 mm, and 1 contour. After all the method presented in this paper proposed an adequate ME3DP process parameter optimization that can be applied to other systems with a large number of processing parameters.

1.3.3 Build Time

One of the process limitations of ME3DP is the lengthy build time compared to some current manufacturing technologies. For example, it would take several minutes to print a one inch

cube using ME3DP while injection molding can process several cubes per minute. This constraint comes directly by the nature of the ME3DP process where speed deposition is limited by the fusing time of layers/rasters, surface quality, and dimensional accuracy. A significant change of build time for ME3DP technologies that compete with current mass production methods are not likely to occur without major technological advances. Studies available in literature on ME3DP mostly focus on parameter optimization and build orientation [19, 29, 30] to reduce build time with the existing technology available. Thrimurthulu [19] identified the conflicting parameters between layer thickness and part deposition time, where usually one of the two qualities has to be compromised to improve the other. Therefore, through real coded genetic algorithm and the optimization of parameters created a model that provides optimum part deposition orientation to improve surface quality and decrease build time at an equilibrium point. The capabilities of this system were validated on two case studies, one an axisymmetric part and a typical 3D. Figure 1.7 is the graphical output obtained for the axisymmetric part optimum part deposition orientation, where Figure 1.7a represents part deposition for best surface quality and Figure 1.7b represents the best part orientation for minimum build time. The minimization of both qualities in this study relies in averaging the impact of build time vs surface quality. Although this study does not solve completely the issue of conflicting parameters, surface quality vs build time, it provides a fair estimate to minimize the impact between them through optimum part deposition and parameter optimization.

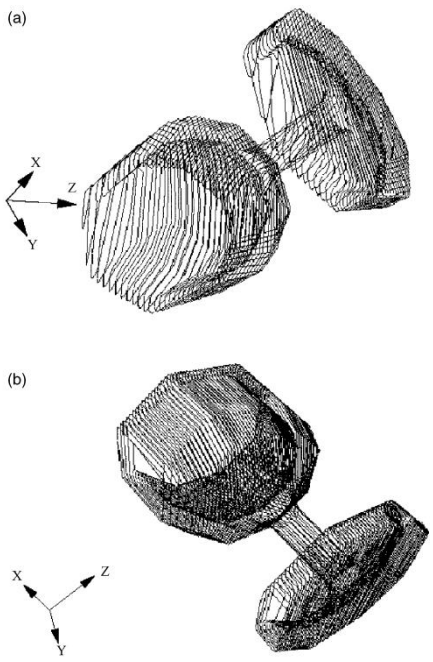

Figure 1. 7 Graphical output from developed system of optimum part deposition [19]

Kumar et al [29] studied the relationship between processing parameters layer thickness, raster angle, orientation, contour width, and raster width with relationship to build time and support material volume. For this study a 2^5 full factorial design of experiments methodology was employed. A total of 32 experiments were carried out and analyzed using ANOVA which discovered that besides layer thickness, part build orientation had the highest impact on build time and support material volume. Nancharaiah [30] used design of experiments (DOE) to optimize ME3DP processing time. The study was based on three processing parameters: layer thickness, air gap, and raster angle. Through ANOVA the study concluded that layer thickness contributes 66.57% on processing time at 99% confidence level, air gap contributes 30.77% at 95% significance.

1.3.4 Anisotropy

The deposition orientation in ME3DP is known to influence the final mechanical properties of a printed part. This directional dependency or anisotropy is a common issue in additive

manufacturing technologies. Mechanical properties of printed parts are important in the area of rapid prototyping, as prototypes must have adequate mechanical reliability for tooling and demonstration purposes. This characteristic is especially important for ME3DP produced end products/parts, where they must have similar mechanical properties as those produced using traditional manufacturing in order to withstand in-service loadings and operation requirements [31]. Unlike other anisotropic materials like wood, ME3DP anisotropic properties are not influenced solely by the building material, the effect depends mostly on the direction of the building layers and adhesion between them. Most studies found in literature deal with processing parameter optimization and build orientation to reduce anisotropic properties [32 – 35]. An early study of anisotropy in ME3DP by Es-said et al [32] based their article in comparing 5 different raster pattern orientations to examine their behavior under tensile strength, modulus of rupture, and impact resistance. The material used for this study was ABS and Figure 1.8 represents the schematic representation of the 5 raster patterns used in this study along with their respective tensile test rupture geometry. The 0° raster pattern recorded the highest values on every test. The ultimate tensile strength data recorded for the 0° raster pattern direction, had a higher value of almost three times if compared to the lowest, the 45° direction, and 30% higher than the second highest the 45° and 0° direction. This results show the effect of direction in final mechanical properties. Similar results were seen among the rest of the mechanical tests, which made Es-said et al conclude the high importance of pattern direction on mechanical properties.

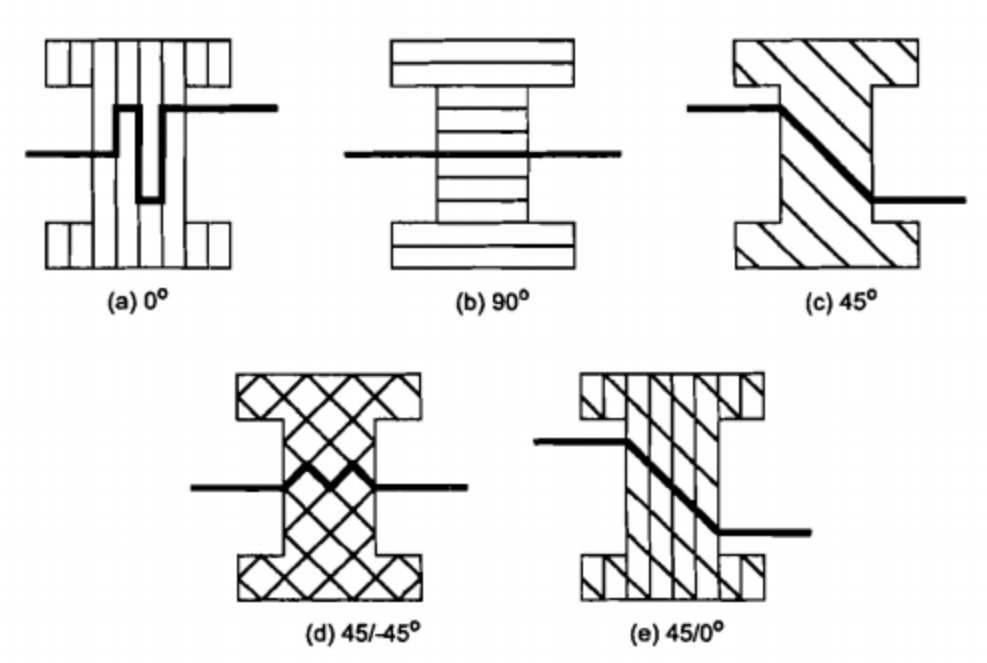

Figure 1. 8 Schematic representation of raster pattern along with rupture geometry for the 5 systems in tensile testing [32]

An interesting study by Ahn et al [33] displays the comparison between ME3DP specimens and injection molded specimens both made with the same grade of ABS. In this study Ahn et al used a DOE approach to examine the effects of process parameters such as raster orientation, air gap, raster width, color, and model temperature on the mechanical properties of the printed specimens under tension and compression. After process optimization Ahn et al [33] found superior mechanical properties on specimens printed with an - 0.003 inch overlap, these specimens reported a 65 to 72 percent of strength compared to injection molded specimens in tensile strength, and 80 to 90 percent on compressive strength. Five different build orientations for the tensile strength test specimens were selected for this study: 0°, 45°/-45°, 0°/90°, and 90°. The pattern with the 0° build orientation recorded the highest strength with 18.72 MPa which represents 72% of the total strength of the injection molded parts. For the compression testing only two different build orientations were compared: 45°/-45°, and 0°/90°, both recorded similar compressive strengths to which the authors concluded that build orientation has a lesser impact during compressive forces.

Bellini et al [34] interpreted that the internal architecture of a part fabricated using ME3DP is not significantly different from a fiber reinforced composite structure. This analogy allowed the use of analytical tools developed for earlier anisotropic products. From previous studies it was determined that the first step for better understanding of the mechanical properties in composite materials is to test the single "fiber" [35] that is why Bellini et al [34] tested the mechanical properties of the filament used in the ME3DP process and the ME3DP roads or "rasters", the results showed similar tensile strength and young modulus between the filament and ME3DP roads. The only difference was shown on the maximum strain were the ME3DP roads represented one third of the filament. From this data the authors concluded that the extrusion process does not have a considerable effect on tensile strength and modulus of the material but notably effects on maximum strain [34]. In order to test the anisotropy nature of the ME3DP process, Bellini et al printed 6 different build orientations depicted on Figure 1.9 to perform tensile testing. From Figure 1.9 the specimens on the left cube represents the different building orientation of parts printed at 0° and 90°, the cube on the right represents the building orientation of the 45° and -45° raster angle. The results of the tensile test are depicted on Figure 1.10, through a MATLAB function stress-strain curves of the data points taken from the tensile test provided the averaged stress-strain curves of the different build orientations. As it was expected the xz orientation showed the lowest tensile strength, due to the sample being pulled in the direction where bonding is the weakest, perpendicular to the raster pattern direction. The yz parts showed the highest strength and young modulus because the tensile load was in the same direction as the build orientation, the rasters were aligned with the tensile direction. Bellini concluded that mechanical properties are considerably dependent on two modeling phases: the building direction (raster pattern) and the chosen path (building orientation).

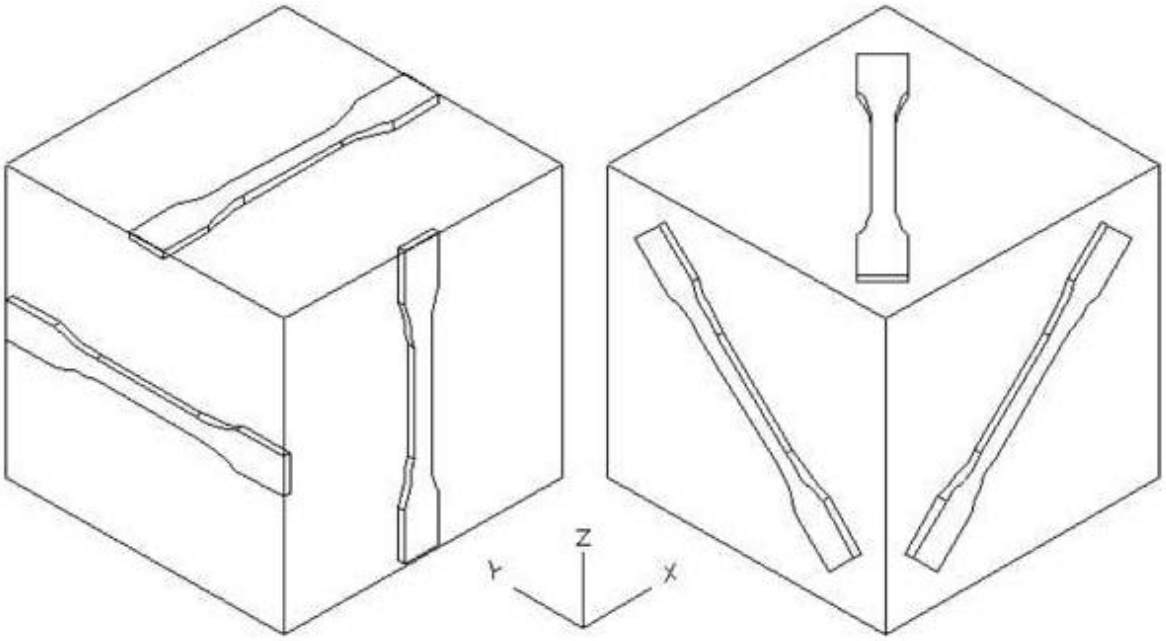

Figure 1. 9 Building orientations for tensile test specimens [34]

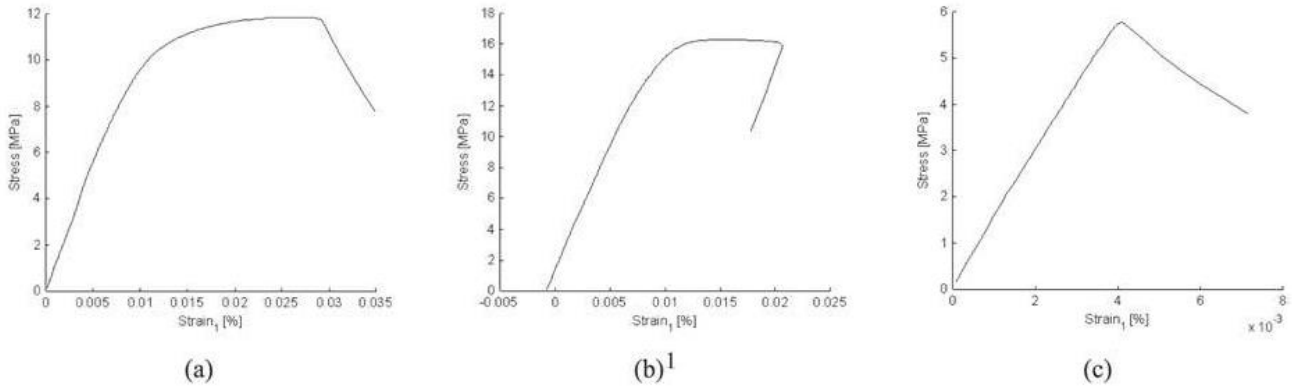

Figure 1. 10 Stress strain curves a) xy direction b) yz direction c) xz direction [34]

ME3DP is a promising technology for the production of specific need, low volume products such as replacement parts for larger systems and custom products [36]. With recent increments of production of ME3DP components and finished goods, Ziemian et al [36] noticed the importance of a thorough investigation of the effects of build orientation in key mechanical properties of ME3DP components. The goal of the project was to quantitatively analyze the potential of ME3DP to fully evolve from rapid prototyping to rapid manufacturing through the

evaluation of the anisotropic properties of the process. Key mechanical properties like tensile, compressive, flexural, impact and fatigue strength properties of ME3DP specimens were compared with injection molded parts made with the same base ABS material. The study used recommendations on processing parameter optimization from previous works to focus solely on the significance in the direction of polymer roads relative to the loading direction of the part. The evaluation took place on 4 different raster orientations: longitudinal 0°, diagonal 45°, transverse 90°, and alternating at 45° (45°/-45°). The tensile test results indicated that the 0° raster orientation had the highest ultimate and yield strength with 25.72 and 25.51 MPa respectively, this was expected as the 0° raster orientation deposits the material parallel to the specimen's longitude which also corresponds to the direction of the tensile load during the test. The transverse direction or 90° scored the lowest ultimate which represented 56.23% percent of the 0° specimens with 14.56 MPa following the diagonal 45° with 16.22 MPa and alternating (45°/-45°) with 19.36 MPa. Figure 1.11 represents an SEM image of a longitudinal 0° fracture surface, in this image a predominantly brittle fracture can be observed with localized micro-shearing in each individual fiber face. Thus, tensile strength is heavily dependent on the strength of the ABS material than specimens with orientations other than 0° as it is the case with the 90° fracture surface represented in Figure 1.12 were most of the failure occurred in the predominantly weak interface between layered ABS fibers [36]. The diagonal and alternating 45° orientation displayed a mixture of individual rupture fibers and failure due to poor interfacial adhesion as it can be seen on Figure 1.13.

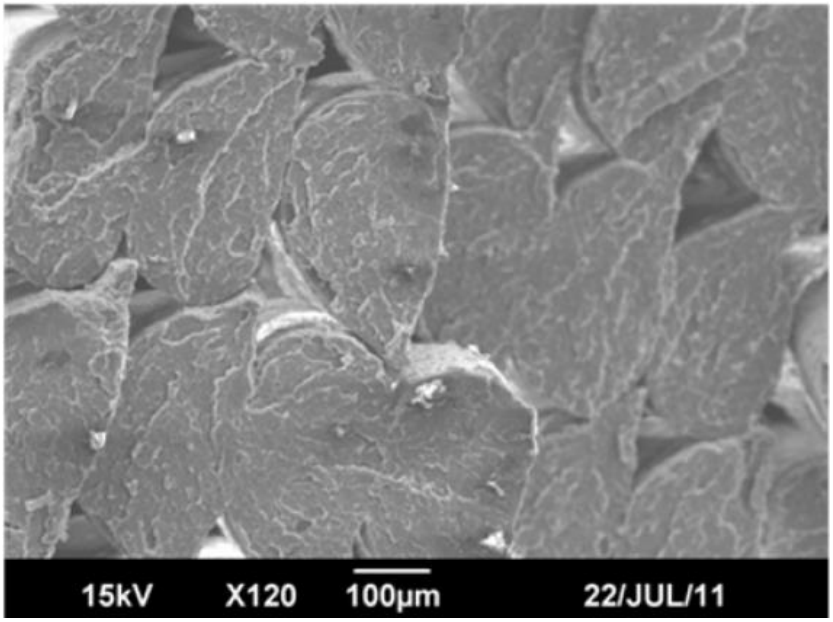

Figure 1. 11 Fracture surface of Longitudinal 0 degree [36]

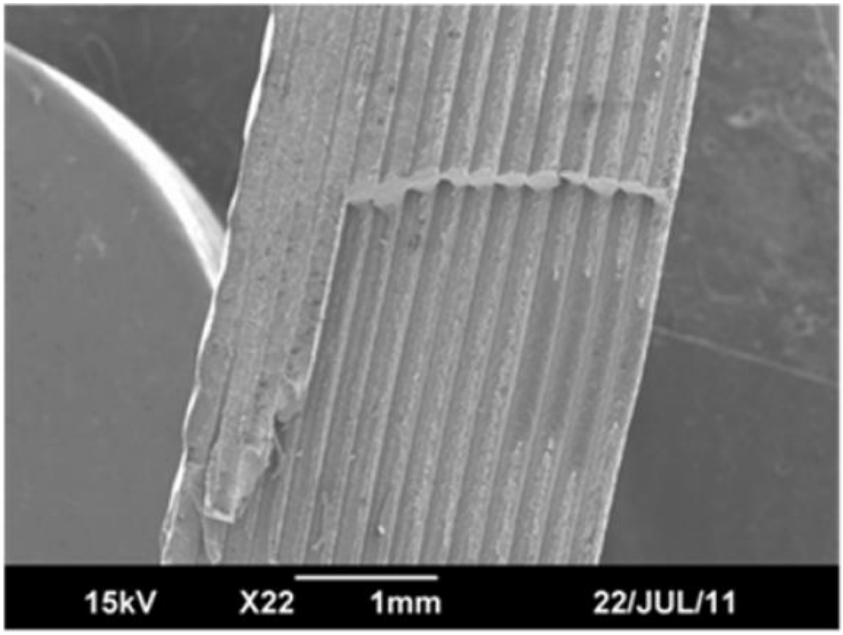

Figure 1. 12 Fracture surface of transversal 90 degree [36]

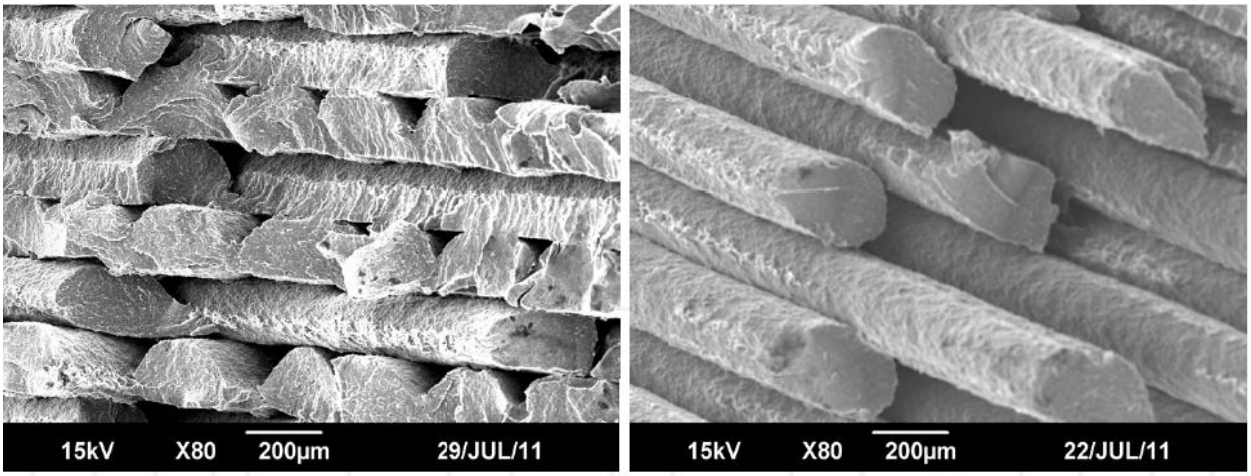

Figure 1. 13 Fracture surface a) Alternating 45/-45 degree b) Diagonal 45 degree [36]

During compression test, the transversal orientation or 90° obtained the highest mean yield strength with 29.48 MPa following the 0° with 28.83 MPa, alternating 45°/-45° with 28.14 MPa, and diagonal 45° with 24.46 MPa. Compression tests in polymers result in higher strengths than those obtained in tension [33], as it was the case of this study were the average yield strength in tension was 56% compared to the average obtained in compression. Statistically differences were not found on the 0°, 90° and 45°/-45° raster directions, the only difference was found in the 45° which represented roughly 83% of the highest scored obtained by the 90° build orientation. In order to determine flexural properties three-point bending test was performed. Since build orientations 0° and alternating 45° did not break during the test, for comparison reasons yield strength over ultimate strength were evaluated. The highest mean yield strength belonged to the 0° raster orientation with 34.2 MPa, following the alternating 45° with 26.5 MPa, the diagonal 45° with 21.3 MPa, and transverse 90° with 20.8 MPa [36]. Flexural strengths are usually higher than tensile strengths because of the compressive and tensile stresses that are subjected during testing [36]. There is a significant difference of 60.9% between the 0° and 90° raster orientation. Through hoc analysis the impact of raster orientation further indicates a significant difference of all paired means except to the 45° and 90° angle were mean yield strength were 21.3 and 20.8 MPa

respectively. As it was the case for the tensile and flexural test, the 0° build direction scored the highest impact energy during impact test with 2.991 (J/cm) and the lowest impact energy belonged to the transverse 90° orientation. A post hoc comparison of the results indicated that there was a significant difference for all paired comparisons except for the diagonal 45° and alternating 45°, which implies the presence of anisotropic characteristics pertaining impact energy [36]. When analyzing the feasibility of ME3DP becoming a rapid manufacturing tool, Ziemian et al [36] remarks the importance of assessing raster orientation effects on fatigue properties. For this a tension-tension loading configuration was employed with a maximum fatigue load of 70% of the mean failure load determined from previous tensile testing. The highest number of cycles to failure was experienced by the alternating 45°/-45° with 4916 cycles, following the longitudinal 0° with 4557 cycles, transverse 90° with 1616, and diagonal with 1312 cycles. There was a big difference between the diagonal 45° that represented 26.7% of the total number of cycles to fail experienced by the alternating 45° orientation. After post hoc comparison it was determined that every pair except alternating 45° and 0° were statistically different which confirm the significant effect of build orientation on fatigue properties [36]. Ziemian concluded that build orientation had a significant orientation for tensile, compressive, flexural, impact and fatigue strength properties through experimental data, and statistical analysis like Tukey and ANOVA. Although Ziemian did not present an approach to diminish the anisotropy effects of ME3DP this work can be used to determine optimum raster orientation for a given part based on the expected in service loads or as a point of reference for analytical models.

Most of the previously presented studies on anisotropy generally deal with parameter optimization and experimental analysis to determine dependency/optimization of build orientation on different mechanical properties. The following studies entail a different approach to diminish

anisotropic properties by creating new 3D printable materials that diminish build orientation dependence on the final mechanical properties of the part. Shaffer et al [37] presented a novel approach to mitigate the effect of layer to layer adhesion on mechanical properties by blending common 3D printable materials with specific radiation sensitizers and exposing them to ionizing radiation in order to increase crosslinks among the polymer chains in the ME3DP part. Two polymer systems were used in this study, the first was composed of acrylate monomers: methyl acrylate (MA) and isobornyl acrylate (IBoA) combined with 0.1 wt% 2,2-dimethoxy-2-pheynlacetophenone (DMPA) which serves as the photo-initiator and blended with radiation sensitizer trimethylolpropane (TMPTA) [36]. The second system consisted in PLA blended with triallysocynurate (TAIC), a radiation sensitizer also known as 1.3.5-triallyl-1,3,5-triazine-2,4,6(1H,3H,5H)-trione, Figure 1.14 shows a graphical representation of the process that took place during the blending of both polymer systems.

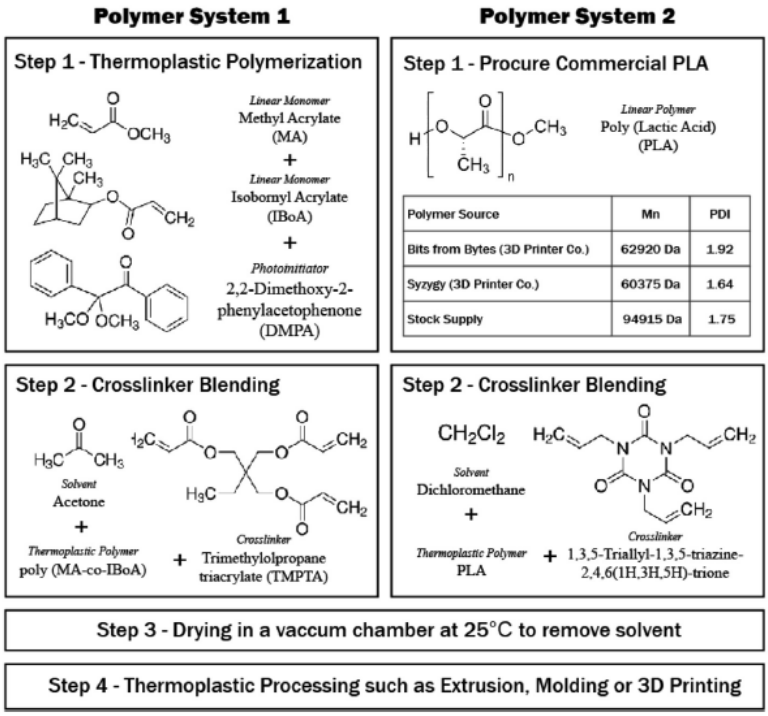

Figure 1. 14 Shcematic representation of blending process [37]

After printing specimens of both systems in 3 different raster pattern orientations (vertical 0°, diagonal 45°, and horizontal 90°) ionizing radiation doses were applied with 10 and 50 kGy (kilogray) at different temperatures of 0°C, 20°C, 40°C, and 60°C during irradiation. Tensile test was performed and the results for the PLA + TAIC can be observed on Figure 1.15, tensile test specimens for the MA/IBoA + DMPA results were not presented because they did not present mechanical stability after irradiation. Figure 1.15 shows that the irradiation at 60°C improved significantly ultimate strength and strain from the control system.

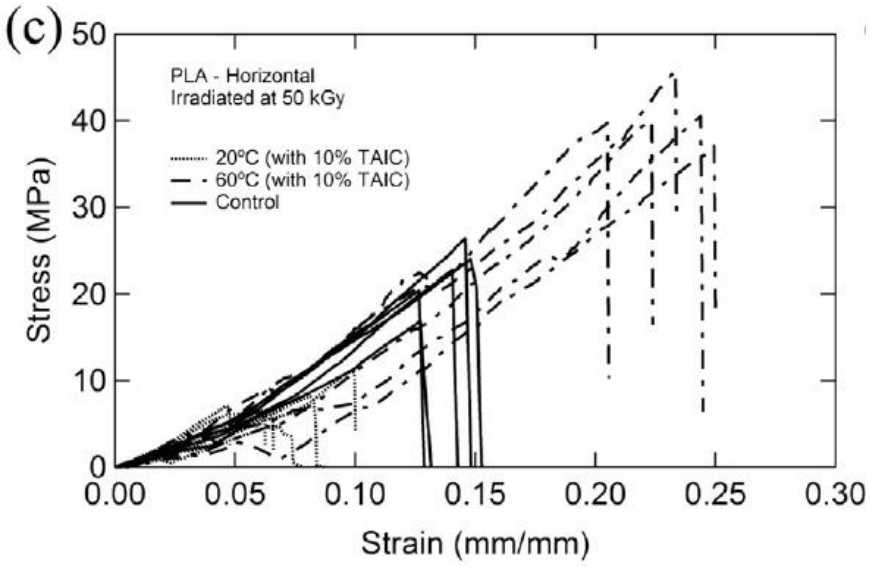

Figure 1. 15 Stress-strain curves for PLA + TAIC system [37]

From Figure 1.16a the anisotropic nature of ME3DP can be appreciated through the stress-strain taken from the tensile testing performed on the baselines with the different build orientations. Figure 1.16b shows the crosslinked sensitized PLA at different radiation temperatures printed in the vertical and horizontal direction. From this image it is possible to observe the huge drop in ultimate tensile strength and strain on the PLA + TAIC irradiated at 20 °C printed in the horizontal direction compared to the higher ultimate strength and strain recorded of the same system printed at a vertical direction. This gap is significantly reduced by the PLA + TAIC irradiated at 60 °C showing a decrease in anisotropy, that can be further confirmed by the increment in ultimate strength and strain if compared to its baseline printed in the same direction[37].

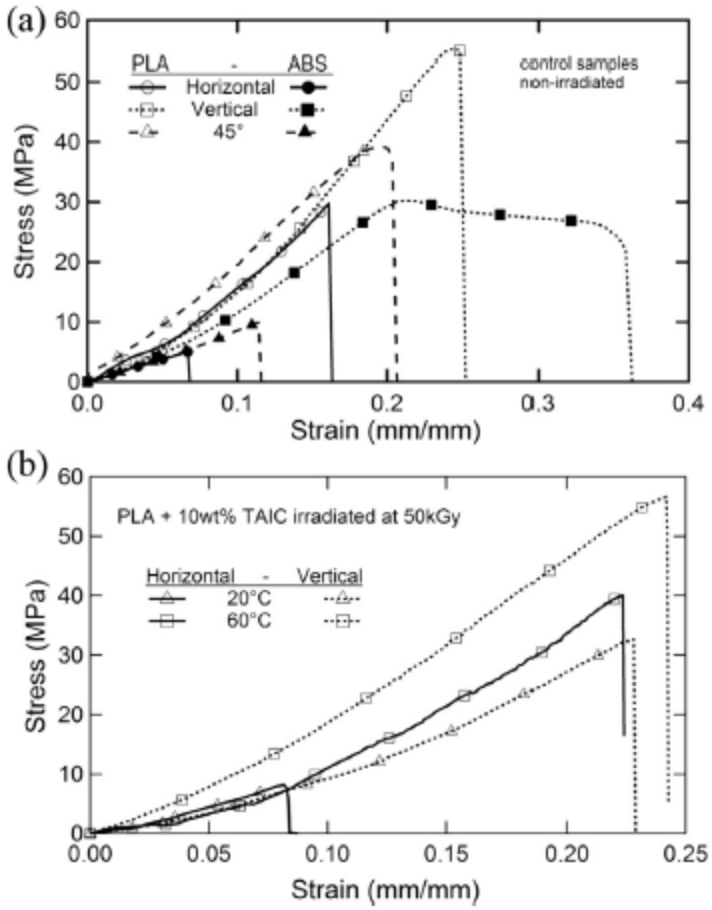

Figure 1. 16 Stress-strain diagrams a) control system b) PLA + TAIC irradiated at 50kGy [37]

Torrado et al [38] studied the effects of build orientation for various additives and polymer blends based on ABS. In this study 6 different polymer/non-polymer composites and 4 polymer blends were printed in two directions, horizontal (XYZ) and vertical (ZXY) as it is graphically represented on Figure 1.17.

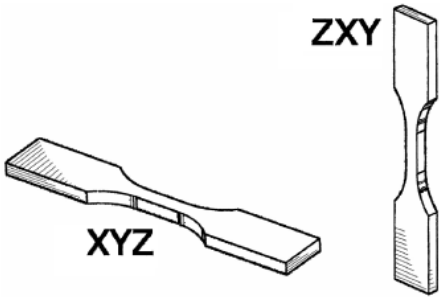

Figure 1. 17 Print directions [38]

The ABS polymer composites and blends were processed using a twin screw extruder to create a 1.75 mm monofilament that was later printed into tensile test specimens. The ultimate tensile strength (UTS) was the metric used to test anisotropy by calculating the percent difference between build orientations as it is expressed in Equation 1.2.

Equation 1. 2 [38]

$$\Delta(\%)_{UTS} = \frac{UTS_{XYZ} - UTS_{ZXY}}{UTS_{XYZ}}$$

Every material system used in this study along the results of the mechanical test for both directions can be seen on Figure 18. On Figure 18 “H” and “V” represent the build orientation horizontal and vertical respectively [38].

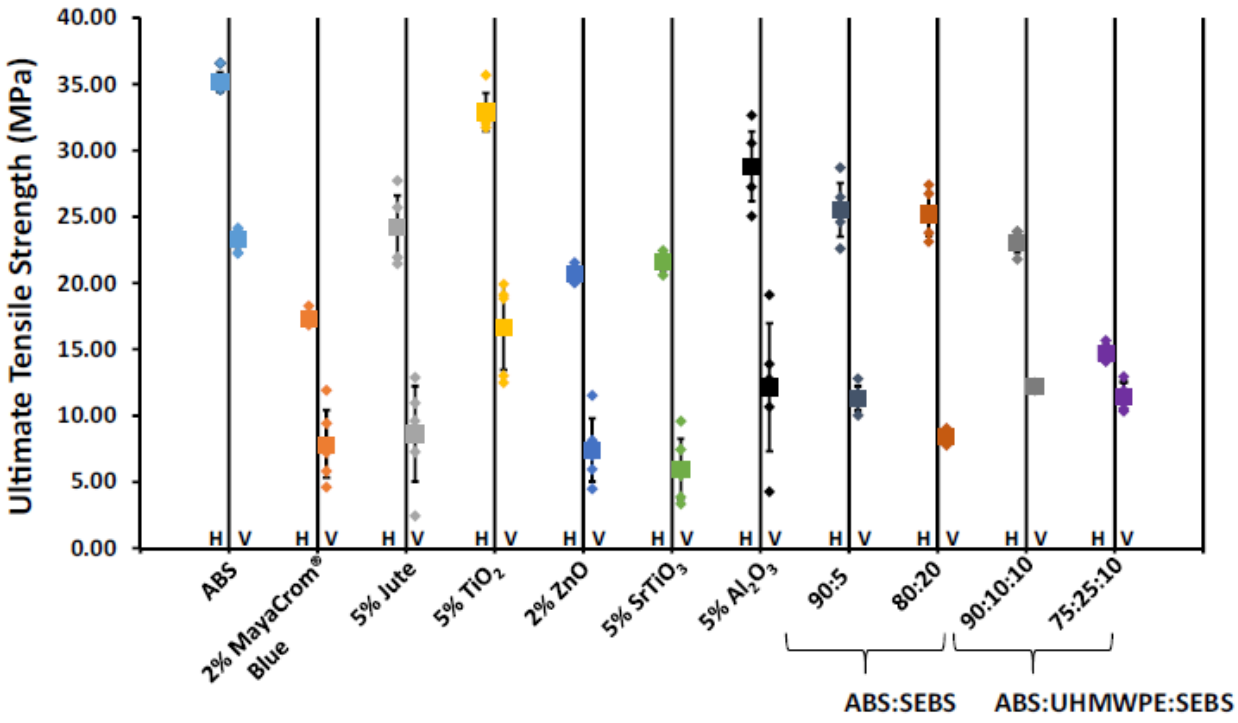

Figure 1. 18 Ultimate tensile strength in both directions [38]

The test results indicate that none of the polymer composites blends nor composites improve the UTS of the baseline. Out of the composites and blends, the 5% titanium dioxide composite recorded the highest UTS value of 32.9 MPa that was slightly below the UTS ABS baseline of 33.96 MPa. The material that presented the lowest anisotropy was ABS blended with ultra high molecular weight polyethylene (UHMWPE) with elastomer styrene ethylene butylene styrene (SEBS) at a 75:25:10 ratio, this material tested a relative difference of 22% compared to the 47% difference in UTS from the two build directions presented in the ABS baseline.

Material development seems like a promising method to diminish anisotropy in ME3DP systems. The fusion between layers and rasters seem to be the key factor in reducing mechanical properties anisotropy. Poor interfacial adhesion is prone to create a larger anisotropy effect while failure within individual rasters creates lower anisotropy as it was the case for ABS:UHMWPE:SEBS on the work presented by Torrado et al [38].

1.4 Material Availability

Material availability is an important aspect for the development of ME3DP. The selection of materials available for ME3DP represents a very small fraction of materials available in comparable technologies on conventional manufacturing (e.g. injection molding) [6]. This narrow spectrum of materials available for ME3DP represents a barrier for application on industries that employ different material requirements than those available for this technology. Development of ME3DP materials with a vast range of material properties would diminish this barrier and increase the applicability of this technology. ME3DP materials depend on certain rheological qualities that enable the formation process through deposition and fusion between rasters and layers to create an object. Relatively low glass transition temperatures, low shrinkage tendency after cooling, and medium to high melt flow rates are some of the desired qualities for ME3DP materials. These qualities are not present on every polymer which increases the difficulty in the creation of new materials compatible with the technology. Two viable approaches to increment the number of materials available for ME3DP are polymer blending and polymer compositing through the alteration of ME3DP compatible polymers to enhance a targeted physical quality.

In the next two sections of this study an introduction to polymer blending and compositing will be presented along a literature review of those practices in ME3DP. It must be noted that these two approaches represent the core of this study as these techniques were applied to develop novel ME3DP materials that will be introduced in the following chapters. Thus, a review of current polymer blending and polymer compositing studies will be introduced to remark the importance these techniques play on the development of ME3DP.

1.4.1 Polymer Blending

The field of polymer sciences has evolved significantly for the past decades thanks to the evolution of polymer synthesis. First from the polymerization of monomers, then from random copolymerization which demonstrated to be an effective technique to improve or modify properties of known polymers, to finally the more systematic approach of block-and-graft copolymerization [39]. According to Paul, there are still concepts in polymer synthesis that have yet to be explored, on the other hand that does not mean that new chemical structures or organizations are necessary "to meet new needs or to solve old problems" as polymer blending can be used to tailor physical qualities from existing polymers [39]. The term of polymer blend refers to the physical rather than chemical (modifying chemical structures) approach of blending polymers. Twin screw extruders are industry standard for polymer blending and impose a more economical method to create polymers that combine more than one desired physical property [40].

In the field of AM by ME3DP, polymer blending has been proven to be a viable approach to develop new materials compatible with the technology. ME3DP largest company Stratasys, commercially carries a variety of polymer blends, an example is a polymer blend based on ABS and PC which combines the heat resistance properties of PC with the elastic properties of ABS [41]. From literature Torrado et al examined the anisotropic nature for polymer blends based on ABS and an elastomer styrene ethylene butadiene styrene (SEBS) [38]. Major findings in this study showcased the decrease on mechanical anisotropy of a ternary blend of ABS:UHMWPE:SEBS. Chen et al [42] developed ME3DP scaffolds for tissue engineering by blending PLA with thermoplastic polyurethane (TPU). TPU is a highly elastic material composed of flexible segments (polyesther) and hard segments (benzyl structure) that exhibits good biocompatibility, good abrasion resistance, and high elongation. However, TPU lacks mechanical

strength and experiences poor shape fixity. On the other hand, PLA offers good mechanical strength, high rigidity, and it is highly biocompatible and biodegradable. This polymer blend enhanced ductility on PLA, and increased its tensile and impact strength. The PLA/TPU blend along the ability to easily control the architecture with ME3DP improved the strength, and durability, of the biomaterial scaffolds.

In Chapter 3, a published article from the author will be presented, entailing the development of a polymer blend in an effort to expand ME3DP capabilities through material development.

1.4.2 Polymer composites

Polymer composites are materials that consists of two or more chemically and physically different phases separated by distinct interfaces [42]. The reason behind polymer compositing is to achieve systems with more useful structural or functional properties that were not attainable by any of the constituents alone [42]. In ME3DP polymer composites are enabling the expansion of the technology into different fields thanks to the modification of physical properties of ME3DP materials through the addition of fillers. Technologies like ME3DP provide the capability to deposit dielectric, conductive materials, or materials with different electrical properties in a volumetric scale at an almost arbitrary fashion [43]. This, along recent developments in polymer composites of materials with high dielectric and reasonable loss tangents, compatible with the technology, have opened the door for the development of antennas with optimized performance and size [43]. Castro et al [44] explored the effects on relative permittivity and loss tangent in antennas build by ME3DP with different polymer composites. The polymer composites were based in two different polymer matrices cyclo-olefin polymer (COP) and ABS reinforced with ceramics $Ba_{0.5}5Sr_{0.45}TiO_3$, $MgCaTiO_2$, and TiO_2. COP has a high melting temperature of 280° C and T_g of

136° C, it is resistant to solvents and acids, and also holds superb electromagnetic properties with εr~2.3 and tanδd <0.0005 at 17 GHz [44]. Compatibility of the polymer blends with ME3DP can be observed in Figure 1.19 where an SEM image of the 30% v/v COP- TiO_2 composite filament's cross section is shown along the top view of the ME3DP printed thin sheet sample.

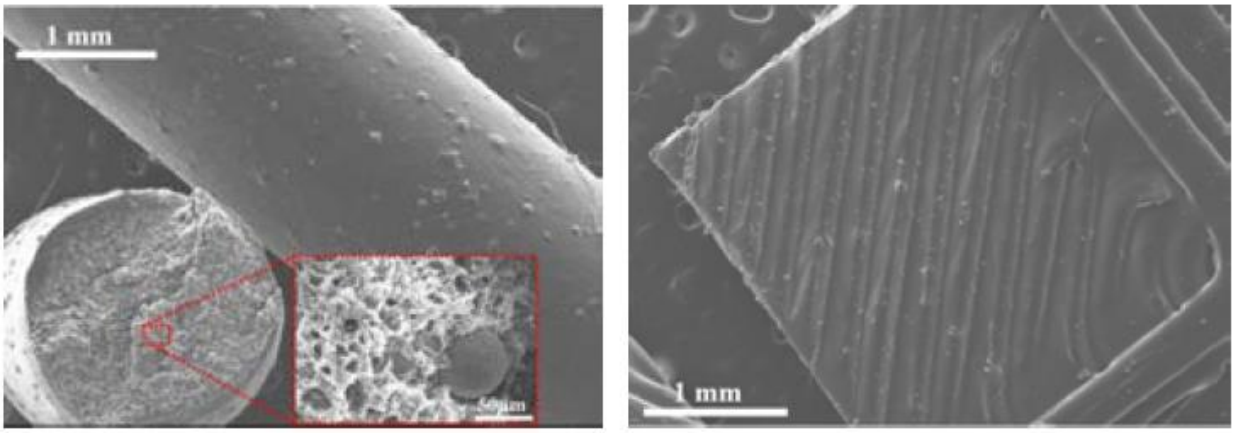

Figure 1. 19 SEM image of COP-TiO2 30% v/v coss section and thin sheet [44]

The results obtained from the measured electromagnetic performance showed an increase of relative dielectric permittivity of the composites from εr~2.3 of COP to εr~4.88 and tanδd <0.0005 for the 25% v/v COP- $Ba_{0.5}5Sr_{0.45}TiO_3$ an increase of relative permittivity of over 100%. Similar results were observed for the other composites in the study showing very promising features for enabling next generation high-performance 3D RF and microwave devices using ME3DP [44].

In the field of biomaterials, ME3DP has become an important tool for the development of tissue engineered scaffolds due to the manufacturing flexibility ME3DP has to easily prepare scaffolds with customizable design of size, porosity, and interconnections between channels which are important factors in the mechanical properties, and cell growth proficiency [42]. Current ME3DP compatible polymers do not have all the properties required to create optimum tissue engineering scaffolds. Polymer composites have been developed to improve cell growth and mimic

human bone properties. Natural bone is a porous material that contains voids in varying sizes, it is composed of connective tissue consisting in a polymeric phase (collagen), ceramic phase (minerals), and water [45]. Kalita et al [45] developed a polymer composite blend based on high shear mixing polypropylene polymer (PP) with tricalcium phosphate ceramic (TCP) and fabricated controlled porosity PP-TCP composite scaffolds using ME3DP. PP has great cracking resistance and high flex life, it has biomaterial properties and has been previously used for finger joint prostheses [45]. Calcium phosphate ceramics like TCP have been utilized as bone substitute materials and are widely used in the health care industry [45]. After creating feedstock material for the PP-TCP material, ME3DP was used to fabricate controlled porosity scaffolds with 3D interconnectivity, Figure 1.20 is a graphical representation of the scaffolds fabricated with ME3DP.

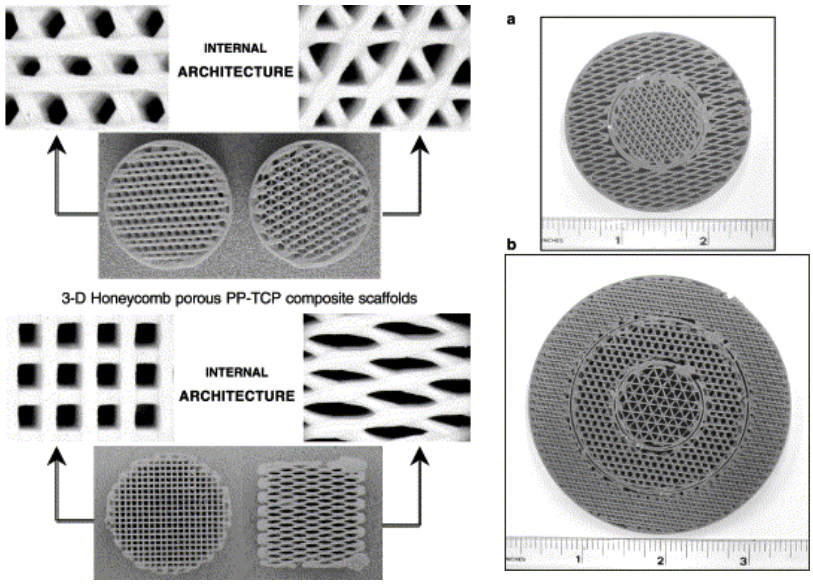

Figure 1. 20 PP-TCP composite scaffolds with different internal architectures [45]

The scaffolds were characterized for their physical, mechanical, and biological properties. Different architecture results showed an increase in pore size diminishes the compressive strength of the scaffolds, samples with 36% volume porosity and 16 µm pore size showed the best

mechanical properties under compression [45]. The biocompatible analysis revealed non-toxicity of the composite and proved successful attachment of OPC1 cells to the substrate. Polymer blending enabled the use of ceramics to mimic human bone chemical composition that enhance cell growth without sacrificing mechanical stability by compounding with a polymer to decrease the inherent brittleness of ceramics. Similar studies like the one produced by Schantz et al [46] where an assessment of polymer-ceramic scaffolds, composed of polycaprolactone and calcium phosphate made by ME3DP, also indicated enhancement in biocompatibility for cell growth from compounding this polymer-ceramic material system. Also Korpela et al [47] proved the success of polymer composite in ME3DP for biomedical applications in the development of scaffolds using a polymer composite based on poly(e-caprolactone) and bioactive glass which increased mechanical stability and cell growth proliferation.

Many polymer composites in ME3DP partake on the enhancement of mechanical properties for the creation of more robust parts. Carbon fiber is one the most used filler in polymer composites for ME3DP because of its strength, light weight and good processability with polymers. Love et al [48] created a polymer composite based in ABS and short carbon fibers and was able to increase its strength 200% and modulus by 400%. Shofner et al [49] used ABS with vapor grown carbon fibers and experienced a 60% increase in tensile strength. Sarvestani et al [50] used continuous carbon fiber reinforcement in nylon and was able to get 580 MPa of tensile strength and 52.4 GPa modulus. Ning et al [51] compared the effects of carbon fiber content and length in ABS, in this study it was found that 150 μm carbon fibers had a larger effect on tensile strength and Young's modulus than shorter 100 μm carbon fibers. Besides carbon fiber, other composites have been created using metals, ceramics and various fibers to enhance the mechanical properties of ME3DP materials [52 – 59].

Polymer compositing has proven to be a viable option to enhance physical properties that are not inherent in polymers. This technique has introduced ME3DP into a number of new applications and it will continue to expand with the creation of new novel materials compatible with the technology.

1.5 References

[1] B.H. Stuart, Polymer Analysis, John Wiley & Sons, 2008.

[2] T. T. Wohlers and T. Caffrey, Wohlers Report 2016: 3D Printing and Additive Manufacturing State of the Industry Annual Worldwide Progress Report. Fort Collins, CO: Wohlers Associates, 2016.

[3] T. T. Wohlers, Wohlers Report 2013: 3D Printing and Additive Manufacturing State of the Industry Annual Worldwide Progress Report. Fort Collins, CO: Wohlers Associates, 2013.

[4] Go, Jamison, and A. John Hart. "A Framework for Teaching the Fundamentals of Additive Manufacturing and Enabling Rapid Innovation." *arXiv:1510.09070 [physics]*. 2015

[5] Standard Terminology for Additive Manufacturing Technologies. ASTM International, 2013.

[6] Ford, Sharon. "Additive Manufacturing Technology: Potential Implications for U.S. Manufacturing Competitiveness." Journal of International Commerce and Economics. Published electronically September 2014.

[7] First 3D-printed aircraft component takes to skies at FRCSE | NAVAIR - U.S. Navy Naval Air Systems Command - Navy and Marine Corps Aviation Research, Development, Acquisition, Test and Evaluation, (n.d.). http://www.navair.navy.mil/index.cfm?fuseaction=home.NAVAIRNewsStory&id=6494 (accessed February 2, 2017).

[8] P Kumar, IPS Ahuja, R Singh. "Application of fusion deposition modelling for rapid investment casting – a review", International Journal of Materials Engineering Innovation. 3 (2012) 204–227.

[9] D. Roberson, C.M. Shemelya, E. MacDonald, R. Wicker, Expanding the applicability of FDM-type technologies through materials development, Rapid Prototyping Journal. 21 (2015) 137–143. doi:10.1108/RPJ-12-2014-0165.

[10] A. Arivazhagan, A. Saleem, S.H. Masood, M. Nikzad, K.A. Jagadeesh, Study of dynamic mechanical properties of Fused Deposition Modeling processed Ultem material, American Journal of Engineering and Applied Sciences. 7 (2014) 307–315.

[11] L.M. Galantucci, F. Lavecchia, G. Percoco, Experimental study aiming to enhance the surface finish of fused deposition modeled parts, CIRP Annals - Manufacturing Technology. 58 (2009) 189–192.

[12] S.H. Masood, Intelligent rapid prototyping with fused deposition modelling, Rapid Prototyping Journal. 2 (1996) 24–33.

[13] B.C. Gross, J.L. Erkal, S.Y. Lockwood, C. Chen, D.M. Spence, Evaluation of 3D Printing and Its Potential Impact on Biotechnology and the Chemical Sciences, Anal. Chem. 86 (2014) 3240–3253.

[14] O.A. Mohamed, S.H. Masood, J.L. Bhowmik, Optimization of fused deposition modeling process parameters: a review of current research and future prospects, Advances in Manufacturing; Shanghai. 3 (2015) 42–53. doi:http://0-dx.doi.org.lib.utep.edu/10.1007/s40436-014-0097-7.

[15] A. Bagsik, V. Schöppner, and E. Klemp. "FDM part quality manufactured with Ultem* 9085." 14th international scientific conference on polymeric materials. Vol. 15. 2010.

[16] R. Anitha, S. Arunachalam, P. Radhakrishnan, Critical parameters influencing the quality of prototypes in fused deposition modelling, Journal of Materials Processing Technology. 118 (2001) 385–388. doi:10.1016/S0924-0136(01)00980-3.

[17] T. Nancharaiah, D.R. Raju , V.R. Raju, An experimental investigation on surface quality and dimensional accuracy of FDM components. Int J Emerg Technol (2010) 1(2):106–111

[18] D. Ahn, J.-H. Kweon, S. Kwon, J. Song, S. Lee, Representation of surface roughness in fused deposition modeling, Journal of Materials Processing Technology. 209 (2009) 5593–5600. doi:10.1016/j.jmatprotec.2009.05.016.

[19] K. Thrimurthulu, P.M. Pandey, N. Venkata Reddy, Optimum part deposition orientation in fused deposition modeling, International Journal of Machine Tools and Manufacture. 44 (2004) 585–594. doi:10.1016/j.ijmachtools.2003.12.004.

[20] P.M. Pandey, N. Venkata Reddy, S.G. Dhande, Improvement of surface finish by staircase machining in fused deposition modeling, Journal of Materials Processing Technology. 132 (2003) 323–331. doi:10.1016/S0924-0136(02)00953-6.

[21] P.M. Pandey, N.V. Reddy, S.G. Dhande, Virtual hybrid-FDM system to enhance surface finish, Virtual and Physical Prototyping. 1 (2006) 101–116. doi:10.1080/17452750600763905.

[22] L.M. Galantucci, F. Lavecchia, G. Percoco, Experimental study aiming to enhance the surface finish of fused deposition modeled parts, CIRP Annals. 58 (2009) 189–192. doi:10.1016/j.cirp.2009.03.071.

[23] A. Garg, A. Bhattacharya, A. Batish, On Surface Finish and Dimensional Accuracy of FDM Parts after Cold Vapor Treatment, Materials and Manufacturing Processes. 31 (2016) 522–529. doi:10.1080/10426914.2015.1070425.

[24] A. Noriega, D. Blanco, B.J. Alvarez, A. Garcia, Dimensional accuracy improvement of FDM square cross-section parts using artificial neural networks and an optimization algorithm, Int J Adv Manuf Technol. 69 (2013) 2301–2313. doi:10.1007/s00170-013-5196-2.

[25] O.A. Mohamed, S.H. Masood, J.L. Bhowmik, Optimization of fused deposition modeling process parameters for dimensional accuracy using I-optimality criterion, Measurement. 81 (2016) 174–196. doi:10.1016/j.measurement.2015.12.011.

[26] A.K. Sood, R.K. Ohdar, S.S. Mahapatra, Improving dimensional accuracy of Fused Deposition Modelling processed part using grey Taguchi method, Materials & Design. 30 (2009) 4243–4252. doi:10.1016/j.matdes.2009.04.030.

[27] J.W. Zhang, A.H. Peng, Process-Parameter Optimization for Fused Deposition Modeling Based on Taguchi Method, Advanced Materials Research. 538–541 (2012) 444–447. doi:10.4028/www.scientific.net/AMR.538-541.444.

[28] R.K. Sahu, S.S. Mahapatra, A.K. Sood, A Study on Dimensional Accuracy of Fused Deposition Modeling (FDM) Processed Parts using Fuzzy Logic, Journal for Manufacturing Science & Production. 13 (2013) 183–197. doi:10.1515/jmsp-2013-0010.

[29] G.P. Kumar, S.P. Regalla, Optimization of Support Material and Build Time in Fused Deposition Modeling (FDM), Applied Mechanics and Materials. 110–116 (2012) 2245–2251. doi:10.4028/www.scientific.net/AMM.110-116.2245.

[30] T. Nancharaiah, Optimization of Process Parameters in FDM Process Using Design of Experiments, International Journal on Emerging Technologies. 2(1): (2011) 100-102.

[31] B. Caulfield, S. Lohfeld, P.E. McHugh, Dependence of mechanical properties of polyamide components on build parameters in the SLS process, (2007). doi:10.1016/j.matprotec.2006.09.007.

[32] O.S. Es-Said, J. Foyos, R. Noorani, M. Mendelson, R. Marloth, B.A. Pregger, Effect of Layer Orientation on Mechanical Properties of Rapid Prototyped Samples, Materials and Manufacturing Processes. 15 (2000) 107–122. doi:10.1080/10426910008912976.

[33] S.-H. Ahn, M. Montero, D. Odell, S. Roundy, P.K. Wright, Anisotropic material properties of fused deposition modeling ABS, Rapid Prototyping Journal. 8 (2002) 248–257. doi:10.1108/13552540210441166.

[34] A. Bellini, S. Güçeri, Mechanical characterization of parts fabricated using fused deposition modeling, Rapid Prototyping Journal. 9 (2003) 252–264. doi:10.1108/13552540310489631.

[35] F.L. Matthews, Composite Materials : Engineering and Science, Springer Netherlands, 1993. //www.springer.com/us/book/9780412559709 (accessed March 9, 2018).

[36] C. Ziemian, M. Sharma, S. Ziemian, Anisotropic Mechanical Properties of ABS Parts Fabricated by Fused Deposition Modelling, Mechanical Engineering. (2012). https://digitalcommons.bucknell.edu/fac_books/72.

[37] S. Shaffer, K. Yang, J. Vargas, M.A. Di Prima, W. Voit, On reducing anisotropy in 3D printed polymers via ionizing radiation, Polymer. 55 (2014) 5969–5979. doi:10.1016/j.polymer.2014.07.054.

[38] A.R. Torrado, C.M. Shemelya, J.D. English, Y. Lin, R.B. Wicker, D.A. Roberson, Characterizing the effect of additives to ABS on the mechanical property anisotropy of specimens fabricated by material extrusion 3D printing, Additive Manufacturing. 6 (2015) 16–29.

[39] D.R. Paul, Polymer Blends, Elsevier, 2012.

[40] C. Koning, M. Van Duin, C. Pagnoulle, R. Jerome, Strategies for compatibilization of polymer blends, Progress in Polymer Science. 23 (1998) 707–757.

[41] PC-ABS Material for Fortus 3D Printers, (n.d.). http://www.stratasys.com/materials/fdm/pc-abs (accessed March 1, 2017).

[42] S. Thomas, K. Joseph, S.K. Malhotra, K. Goda, M.S. Sreekala, Polymer Composites: Macro- and Microcomposites, John Wiley & Sons, Incorporated, Hoboken, GERMANY, 2012. http://ebookcentral.proquest.com/lib/utep/detail.action?docID=867652 (accessed March 16, 2018).

[43] J. O'Brien, M.F. Córdoba-Erazo, E. Rojas, J. Castro, M. Abdin, G. Mumcu, J. Wang, K. Church, P. Deffenbaugh, T. Weller, Miniaturization of microwave components and antennas using 3D manufacturing, in: 2015 9th European Conference on Antennas and Propagation (EuCAP), 2015: pp. 1–4.

[44] J. Castro, E. Rojas, A. Ross, T. Weller, J. Wang, High-k and low-loss thermoplastic composites for Fused Deposition Modeling and their application to 3D-printed Ku-band antennas, in: 2016 IEEE MTT-S International Microwave Symposium (IMS), 2016: pp. 1–4. doi:10.1109/MWSYM.2016.7540068.

[45] S.J. Kalita, S. Bose, H.L. Hosick, A. Bandyopadhyay, Development of controlled porosity polymer-ceramic composite scaffolds via fused deposition modeling, Materials Science and Engineering: C. 23 (2003) 611–620. doi:10.1016/S0928-4931(03)00052-3.

[46] J.-T. Schantz, A. Brandwood, D.W. Hutmacher, H.L. Khor, K. Bittner, Osteogenic differentiation of mesenchymal progenitor cells in computer designed fibrin-polymer-ceramic scaffolds manufactured by fused deposition modeling, J Mater Sci: Mater Med. 16 (2005) 807–819. doi:10.1007/s10856-005-3584-3.

[47] S.J. Kalita, S. Bose, H.L. Hosick, A. Bandyopadhyay, Development of controlled porosity polymer-ceramic composite scaffolds via fused deposition modeling, Materials Science and Engineering: C. 23 (2003) 611–620. doi:10.1016/S0928-4931(03)00052-3.

[48] L.J. Love, V. Kunc, O. Rios, C.E. Duty, A.M. Elliott, B.K. Post, R.J. Smith, C.A. Blue, The importance of carbon fiber to polymer additive manufacturing, Journal of Materials Research. 29 (2014) 1893–1898. doi:10.1557/jmr.2014.212.

[49] M.L. Shofner, K. Lozano, F.J. Rodríguez-Macías, E.V. Barrera, Nanofiber-reinforced polymers prepared by fused deposition modeling, J. Appl. Polym. Sci. 89 (2003) 3081–3090. doi:10.1002/app.12496.

[50] A. N. Sarvestani, N. van de Werken, P. Khanbolouki, M. Tehrani, 3D Printed Composites With Continuous Carbon Fiber Reinforcements, (2017) V002T02A031. doi:10.1115/IMECE2017-72041.

[51] F. Ning, W. Cong, Z. Hu, K. Huang, Additive manufacturing of thermoplastic matrix composites using fused deposition modeling: A comparison of two reinforcements, Journal of Composite Materials. (2017) 0021998317692659. doi:10.1177/0021998317692659.

[52] K. Boparai, R. Singh, H. Singh, Comparison of tribological behaviour for Nylon6-Al-Al2O3 and ABS parts fabricated by fused deposition modelling, Virtual and Physical Prototyping. 10 (2015) 59–66. doi:10.1080/17452759.2015.1037402.

[53] D. Drummer, S. Cifuentes-Cuéllar, D. Rietzel, Suitability of PLA/TCP for fused deposition modeling, Rapid Prototyping Journal. 18 (2012) 500–507. doi:10.1108/13552541211272045.

[54] V. Francis, P.K. Jain, Experimental investigations on fused deposition modelling of polymer-layered silicate nanocomposite, Virtual and Physical Prototyping. 11 (2016) 109–121. doi:10.1080/17452759.2016.1172431.

[55] M. Nikzad, S.H. Masood, I. Sbarski, Thermo-mechanical properties of a highly filled polymeric composites for Fused Deposition Modeling, Materials & Design. 32 (2011) 3448–3456. doi:10.1016/j.matdes.2011.01.056.

[56] A.R.T. Perez, D.A. Roberson, R.B. Wicker, Fracture Surface Analysis of 3D-Printed Tensile Specimens of Novel ABS-Based Materials, J Fail. Anal. and Preven. 14 (2014) 343–353. doi:10.1007/s11668-014-9803-9.

[57] M.A. Ryder, D.A. Lados, G.S. Iannacchione, A.M. Peterson, Fabrication and properties of novel polymer-metal composites using fused deposition modeling, Composites Science and Technology. (n.d.). doi:10.1016/j.compscitech.2018.01.049.

[58] C.M. Shemelya, A. Rivera, A.T. Perez, C. Rocha, M. Liang, X. Yu, C. Kief, D. Alexander, J. Stegeman, H. Xin, R.B. Wicker, E. MacDonald, D.A. Roberson, Mechanical, Electromagnetic, and X-ray Shielding Characterization of a 3D Printable Tungsten–Polycarbonate Polymer Matrix Composite for Space-Based Applications, Journal of Elec Materi. 44 (2015) 2598–2607. doi:10.1007/s11664-015-3687-7.

[59] S.H. Masood, W.Q. Song, Development of new metal/polymer materials for rapid tooling using Fused deposition modelling, Materials & Design. 25 (2004) 587–594. doi:10.1016/j.matdes.2004.02.009.

CHAPTER 2: RESEARCH OBJECTIVES AND PRESENTED PUBLISHED PAPERS

2.1 Research Objectives

In the previous chapter an introduction to ME3DP and the current challenges for mass adoption were introduced to give an overview of current needs and areas of improvement. The main objective of this work was to increase ME3DP adoption by the development of novel materials compatible with the technology. Increasing the range of ME3DP compatible materials will streamline major scale adoption of this technology. In an effort to expand ME3DP applicability through a material perspective, a novel polymer blend and a polymer composite along a complete characterization and processing parameters will be presented. The main research objectives of this dissertation are as followed:

1. The creation of new polymer blends and composites to expand the use of ME3DP technologies.
2. Present the required processing parameters for the creation of tailored novel materials for the use in ME3DP technologies.
3. Phase characterization of the new polymer blends:
    - Scanning transmission electron microscope (STEM).
    - Fourier transform infrared spectroscopy (FTIR).
    - Dynamic mechanical analysis (DMA).
4. Explore mechanical properties and reinforcement of the new polymer blends and composites.
    - Mechanical testing following standard ASTM D638-14.
    - Fractographic analysis using scanning electron microscope (SEM).

5. Characterization of rheological properties of the new blends and composites through melt flow rate (MFR) following ASTM standard 1238-13.

Overall the objective of this work is to present viable methods to create novel ME3DP materials with tailored physical qualities. Along an extensive characterization work that can be used for parameter optimization in ME3DP and provide better understanding of polymer blends/composites. The derivation of objectives one and two are to present processing information that can serve as base for the creation of new tailored ME3DP materials. Objective number three and five refer to the characterization of polymer blends in order to understand present phases, degree of miscibility, and effect on rheological properties. Objective number four pertains to the novel reinforcement method that will be introduced on Chapter 4.

2.2 Published Works

The next chapters of this dissertation, Chapter 4 and 5, are composed of published works by the author. The citations of the published works along their abstract are presented below.

Chapter 3

The material presented in Chapter 3 introduces the development of an elastomeric blend based on ABS. This article was published in the Journal of Virtual and Physical Prototyping cited as follows:

J.G. Siqueiros, K. Schnittker, D.A. Roberson, ABS-maleated SEBS blend as a 3D printable material, Virtual and Physical Prototyping. 11 (2016) 123–131. doi:10.1080/17452759.2016.1175045.

Permission to use the cited article above in this dissertation has been granted by the publisher in Appendix A.

Abstract

A key enabler for the advancement of material extrusion 3D printing is the implementation of new printable materials with a wide variety of physical properties. The focus of this study is the development of 3D printable polymer blends based on compounding acrylonitrile butadiene styrene (ABS) with styrene ethylene butylene styrene. Here the mechanical properties of the resulting novel material systems were manipulated through the change of mixture composition. The novel blends were evaluated based on mechanical testing and fracture surface analysis. Additionally, the rheological characteristics were determined based on melt flow index values. Key results were the significant increase in elongation at break values from 8.53% (ABS baseline) to 1506.57% (rubberised ABS) and the drastic difference in fracture surface morphology when comparing the various blends to ABS.

Chapter 4

The material presented in Chapter 4 introduces the development of a polymer composite based on two polymer matrices with a phosphate glass filler. The article was published in the International Journal of Polymer Science cited as follows:

J.G. Siqueiros, D.A. Roberson, In Situ Wire Drawing of Phosphate Glass in Polymer Matrices for Material Extrusion 3D Printing, International Journal of Polymer Science. (2017). doi:10.1155/2017/1954903.

Abstract

A strategy to increase the amount of materials available for additive manufacturing platforms such as material extrusion 3D printing (ME3DP) is the creation of printable thermoplastic composites. Potential limiters to the incorporation of filler materials into a thermoplastic resin include agglomeration of the filler materials, which can compromise the mechanical properties of the material system and a static morphology of the filler material. A potential solution to these issues is the use of filler materials with low glass transition temperatures

allowing for a change in morphology during the extrusion process. Here, we successfully demonstrate the drawing of phosphate glass particles into a wire-like morphology within two polymeric systems: (1) a rubberized acrylonitrile butadiene styrene (ABS) blend and (2) polylactic acid (PLA). After applying a normalization process to account for the effect of air gap within the 3D printed test specimens, an enhancement in the mechanical properties was demonstrated where an increase in

strength was as high as 21% over baseline specimens. Scanning electron microanalysis was used to characterize the fracture surface and wire drawing efficacy. Factors affecting the ability to achieve wire drawing such as polymer viscosity and print temperature are also highlighted.

Permission to use the cited article above in this dissertation has been granted by the publisher in Appendix B.

CHAPTER 3: ABS-MALEATED SEBS BLEND AS A 3D PRINTABLE MATERIAL

3.1 Introduction

Material extrusion 3D printing (ME3DP) is a technology where a 3D object is created through the deposition of a material (typically a thermoplastic) in a layer-by-layer manner by means of extrusion through a heated nozzle. Originally marketed under the moniker fused deposition modelling (FDM), this 3D printing method has become ubiquitous in educational, industrial, and home-use settings. As a whole, 3D printing has been evolving at an increased pace because of the numerous benefits this technology has over conventional manufacturing methods, such as machining. The rapid growth of 3D printing platforms based on FDM is due to expiration of the original patents on this technology [1] in 2009 [2]. The well-known advantages of 3D printing technology include the ability to print complex shapes and a rapid design to product cycle [3]. There are also disadvantages to the use of ME3DP in a manufacturing setting; one being the lack of variety available for materials with a diverse set of physical properties that can be employed for particular or specific applications. Therefore, a key enabler for the advancement of 3D printing as a technology is the creation of more materials with a greater diversity in physical properties compatible with current 3D printing technologies. The possibility to print a selection of materials with different physical properties in combination with the complex shapes that can only be reproduced by additive manufacturing (AM) enables ME3DP to be a very powerful technology that could bring major innovations in the manufacturing field and beyond [4].

As previously mentioned, ME3DP relies on the extrusion of a thermoplastic filament through a heated nozzle. The most common polymers currently used particularly among desktop-grade systems are acrylonitrile butadiene styrene (ABS) and polylactic acid. Recently, interest in

flexible materials for polymer based 3D printing platforms has increased due to the potential for creating multifunctional all 3D printed parts, such as mechanical actuators [5]. The 'Tango' product line offered by Stratasys for Objet printers is a key example. In the area of ME3DP, polyurethanes have become the flexible material of choice, namely the commercially available NinjaFlex®. The focus of the work presented in this paper reflects on the development of a new material system based on blends composed of ABS and the thermoplastic elastomer styrene ethylene butylene styrene grafted with maleic anhydride (SEBS-g-MA), at various concentration levels. The variation in SEBS-g-MA content levels allows for tunability of the viscoelastic properties of the resulting material, which reflects on the final elastic behavior of the filament and printed part. ABS is a thermoplastic composed of three monomers; acrylonitrile, butadiene, and styrene and the combination of these three monomers at different levels enables a wide variety of properties [6].

For this study, two different grades of commercially available ABS were utilized: (1) MG47 and (2) MG94. Both resin types were produced by SABIC (Pittsfield, MA) under the Cyclolac™ product line. The MG47 grade is considered a multipurpose injection-molding grade of ABS [7]. The MG94 grade possesses a higher melt flow index (MFI), which is indicative of a lower molecular weight. It has been observed that molecular weight has an effect on the compounding behavior in polymers [8] where lower molecular weight equates to a higher level of blending.

From previous studies performed by Torrado, it was found that lower molecular weight ABS grades exhibited an enhanced mixing behavior when compounded with SEBS-g-MA [9]. During this study, an evaluation of both MG94 and MG47 was performed where both grades were compounded with SEBS-g-MA grade FG1901-GT (Kraton, Houston, TX, USA) where the

composition of this material is styrene, ethylene, and butylene combined with 1.4–2.0% by weight maleic anhydride [10]. Blends of various ratios (by weight) of ABS and SEBS-g-MA were created by a twin screw compounding/extrusion process. The physical properties of these blends were evaluated based on mechanical testing, scanning electron microscopy, and MFI measurements. In cases where test coupons were necessitated, specimens were fabricated through the use of a desktop-grade 3D printer.

3.2 Experimental Procedure

The various blend combinations of ABS with SEBS-g-MA used in this study are tabulated in Table 3.1, where it is noted that blends of (based on wt. % SEBS-g-MA) 25%, 50%, and 75% by weight SEBS were compounded. In the case of MG94, an additional blend of 90% SEBS-g-MA was compounded and evaluated. A blend composed of ABS grade MG47 compounded with 90% by weight SEBS-g-MA was also extruded, however we were unable to print objects on our printer, therefore we have excluded this particular mixture from our study. The polymer blends were created through the use of a Dr Collin twin screw extruder/compounder (Model ZK 25 T, Dr Collin GmbH, Ebersberg, Germany) which was configured to produce a monofilament with a diameter of 1.75 mm in order to be compatible with most desktop- and industrial-grade material extrusion 3D printers.

Table 3. 1 ABS:SEBS-g-MA Blends

MG47 100% (Baseline)	**ABS MG94 100% (Baseline)**
ABSMG47: SEBS-g-MA 75:25	ABSMG94: SEBS-g-MA 75:25
ABSMG47: SEBS-g-MA 50:50	ABSMG94: SEBS-g-MA 50:50
ABSMG47: SEBS-g-MA 25:75	ABSMG94: SEBS-g-MA 25:75
	ABSMG94: SEBS-g-MA 10:90

Prior to the extrusion process, the resins (which were in pellet form) were dried using a compressed air dryer (Dri-Air CFAM Micro-Dryer, East Windsor, Connecticut, USA). The drying cycle for the ABS MG47 was carried out at a temperature of 90°C for a time period of 2 hours, ABS MG94 was dried at 80°C for a period of 2 hours, and the SEBS-g-MA Kraton FG1901-GT was dried at 60°C for 1 hour. The drying parameters were inferred from the manufacturer-supplied material data sheets. The extruding parameters were slightly modified for each blend in order to obtain homogeneous compounding results and to optimize the overall quality of the filament as seen in Table 3.2. It was found necessary to increase the processing temperature with an increase in the content of SEBS-g-MA, as the slightly higher temperatures improved the mixing of SEBS-g-MA with ABS whether the grade was MG47 or MG94.

Table 3. 2 ABS: SEBS-g-MA Blends Extruding Parameters

Material	T zone 1 (°C)	T zone 2 (°C)	T zone 3 (°C)	T zone 4 (°C)	T zone 5 (°C)	T zone 6 (°C)	RPM Main	Pressure Main Screws	Melt Pump Pressure
ABSMG47: SEBS-g-MA									
100:0	200	210	220	220	210	190	48	90	75
75:25	210	230	240	240	210	195	45	90	55
50:50	210	235	245	245	215	200	43	90	52
25:75	210	240	250	250	220	200	35	90	48
ABSMG94: SEBS-g-MA									
100:0	200	210	210	210	200	190	28	90	54
75:25	200	210	210	210	200	190	28	90	48
50:50	200	210	215	215	210	195	33	90	34
25:75	200	210	215	215	210	195	36	90	39
10:90	200	210	215	215	210	195	39	90	40

Tensile testing was carried out following the ASTM standard D638-10 [11]. Specimens were 3D printed following specifications for Type V as seen in Figure 3.1. In order to demonstrate ME3DP compatibility, the specimens were printed with a Lulzbot Taz 4 (Aelph Objects Inc, Loveland, Colorado, USA) outfitted with a 0.6 mm nozzle diameter. Our unit was modified over the stock version by the running of a custom Marlin open source firmware and the addition of an

E3D V6 hot end (E3D-Online Limited, Chalgrove, Oxfordshire, UK). The specimens were printed with 100% infill and a raster height of 0.27 mm in the XYZ print orientation. For an explanation of standard AM print terminologies, we invite the reader to examine the ASTM F2921 standard [12] and a previous study on the evaluation of novel 3D printed materials by Torrado et al. [13]. As was the case in the extrusion process of the various blends, it was necessary to modify the printing parameters for each blend as shown in Table 3.3 where again, the temperature was raised coincident with the content of SEBS-g-MA. However, rather than to facilitate blending, during the printing process the higher temperature was needed in order to reduce back flow forces that caused the flexible filament to clog in the 3D printer drive gear system. We found the incremental increase in temperature led to a higher flow rate which diminished the back flow forces mitigating the clogging issue. The MG47-based blends were more prone to system clogging during the printing process, which is an expected occurrence due to the higher molecular weight of this grade compared to MG94, where longer polymer chains yield a greater flow resistance or viscosity [14].

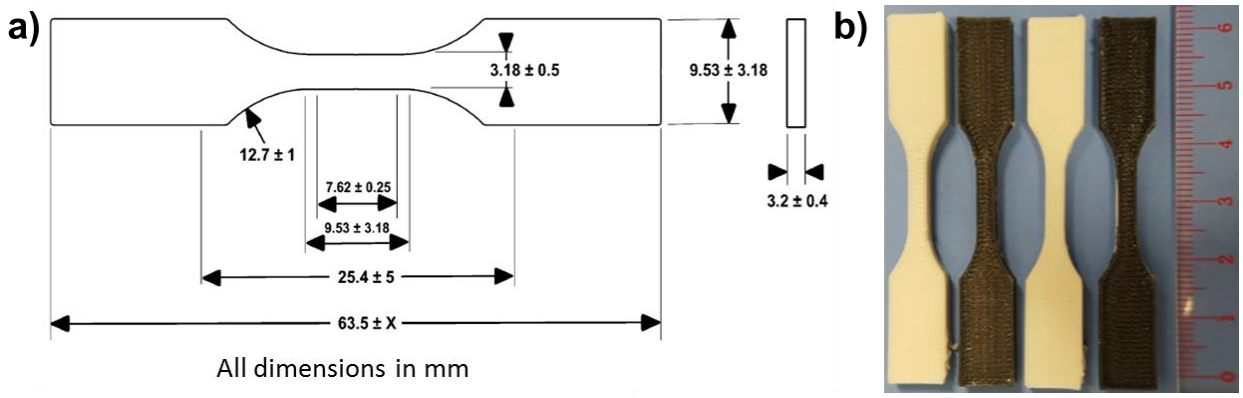

Figure 3. 1 a) Schematic of ASTM 638 Type V Test Specimen [13] and b) examples of 3D Printed specimens where white specimens are based on ABS MG47 and black specimens are based on ABS MG94.

Table 3. 3 ABS: SEBS-g-MA Blends Printing Parameters

Material	Nozzle Temperature (°C)	Bed Temperature (°C)	% Infill	Travel Feedrate (mm/s)

ABSMG47:SEBS-g-MA				
100:0	230	110	100	60
75:25	250	110	100	60
50:50	265	110	100	30
25:75	280	110	100	30
ABSMG94: SEBS-g-MA				
100:0	230	110	100	60
75:25	235	110	100	60
50:50	245	110	100	30
25:75	255	110	100	30
10:90	265	110	100	30

Tensile testing was performed using an Instron 5866 (Instron, Norwood, Massachusetts, USA) tensile testing machine equipped with a 10 kN load cell. The test speed was 10 mm/min at a temperature of 24°C as specified in the ASTM D638-10 [11] standard for rigid and semi-rigid specimens of the Type V geometry. Sample pools of 10 specimens were tested and the resulting stress, strain, and Young's modulus were recorded. Fracture surface analysis (fractography) was conducted using a Hitachi TM-1000 scanning electron microscope (SEM; Hitachi High-Technologies Europe GmbH, Germany) operating at 15 kV accelerating potential and equipped with a backscatter electron detector. As we were examining non-conductive polymeric surfaces, the specimens were first sputter coated with a gold palladium (Au/Pd) target in a Gatan sputter coater Model 682 Precision Etching Coating System (Gatan, Inc., Pleasanton, CA, USA) to reduce electron charging. Two to three representative specimens from each sample pool were selected for SEM microanalysis. The selection of more than one representative from each sample pool for the fracture surface analysis gave the opportunity to learn about the failure modes within each elastomeric blend and to establish a correlation between fracture morphology and blend ratios. Rheological testing was performed using a Tinius Olsen MP1200 melt flow indexer (Tinius Olsen, Horsham, Pennsylvania, USA) following the ASTM D1238-13 standard (procedure A) [15]. In

order to perform this test, 7 g of material from each elastomeric blend experiment was pelletized and introduced to the melt flow indexer. In order to provide an accurate relative comparison, all tests were conducted using the same machine-operating parameters; a temperature of 230°C and a 3.8 kg test load.

3.3 Results

3.3.1 Tensile Testing

Tensile test results are tabulated in Table 3.4 and graphically represented in Figures 3.2 and 3.3 for the blends examined in this study. It can be seen that, in terms of mechanical properties, both grades of ABS responded similarly to one another in response to an increase in the amount of SEBS-g-MA. Ultimate tensile stress (UTS) and per cent elongation (%El or strain) for different blend ratios indicate that the polymeric blends have physical properties which follow a rule of mixtures type of behavior for the constituents; in this case ABS and SEBS-g-MA, which is indicative of a miscible blend [16]. The UTS of the blends decreased as the SEBS-g-MA content increased, which was expected as the addition of the elastomer tends to reduce the UTS of the stronger polymer (in this case ABS) and acts as a rubber toughening agent increasing resistance to tensile strain. There are examples in the literature pertaining to this so-called ‘rubber toughening effect’ of SEBS-g-MA, such as the studies by Oshinki et al. [17], where a creation of a super-tough polyamide was achieved by the blending of SEBS-g-MA with nylon-6,6, the work published by Tjong et al. [18] pertaining to polypropylene toughened by the addition of SEBS-g-MA, and a study related to the rubber toughening effect of SEBS-g-MA for PA6/PP/organoclay nanocomposites performed by Kusmono et al. [19].

Similar to the observations made related to the Young’s modulus decreased as the content of SEBS-g-MA was increased. The relationship between the reduction in Young’s modulus and

the content of SEBS-g-MA provides some degree of tunability in the stiffness of the material allowing for the possibility to fabricate custom devices where shock absorption is required. Figure 3.2 is an example of a bumper (shock absorber) that was replaced in a Brabender Granu-Grinder (C.W. Brabender, South Hackensack, New Jersey) by ME3DP using the ABS MG94 SEBS-g-MA 50% blend.

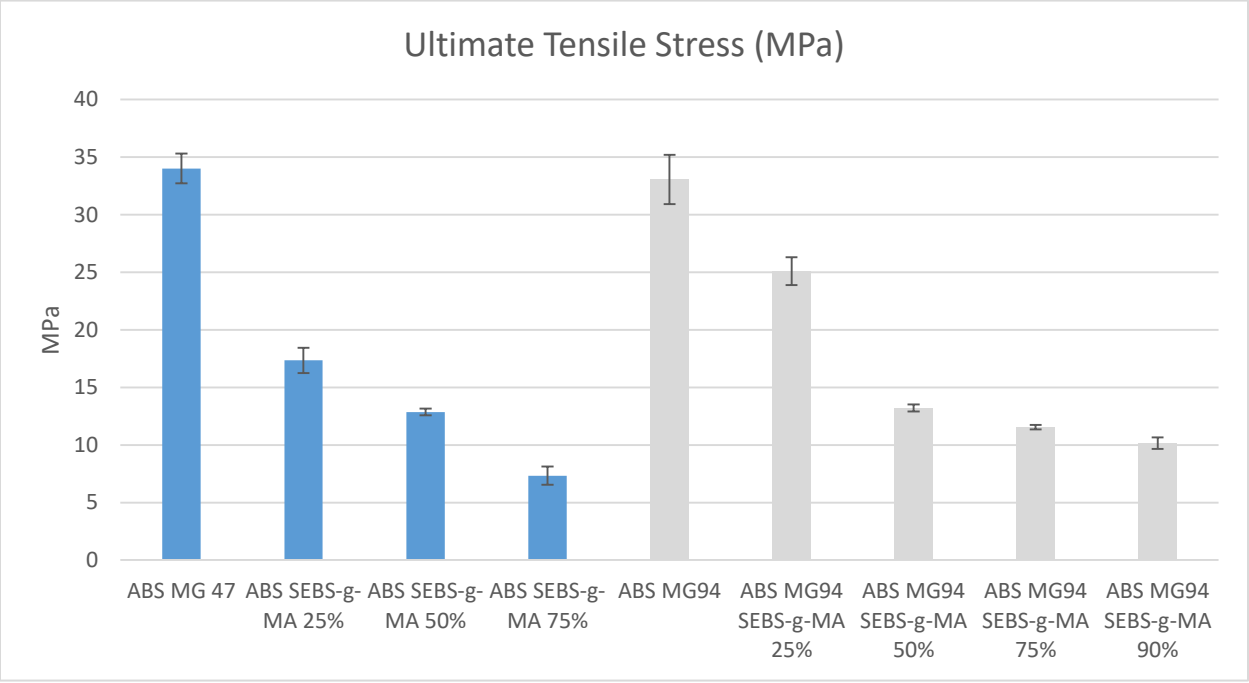

Figure 3. 2 UTS values for the blends evaluated in this study

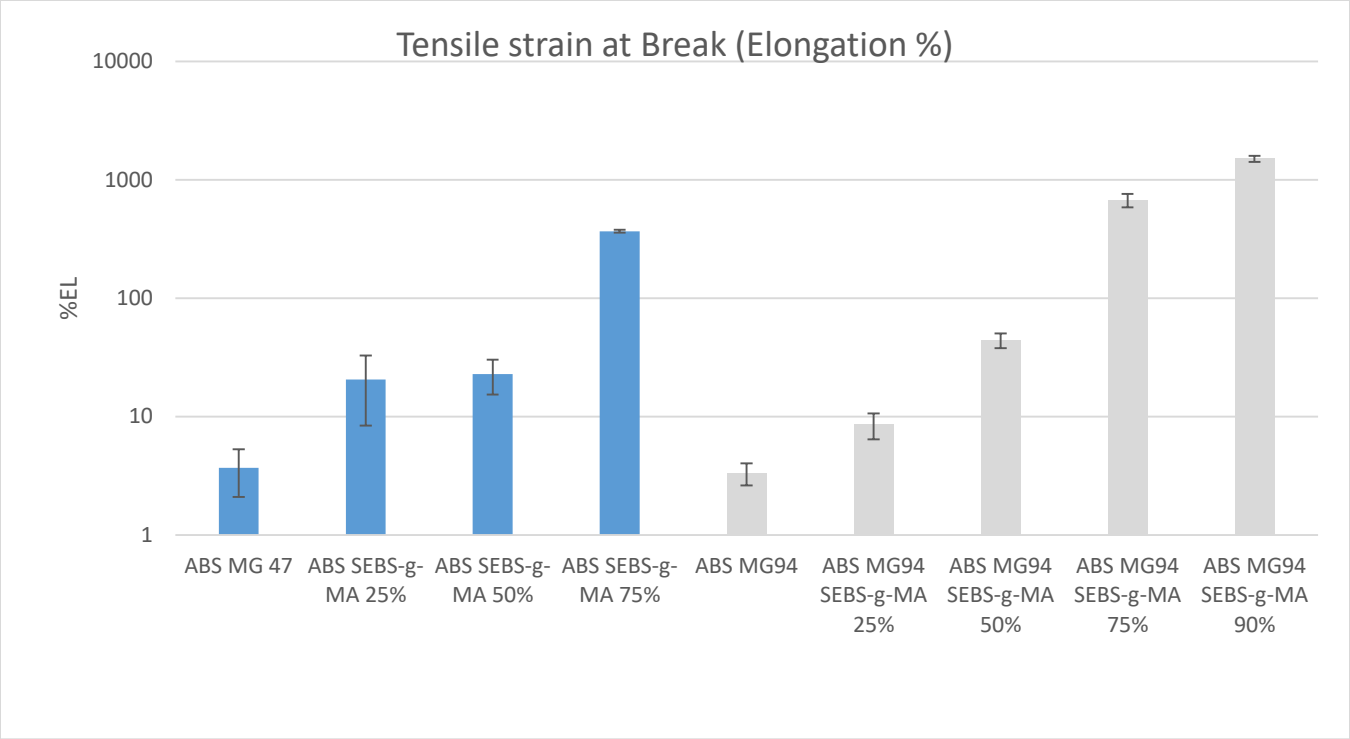

Figure 3. 3 % Elongation values for the materials tested

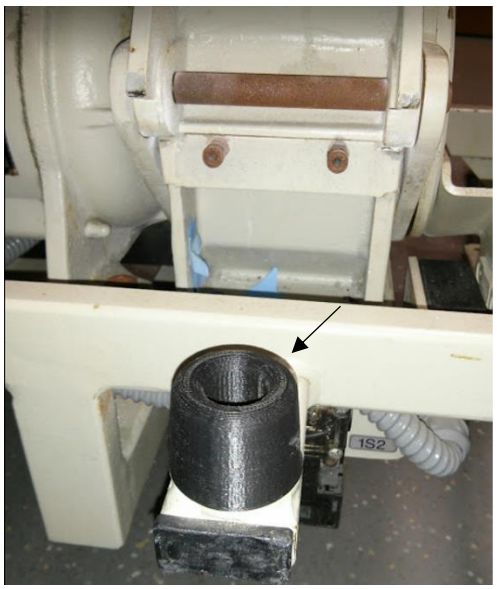

Figure 3. 4 ABS MG94 SEBS-g-MA Shock Absorber (Bumper)

A notable observation made during this study was the ability to tune the strain withstood by the material at failure (in terms of %El) from 3.32% for the baseline ABS MG94 material to

1506.57% for the ABS MG94 SEBS-g-MA 90% blend. Similar effects in elongation percentages were shown by the ABS MG47 blends but at lower relative degrees of difference. The significant change in mechanical properties of these blends without compromising the compatibility with ME3DP platforms endorses the use of this material for 3D printing applications where a discrete degree of elasticity would be required such as the aforementioned shock absorber or a mechanical actuator.

Table 3. 4 ABS: SEBS-g-MA Blends Tensile Test

Material	Ultimate Tensile Stress (MPa)	Tensile strain at Break (Standard) (Elongation %)	Modulus (Automatic Young's) (MPa)
ABS MG 47	34.01 ± 1.3	3.694 ± 1.6	2161.48 ± 274.7
ABS SEBS-g-MA 25%	17.34 ± 1.1	13.79 ± 4.1	1,391.00 ± 140.3
ABS SEBS-g-MA 50%	12.86 ± 0.3	22.83 ± 7.5	675.65 ± 151.0
ABS SEBS-g-MA 75%	7.33 ± 0.8	368.20 ± 10.3	70.77 ± 21.3
ABS MG94	33.04 ± 2.14	3.32 ± 0.7	2280.29 ± 341.6
ABS MG94 SEBS-g-MA 25%	25.09 ± 1.2	8.53 ± 2.1	1484.16 ± 141.7
ABS MG94 SEBS-g-MA 50%	13.21 ± 0.3	44.18 ± 6.4	690.25 ± 88.4
ABS MG94 SEBS-g-MA 75%	11.55 ± 0.2	672.96 ± 88.2	43.08 ± 4.46
ABS MG94 SEBS-g-MA 90%	10.16 ± 0.5	1506.57 ± 90.1	14.98 ± 3.69

The analysis of stress–strain curves (Figure 3.5) further exemplifies the effect of the addition of SEBS-g-MA on the amount of plastic deformation endured by the tensile test specimens, most defined by the amount of elongation exhibited by the specimens. A key feature of the stress–strain curves is the behavior observed the case of the 75% by weight SEBS-g-MA blend for both ABS grades and the 90% blend containing ABS MG94. In both cases there is an increase in stress after the onset of plastic deformation. The increase in stress is due to the polymer chains detangling and elongating during the tensile test process. The behavior is most prominent

in the case of the blend of SEBS-g-MA and MG94 and is tantamount to the aforementioned strain hardening effect, which played a role in the planar fracture surfaces.

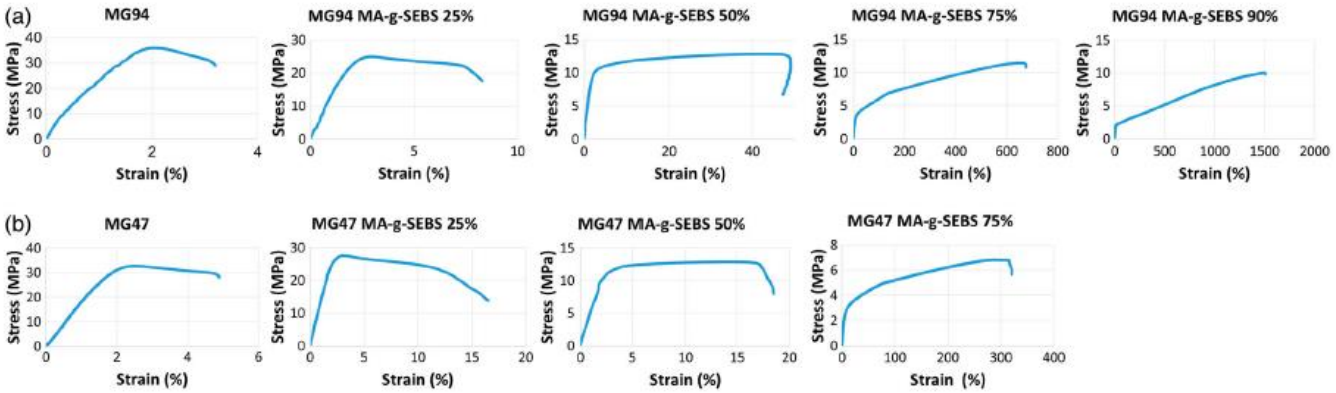

Figure 3. 5 Stress-strain curves for the material system based on (a) ABS grade MG47 and (b) ABS grade MG94. Note the difference in % EL compared to wt. % SEBS-g-MA between the two ABS grades

3.3.2 MFI measurements

Results of MFI measurements are shown in Table 3.5. A notable result is the effect of SEBS-g-MA content on the overall MFI value. Looking first at the blends based on ABS MG47, the lowest concentration blend (a 25% by weight concentration of SEBS-g-MA) the MFI value of 9.06 g/10 min is in between the MFI values for the two constituents where ABS MG47 exhibited an MFI value of 7.42 g/10 min and the SEBS-g-MA grade FG1901-GT exhibited an MFI value of 15.72 g/10 min. The in-between value of this blend was expected and indicative of polymer blending and is analogous to the well-known Fox's law for the calculation of the glass transition temperature (Tg) of a blend given by the equation 3.1 [20]:

$$\frac{1}{T_{g\,Blend}} = \frac{x_1}{T_{g1}} + \frac{x_2}{T_{g2}},$$

where x_1 and x_2 are the weight fraction of the individual polymers. What we observed for the blend of MG94 compounded with a 25% by weight concentration of SEBS-g-MA is a law of

averages-type of behavior. When a Fox's law-type of equation is applied to the case of MFI for the two constituents examined in this study:

$$\frac{1}{MFI_{Blend}} = \frac{x_1}{MFI_1} + \frac{x_2}{MFI_2},$$

the calculated value is 8.54 g/10min which is ~0.52g lower than the measured value. Furthermore, if one were to take a law of averages-type of approach for the prediction of the resultant melt flow index of the binary blend:

$$MFI_{Blend} = x_1 MFI_1 + x_2 MFI_2,$$

the calculated value of the MFI for the 75:25 by weight ratio blend amounts to 9.49 g/10min which is ~0.43 g/10min greater than the measured value.

The deviation from a law of averages-like or Fox's law like behavior increases drastically when the loading of SEBS-g-MA is increased to 50% and 75% in the case of blends based on ABS MG47. At these higher concentrations, the MFI increases to values greater than those of either of the constituents, where the greatest MFI value of the base materials studied here was for the SEBS-g-MA (15.72 g/10 min). At 50% SEBS-g-MA concentration, the MFI was measured to be 23.25 g/10 min where the blend with a concentration of 75% SEBS-g-MA possessed a measured MFI value of 18.55 g/10 min which is less of a deviation than a rule of mixtures-type model, but still higher than the MFI of either constituent and indicative of the rheological aspects of the material being dominated to a greater degree by the SEBS-g-MA. The deviation of MFI values from blending-based models is indicative, that for some mixture ratios, polymer alloying is occurring rather than polymer blending [8].

Further evidence of polymer alloying as opposed to blending is given through observation of the MFI behavior of the blends based on ABS MG94. As compared to the MG47 grade, the MFI of MG94 is much greater (14.83 as compared to 7.42 g/10 min for MG47) which is indicative

of a lower molecular weight. As mentioned above, the previous work by Torrado [9] has reinforced the notion that lower molecular weight polymers mix or blend in a more enhanced manner than a higher molecular weight counterpart. When comparing the behavior between the two ABS grades, the greater propensity to mix for MG94 (leading to alloying rather than blending) of this lower molecular weight version of ABS is observed by the behavior of MFI values of lower SEBS-g-MA concentration. When the mixture was 25% by weight SEBS-g-MA the MFI value was measured to be 28.84 g/10 min which is a strong deviation from a rule of mixtures- type behavior and an indication that polymer alloying occurred. Conversely, as mentioned before, the mixture of 25% by weight SEBS-g-MA with the higher molecular weight MG47 yielded an MFI value following the rule of mixtures type of behavior (9.06 g/10 min). This behavior indicates that the manifestation of alloying occurs at lower concentrations of SEBS-g-MA when the molecular weight grade of ABS is lower meaning that molecular weight not only controls blending, but the onset of alloying as well.

Further examination of the blends based on ABS MG94 reveals that at concentrations of 50% and 75% SEBS-g-MA, the MFI values are still greater than either constituent, however the deviation from mixing model calculations decreases as the concentration shifts in favor of SEBS-g-MA. In the case of a by weight concentration of 90% SEBS-g-MA it can be said that polymer blending rather than polymer alloying is occurring because the MFI value of 15.35 g/10 min is extremely close to the predicted MFI value of 15.53 g/10 min.

It should be noted that the MFI values do not completely correlate with the 3D printer parameters. In terms of feed rate, for the case of the blends based on ABS grade MG47, the increase in MFI correlated with a decrease in feed rate for the 50, and 75% SEBS-g-MA blends, which is expected as the increase in material flow has to be balanced by a decrease in the amount of material

supplied to the liquefier. The same trend was also observed in the case of blends based on MG94 for the 50 and 75% SEBS-g-MA blends. However, in the case of the 90% SEBS-g-MA blend the federate was 30 mm/s while the MFI value was 15.35 g/10 min, a value very close to the MFI value of 14.83 g/10 min observed for the ABS MG94 base resin. The ABS base resin was found to be printable with a feed rate of 60 mm/min.

The material property which has a greater effect on the 3D printer machine parameters is the stiffness of the materials. If one compares the trend of Young's modulus values (Table 3.4) observed during tensile testing to both the print temperature and the filament feed rate, this fact is readily observable. Taking the blend of ABS grade MG94 blended with 25% by weight SEBS-g-MA, the MFI value was 28.84 g/10/min, which is much higher than that of the ABS base resin, but the printable feed rate was found to be 60 mm/s. The stiffness of this blend (inferred from the average Young's modulus of 1484.16 ± 141.7) Higher temperatures were needed to combat backflow issues observed in the printing of these blends as was mentioned previously.

Table 3. 5 ABS: SEBS-g-MA Blends MFI

Material	**Measured Melt Flow Index (g/10min)**	**Fox's Law-type Calculation**	**Law of Averages-type Calculation**
ABS MG47	7.42		
SEBS-g-MA	15.72		
ABS MG47 SEBS-g-MA 25%	9.06	8.55	9.50
ABS MG47 SEBS-g-MA 50%	23.25	10.08	11.57
ABS MG47 SEBS-g-MA 75%	18.55	12.28	13.65
ABS MG94	14.83		
ABS MG94 SEBS-g-MA 25%	28.84	15.04	15.05
ABS MG94 SEBS-g-MA 50%	27.48	15.26	15.28
ABS MG94 SEBS-g-MA 75%	21.17	15.49	15.50
ABS MG94 SEBS-g-MA 90%	15.35	15.63	15.63

3.3.3 Fractography

Differences in mechanical behavior were also observed through the comparison of fracture surfaces between tensile samples printed from the rubberized blends and samples printed from the ABS base resins. The analysis of the fracture surfaces revealed a more ductile behavior, as the weight per cent of SEBS-g-MA was increased regardless of the grade of ABS used. Figure 3.6 presents fracture surfaces from the material system based on ABS MG47. Starting with the baseline ABS specimen (Figure 3.6(a)), the fracture morphology exhibits features indicative of plastic deformation where the samples printed from the blends composed of 50% and 75% by weight SEBS-g-MA exhibit a greater amount of plastic deformation as is seen in Figure 3.7.

The fracture surface of specimens printed from ABS grade MG94 (Figure 3.7) indicates that the print raster interface acted as initiation sites for craze cracks as highlighted by the white arrows. Figure 3.8(a)–(d) represents the fracture surfaces for the (by weight) 25%, 50%, 75%, and 90% by weight SEBS-g-MA blends and, again, illustrates the effect of combining the thermoplastic rubber with ABS not only in terms of fracture morphology difference but in rheological differences as well. Here, the differences between print rasters are somewhat obscured as the blends exhibited different flow characteristics during the 3D printing process as compared to ABS. In terms of fracture behavior, the amount of plastic deformation endured by the tensile specimens increased as weight per cent of SEBS-g-MA increased which agrees well with the mechanical testing values for %El at failure.

However, when examining Figure 3.7(d), there is a notably less evidence of plastic deformation which would normally be attributed to a brittle mode failure. This image corresponds to the fracture surface of the ABS MG94 SEBS-g-MA 90% blend which exhibited the most plastic deformation as indicated by an average of %EI value of 1506.57 ± 90.1%. The high amount of

elongation greatly reduced the cross-sectional area of the test specimen; additionally, there was a strain hardening effect on the polymer due to the elongation of the polymer chains resulting in a final brittle fracture mode. The result was a mechanical behavior similar to the snapping of a rubber band, as depicted in Figure 3.9.

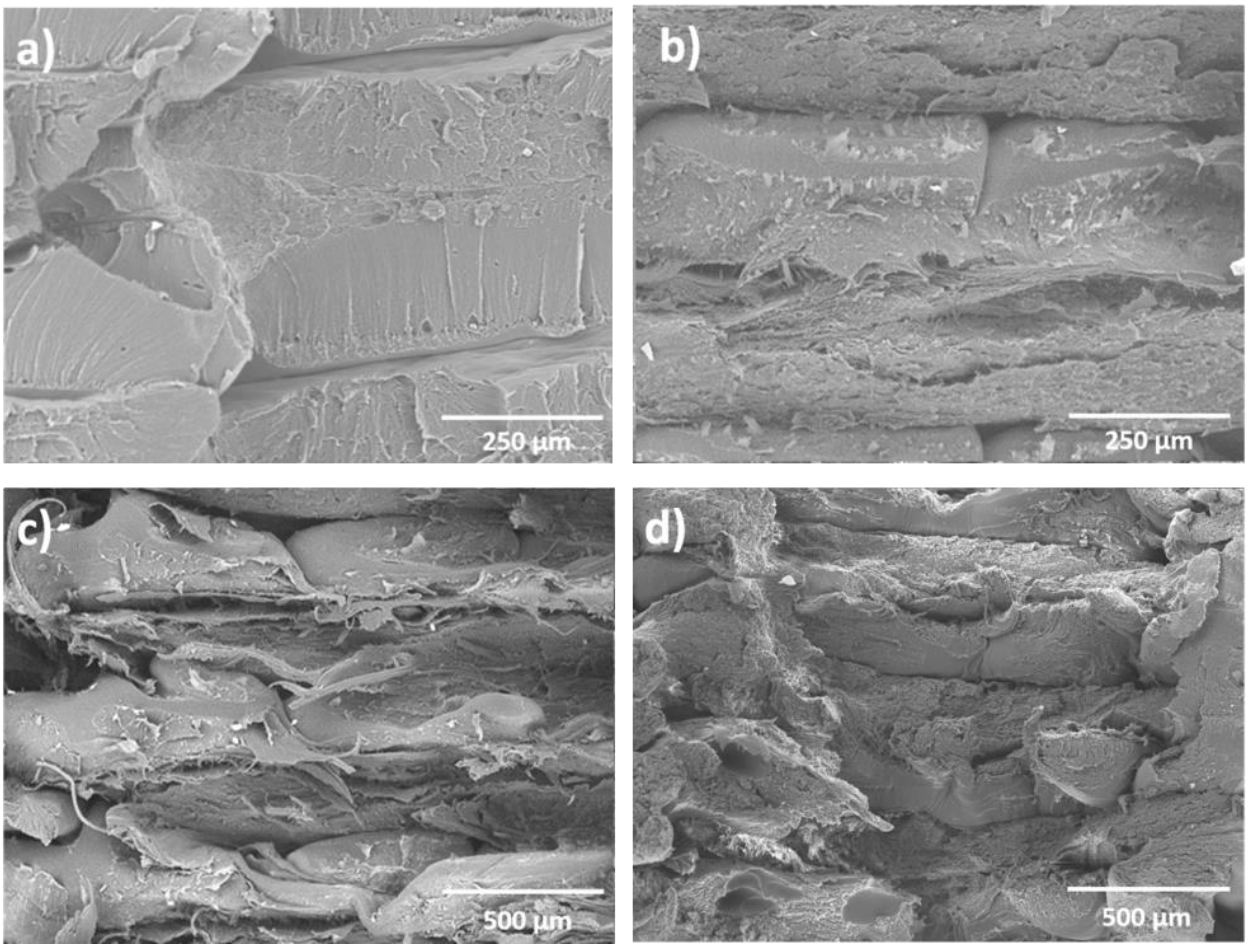

Figure 3. 6 SEM micrographs of specimens based on ABS MG47: a) ABS MG47; b) ABS MG47 SEBS-g-MA 25%; c) ABS MG47 SEBS-g-MA 50%; and d) ABS MG94 SEBS-g-MA 75. Note the increase in plastic deformation corresponding to an increase in SEBS-g-MA content.

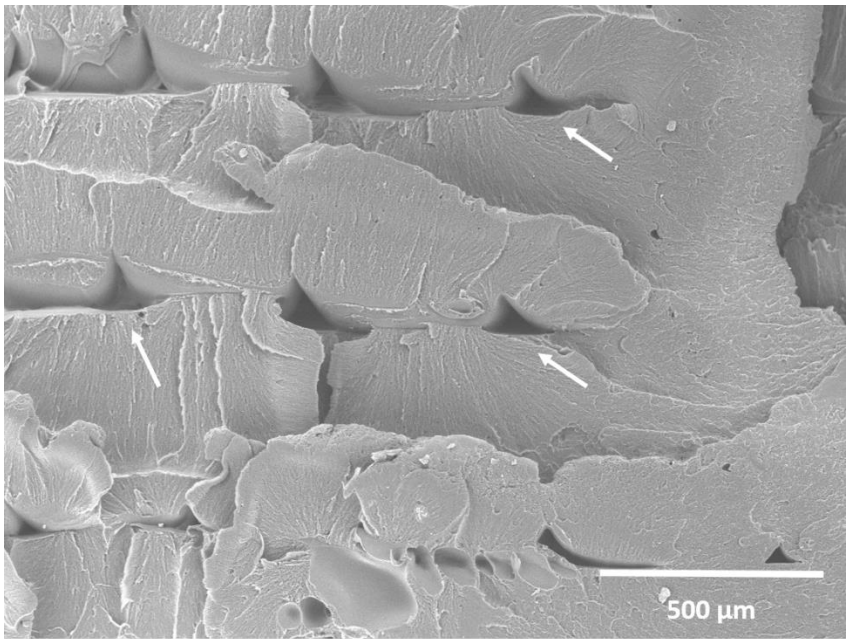

Figure 3. 7 Fracture surface of ABS grade MG94

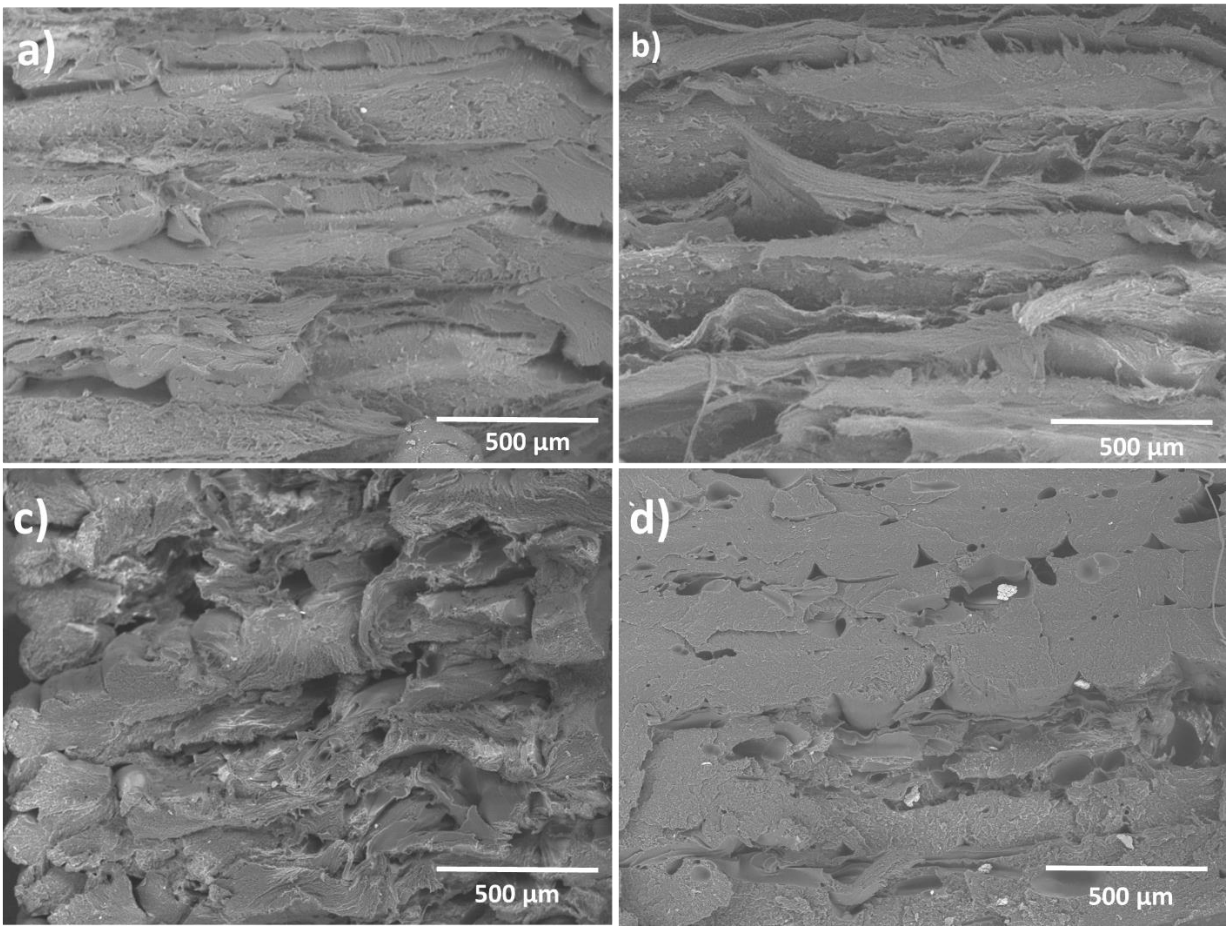

Figure 3. 8 ABS MG94 SEBS-g-MA Blends Fracture Surface Analysis. a) ABS MG94 SEBS-g-MA 25% b) ABS MG94 SEBS-g-MA 50% c) ABS MG94 SEBS-g-MA 75% d) ABS MG94 SEBS-g-MA 90%

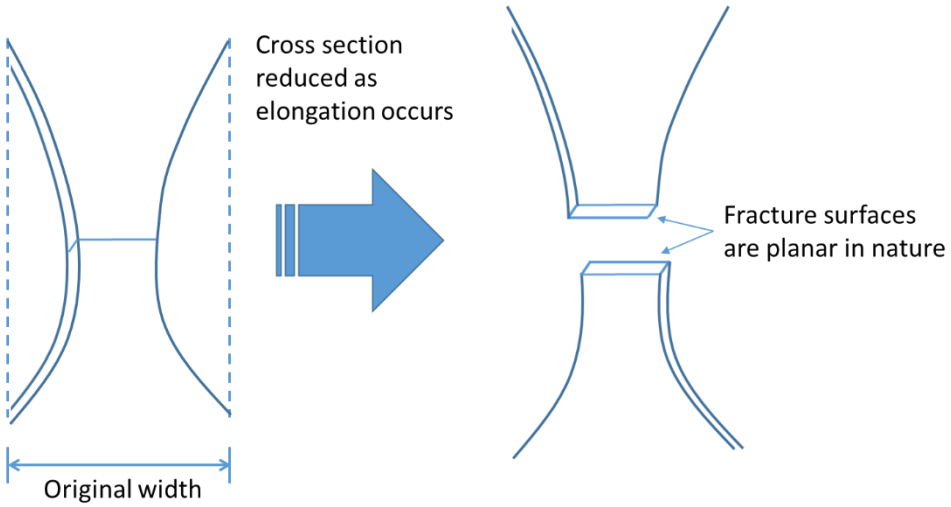

Figure 3. 9 Schematic of the deformation and failure of samples printed from the ABS/90% by weight SEBS-g-MA blend

3.4 Conclusions

We have demonstrated an effort to expand the applicability of ME3DP through increasing the array of materials with different physical properties available for specific applications, in this case applications necessitating tunable flexibility such as shock absorbers and actuators. The capability of mechanical property customization is an advancement over the state of the art where polyurethanes currently occupy the majority of market segment for flexible 3D printable materials. Through blending a material commonly used in 3D printing (ABS) with an elastomer to modify its elastic behavior, a drastic difference in mechanical properties and failure characteristics was observed. The thermoplastic blending process through the use of a twin screw extruder represents a cheaper path to create new materials for 3D printing as compared to the scientific effort that would be required to create new polymers from base chemicals.

The use of two ABS base resins with different molecular weights provided insight into aspects related to the formation of a polymer alloy and overall ability to blend two dissimilar polymeric materials. Here we were unable to create a viable blend from the higher molecular weight ABS MG47 blended with 90% by weight SEBS-g-MA. The most profound were observed for the mixture of ABS MG94 blended with SEBS-g-MA at a weight 90% by weight. This blend exhibited an increase in %El of over 1500% as compared to the base ABS resin.

A key observation made here is that the filament stiffness had a greater effect on the determination of 3D printer print parameters than did the MFI values for the blends tested. Overall, in terms of material printability, we have determined that the MFI range for a rubberized thermoplastic material can be between 15.35 and 28.34 g/10 min. The research effort presented here will be a key enabler for the use of ME3DP in the fabrication of multi-material and multifunctional applications.

3.5 References

[1] Crump, S.S., 1988. The fused deposition modeling (FDM). United States Patent Applications 5,121,329 and 5,340,433.

[2] Lipson, H. and Kurman, M., 2013. Fabricated: the new world of 3D printing. Indianapolis, IN: John Wiley & Sons.

[3] Espalin, D., et al., 2014. Multi-material, multi-technology FDM: exploring build process variations. Rapid Prototyping Journal, 20 (3), 236–244.

[4] Ready, S., Whiting, G., and Ng, T.N., 2014. Multi-material 3D printing. NIP & Digital Fabrication Conference, 2014 (1), 120–123.

[5] Stiltner, L.J., Elliott, A.M., and Williams, C.B., 2011. A method for creating actuated joints via fiber embedding in a polyjet 3D printing process. In 22nd annual international solid freeform fabrication symposium, 8–10 August, Austin, TX, USA.

[6] Rocha, C.R., et al., 2014. Novel ABS-based binary and ternary polymer blends for material extrusion 3D printing. Journal of Materials Research, 29 (17), 1859–1866. doi:10.1557/jmr. 2014.158.

[7] Saudi Basic Industries Corporation, 2015. CYCOLAC™ Resin MG47. Data sheet.

[9] Torrado, A.R., 2015. Defeating anisotropy in material extrusion 3D printing via materials development. Dissertation (PhD). The University of Texas at El Paso.

[8] Shenoy, A.V., Saini, D.R., and Nadkarni, V.M., 1984. Melt rheology of polymer blends from melt flow index. International Journal of Polymeric Materials and Polymeric Biomaterials 10 (3), 213–235.

[9] Torrado, A.R., 2015. Defeating anisotropy in material extrusion 3D printing via materials development. Dissertation (PhD). The University of Texas at El Paso.

[10] Kraton Polymers, 2015. KRATON® FG1901 G Polymer. Data sheet.

[11] American Society for Testing and Materials, 2010. ASTM D638-10. Standard test method for tensile properties of plastics. West Conshohocken, PA: ASTM International.

[12] American Society for Testing and Materials, 2011. ASTM F2921-1. Standard terminology for additive manufacturing—coordinate systems and test methodologies. West Conshohocken, PA: ASTM International.

[13] Torrado, A.R., Roberson, D.A., and Wicker, R.B. 2014. Fracture surface analysis of 3D-printed tensile specimens of novel ABS-based materials. Journal of Failure Analysis and Prevention, 14 (3), 343–353. doi:10.1007/s11668-014-9803-9.

[14] Shenoy, A.V., Saini, D.R., and Nadkarni, V.M., 1983. Rheograms for engineering thermoplastics from melt flow index. Rheologica Acta, 22 (2), 209–222. doi:10.1007/BF01332373.

[15] American Society for Testing and Materials, 2013. ASTM D1238-13. Standard test method for melt flow rates of thermoplastics by extrusion plastometer. West Conshohocken, PA: ASTM International.

[16] Coleman, M.M., Painter, P.C., and Graf, J.F., 1995. Specific interactions and the miscibility of polymer blends. Lancaster, PA: CRC Press.

[17] Oshinski, A.J., Keskkula, H., and Paul, D.R., 1992. Rubber toughening of polyamides with functionalized block copolymers: 2. Nylon-6,6. Polymer, 33 (2), 284–293. doi:10.1016/0032-3861(92)90985-6.

[18] Tjong, S.C., Bao, S.P., and Liang, G.D., 2005. Polypropylene/montmorillonite nanocomposites toughened with SEBS-G-MA: structure–property relationship. Journal of Polymer Science Part B: Polymer Physics, 43 (21), 3112–3126. doi:10.1002/polb.20596.

[19] Kusmono, Z.A., et al., 2008. Influence of SEBS-G-MA on morphology, mechanical, and thermal properties of PA6/PP/organoclay nanocomposites. European Polymer Journal, 44 (4), 1023–1039. doi:10.1016/j.eurpolymj.2008. 01.019.

[20] Brostow, W., et al., 2008. Prediction of glass transition temperatures: binary blends and Copolymers. Materials Letters, 62 (17–18), 3152–3155. doi:10.1016/j.matlet.2008.02.008.

CHAPTER 4: IN SITU WIRE DRAWING OF PHOSPHATE GLASS IN POLYMER MATRICES FOR MATERIAL EXTRUSION 3D PRINTING

4.1 Introduction

A key enabler for the advancement of additive manufacturing (AM) is the creation of new material systems with a wider range of physical properties while maintaining compatibility with 3D printing capital equipment platforms. If we take, for example, material extrusion 3D printing (ME3DP), which is based on the trademarked fused deposition modeling (FDM) technology, there are limitations to the physical attributes of fabricated parts due to the dependence of this AM platform on thermoplastics such as acrylonitrile butadiene styrene (ABS), polylactic acid (PLA), and polycarbonate (PC). As is the case with most thermoplastics, ABS, PLA, and PC have a high molecular weight and their polymer chains weaken rapidly at temperatures approaching their glass transition temperature (Tg) yielding a viscous phase that can be extruded and solidified upon cooling, a characteristic which is the key enabler for FDM-type AM [1]. Brittleness is one detrimental quality that is present in most thermoplastics and can be reduced with the addition of elastomers and plasticizers [2, 3]. Reducing brittleness and improving elastic properties in thermoplastics for ME3DP technologies have been previously studied by Siqueiros et al. [4] where the addition of the elastomer, styrene ethylene butylene styrene grafted with maleic anhydride (SEBS-g-MA) at different loadings (by wt%) was blended into ABS in order to modify its elastic properties while still maintaining compatibility with conventional FDM-type printing platforms. While polymer blending is one strategy for expanding the materials pallet for the ME3DP platform, there is still a limitation to the amount of achievable property augmentation due to the chemical composition and physical similitudes of various miscible polymers. The addition of metals, clays, carbon fibers, and other fillers to polymeric materials has been extensively researched in both academia and industry to enhance more drastically a given desired physical quality in order to

satisfy a given application [5–8]. Improving mechanical properties, modifying thermal conductivity, and increasing elasticity are just a few examples of how polymer physical properties can be altered by the addition of fillers. In the area of ME3DP, this technique has also been applied where many examples can be found in literature [9–21]. In these works, polymers have been doped with metals, carbon fibers, carbon pastes, natural fibers, clays, and other materials in order to alter physical properties such as thermal and electrical conductivity, rheology, stiffness, strength, and elasticity, among other material properties. For example, Hwang et al. [19] explored the effect of the addition of metallic fillers on part warping and thermal conductivity of ABS, Shemelya et al. [21] demonstrated the creation of a tunable radiation shielding material based on a PC matrix loaded with tungsten at different loading percentages, and specific to the application of 3D printing, and Torrado et al. [22] explored the effect of additives on the mechanical property anisotropy based on part build orientation. The addition of fillers into polymers known to be compatible with ME3DP platforms gives the opportunity to expand the application of this manufacturing process without changes to capital equipment as discussed by Roberson et al. [20].

In some cases, the addition of additives has detrimental effects on the mechanical properties of the composite. A well-known problem in the addition of non-polymeric fillers in to ME3DP polymer materials is agglomeration. As mentioned above, Torrado et al. [22] studied the effects of additives on ABS for ME3DP and one of the conclusions drawn from this work was that particle agglomeration affected the overall mechanical properties of ABS, especially the ultimate tensile strength (UTS), where a reduction from 33.96MPa to 20.70MPa was observed due to the addition of 2.5% by weight of Zinc Oxide (ZnO) nanorods. Scanning electron microanalysis revealed that the nanorods had agglomerated. It is worth noting that this previous work did not involve the use of a functionalization process to modify the ZnO prior to melt compounding. From

literature it is known that nonhomogeneous dispersion, agglomeration of particles, and poor attachment of additives to the polymer matrix are the main problems behind these negative effects on mechanical properties [5, 18, 22, 23]. A key aspect of loading polymeric materials with compositing agents such as carbon fibers is that the morphology of the filler material within the polymer matrix is largely predetermined.

The work presented here explores the possibility of loading a polymer matrix with a filler material whose morphology could be altered during the 3D printing process. The filler selected for this study is a phosphate glass (P-glass) which was combined with two polymer systems known for their ME3DP compatibility: (1) PLA, which is commonly used particularly in home-use or desktop gradeME3DP platforms; and (2) a version of the ABS:SEBS-g-MA blend first reported by Siqueiros et al. [4] (ABS blended with SEBS-g-MA in a 50 : 50 by weight ratio). P-glass was chosen as a filler because this material has similar thermal processing parameters to many thermoplastic polymers, meaning that the chance of initiating wire drawing within our matrix materials was likely [24]. The similar processing temperatures enabled an attempt to achieve in situ wire drawing of the P-glass particles within the polymer matrix with the end goal of mitigating particle agglomeration and improving the particle/matrix adhesion by wiring down agglomerated particles of P-glass within the polymer matrix allowing them to act as fiber reinforcement. Besides reducing particle agglomeration and improving mechanical properties, P-glass particles could enhance the insulating properties of these two polymers. Glasses are known for their good thermal insulating properties [25, 26], that is why, in an effort to expand the applications of ME3DP, this composite material could later be used as thermal insulator for a multi-material ME3DP functional component necessitating thermal management such as 3D printed structural electronics [27, 28].

4.2 Experimental Procedure

Phosphate glass was created following a method by Gupta et al. where a mixture composed of a molar composition of 50% tin fluoride (SnF2), 20% tin oxide (SnO), and 30% phosphorous pentoxide (P2O5) [24]. The ingredients were tumble mixed until the desired homogeneity was achieved and then placed into a glassy carbon crucible. The crucible was then placed into an oven (Lindberg/Blue M, Thermo Electron Corporation, Germany) at a temperature of 450°C for 70 minutes. The mixture in its liquid stage was then quenched in a stainless steel pan at room temperature. After quenching, the glass was annealed at 130°C for 90 minutes in a VWR horizontal forced air safety oven (Radnor, PA, USA). The resulting phosphate glass was then processed in a ball mill for 5 minutes. After ball milling the powder was chemically analyzed by X-ray diffraction (XRD) using a Bruker D8 Quest diffractometer (Bruker Corporation, Germany) operating with Cu K-α radiation (1.54 ˚A). The resulting spectra (Figure 4.1) were a 100% match to tin fluorotrioxophosphate (phosphate glass). Figure 4.2(a) is a SEM micrograph of the ball milled phosphate glass particles. Measurement of the particles from the SEM image revealed a highly variable particle size distribution (coefficient of variation = 1.19) with an average size of 9.68μm (Figure 4.2(b)).

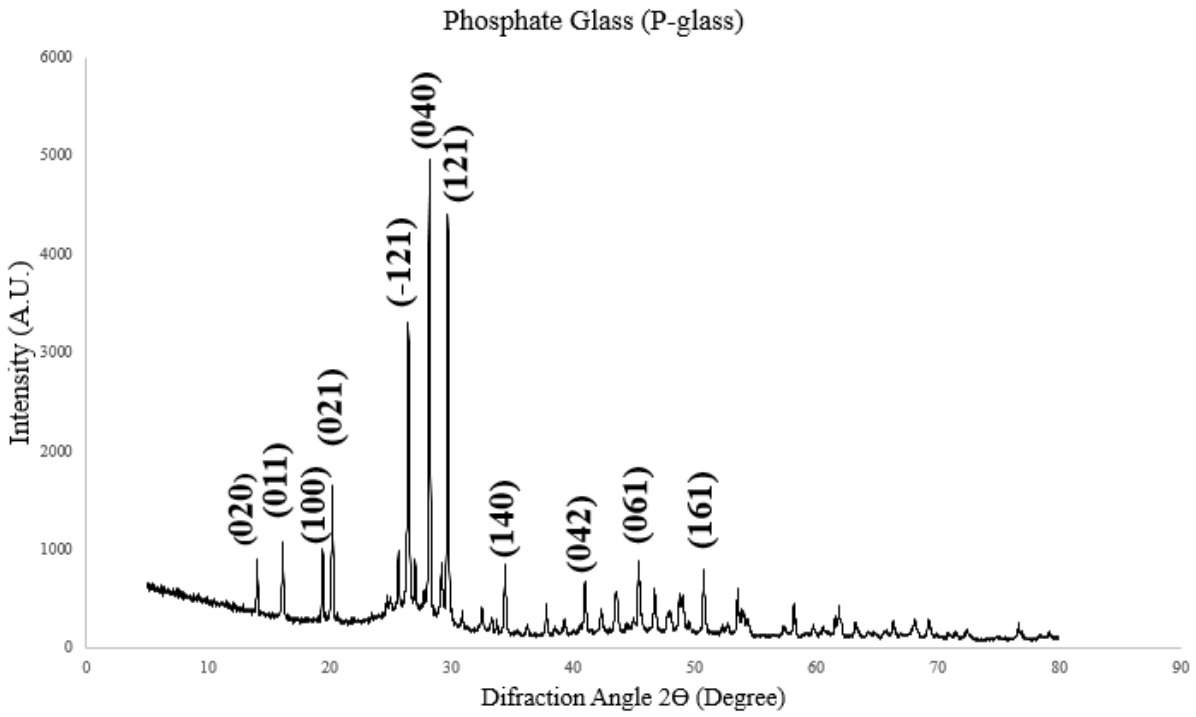

Figure 4. 1 XRD of the P-glass material used in this study

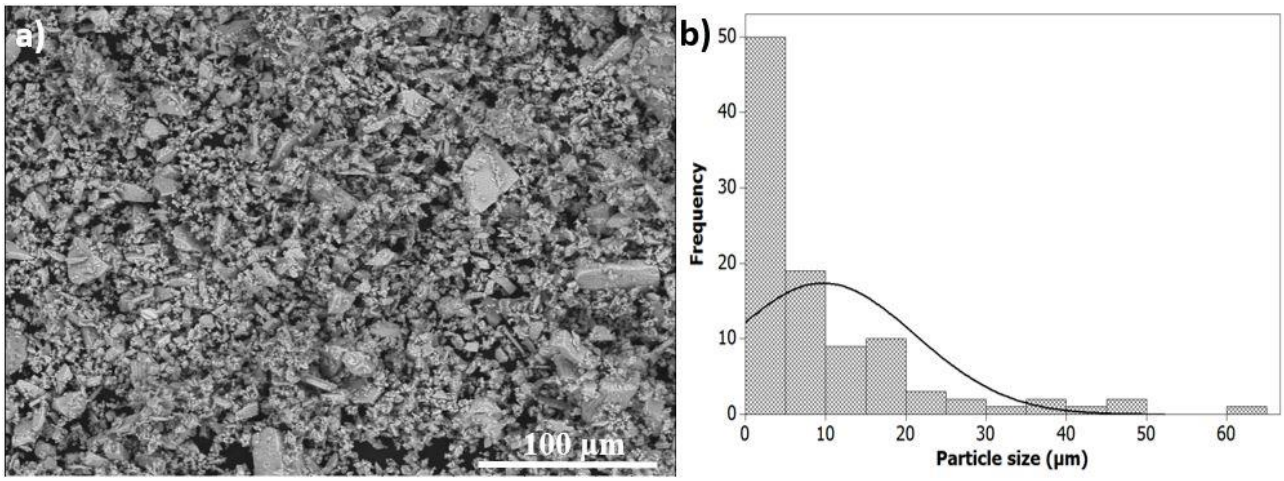

Figure 4. 2 a) SEM micrograph of P-glass particles and b) size distribution of particles

In order to study the behavior of phosphate glass as an additive in polymers known for their ME3DP capabilities, PLA and the ABS-based blend discussed above were used as matrix materials. The polymers used in this study were (1) PLA (grade 4043D NatureWorks, Blair, NE, USA) and (2) a polymer blend composed of a 50 : 50 weight ratio of ABS (grade MG94, SABIC, Pittsfield, MA) and SEBS-g-MA (Grade FG1901 Kraton, Houston, TX, USA). The elastomeric

blend was previously studied by our group for the use in FDM-type processes and was demonstrated as a 3D printable material [4]. All polymers were received in pellet form the respective suppliers. In this study, the ABS:SEBS-g-MA blend was compounded first using a Dr Collin ZK 25 T twin screw extruder compounder (Collin Lab and Pilot Solutions, Inc., Norcross, GA, USA) following parameters documented in Siqueiros et al. [4] and then mechanically pelletized prior to melt compounding with the P-glass particles.

Before melt compounding, the filler material was subjected to a functionalization process intended to facilitate particle/matrix adhesion as well as facilitate improved dispersion of the filler material within the polymer matrix. The functionalization process consisted of a silane treatment on the additive before compounding; it must be mentioned that two different silanes were used in this experiment, one geared for the PLA matrix (3-Glycidyloxypropyl) trimethoxysilane and the other one towards the ABS:SEBS-g-MA blend Vinyltrimethoxysilane both purchased from Aldrich Chemistry (St. Louis, MO, USA). Our group has used a similar functionalization process in prior work where polycarbonate was the matrix material [21]. Before extrusion, the polymer pellets were dried using a compressed air dryer (Dri-Air CFAMMicro-Dryer, EastWindsor, Connecticut, USA). PLA was dried at a temperature of 80∘C for 4 hours and the ABS:SEBS-g-MA blend was dried at 70∘C for a 2-hour period. The limited quantity of phosphate glass necessitated the use of a small batch extruder; therefore, the melt compounding process was performed with the use of a desktop grade Filabot EX2 extruder (Filabot, Barre, VT, USA) in order to accommodate composite batches of 100 g. The extruder was used in conjunction with the belt puller from the Collin ZK 25 T extruder to maintain a constant diameter of 1.75 mm, a standard diameter used on many FDM-type platforms. The extrusion temperatures for the composite systems evaluated in this study are seen in Table 4.1.

Table 4. 1 Extrusion Temperatures

Material System	**Extrusion Temperature °C**
ABS:SEBS-g-MA	210
P-glass 5% - ABS:SEBS-g-MA	230
P-glass 10% - ABS:SEBS-g-MA	235
P-glass 20% - ABS:SEBS-g-MA	240
PLA	190
PLA 2.5% P-glass	205
PLA 5% P-glass	215
PLA 10% P-glass	220
PLA 15% P-glass	235

In order to characterize the mechanical properties of the different polymer composite systems, test specimens were printed using a Lulzbot TAZ 4 (Aelph Objects Inc., Loveland, Colorado, USA) outfitted with a 0.8mm nozzle tip. The printer was modified to accept 1.75mm diameter filament through the installation of an E3D V6 hot end (E3D-Online Limited, Chalgrove, Oxford shire, UK). The test specimens were printed with 100% infill in a rectilinear pattern consisting in alternating layers of 0 and 90 degrees. The dimensions of the specimens followed ASTM standard D638-14 [29] Type V. Figure 4.3 represents the printed tensile test specimens for one of the systems. The printing parameters for all the systems are shown in Table 4.2.

Table 4. 2 Printing Parameters

Material System	**Nozzle Temperature °C**	**Bed Temperature °C**
ABS:SEBS-g-MA Baseline	240	110
ABS:SEBS-g-MA - P-glass 5%	240	110
ABS:SEBS-g-MA - P-glass 10%	240	110
ABS:SEBS-g-MA - P-glass 20%	240	110
PLA Baseline	220	110
PLA - P-glass 2.5%	220	110
PLA - P-glass 5%	220	110
PLA - P-glass 10%	240	110
PLA - P-glass 15%	240	110

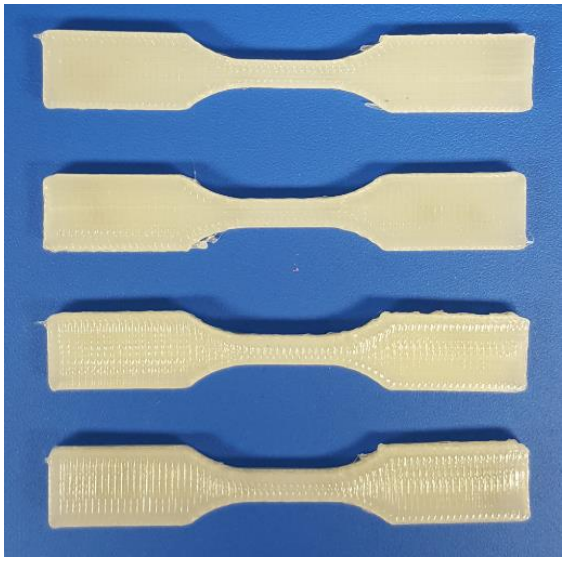

Figure 4. 3 Printed tensile specimens (PLA - Phosphate glass 10%)

Tensile testing was carried out using an Instron 5866 (Instron, Norwood, Massachusetts, USA) loaded with a 10 kN load cell following ASTM standard D638-14 [29]. All tests were performed at a strain rate of 10 mm/min at room temperature on sample pools of 3 to 6 specimens per material system and the UTS and percent elongation at break (% EL) were recorded for each specimen.

Fracture surface analysis of spent tensile test specimens was carried out through the use of a Hitachi TM-1000 scanning electron microscope (SEM; Hitachi High-Technologies Europe GmbH, Germany) operating at a 15 kV accelerating potential and equipped with a backscatter electron detector. Due to the nonconductive nature of polymeric surfaces, the specimens were gold coated using a JEOL Smart Coater (JEOL USA, Inc, Peabody, MA) to reduce electron charging. Two to three different test specimens from each system were analyzed in order to characterize the in situ wire drawing of phosphate glass particles as well as the failure modes and fracture surface morphology within each material system.

Melt flow rate analysis was performed by following ASTM standard D1238-13 [30] (procedure A) using a Tinius Olsen (Horsham, PA, USA) MP1200melt flow indexer (MFI). Prior

to performing the test, filament specimens from the different material systems were pelletized to allow introduction into the melt flow indexer in 7 g sample sizes. For comparison purposes, all the ABS SEBS-g-MA blend systems were tested at a temperature of 230∘C with a 3.8 kg test load. The PLA systems were tested at a temperature of 210∘C with a 2.16kg test load. The melt flow rates of all the systems were collected and will be discussed in greater detail below.

4.3 Results

4.3.1 Fractography

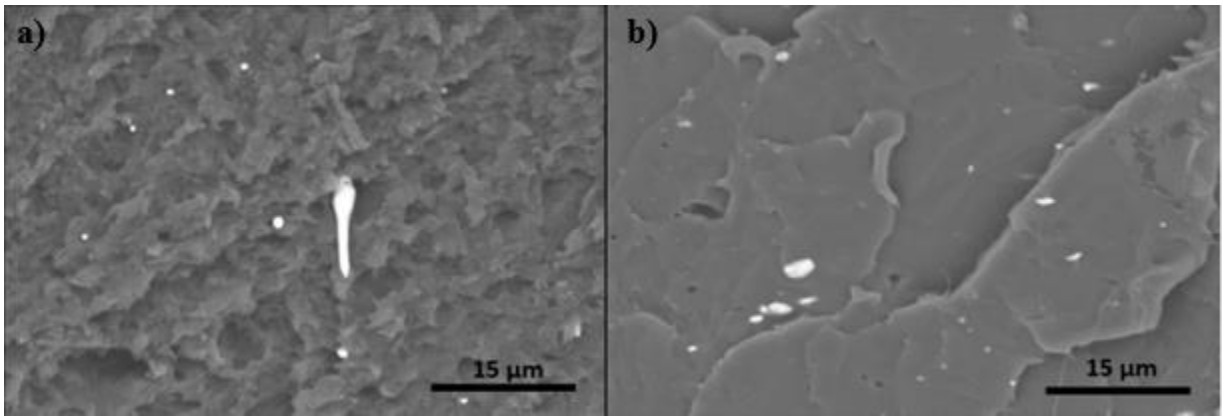

Figure 4. 4 Fracture surface of 5% P-glass loaded into a) ABS:SEBS-g-MA and b)PLA

Fracture surface analysis confirmed the in situ wire drawing of phosphate glass particles within the ABS:SEBS-g-MA polymer matrix as is seen in Figure 4.4(a). Phosphate glass particles were elongated into a rod shape form with diameters ranging from 0.5 to 2 μm. The presence of drawn wires supports the theory and motivation behind this study: because of the similar processing temperatures between polymers and P-glass at the moment of deposition during the 3D printing process, particles of P-glass would experience enough shear forces that would make them elongate within the polymer matrix. In contrast, PLA loaded with 5% P-glass did not show signs of wire drawing as can be observed in Figure 4.4(b). Examination of the PLA specimens loaded with P-glass under SEM revealed that the P-glass particles did not show signs of elongation (Figure 4.5). This could be due to the low viscosity of PLA during filament extruding and ME3DP.

Viscosity plays an important role in the elongation of the P-glass particles; in this study the ABS:SEBS-g-MA blend which has a higher T_g of around 120°C compared to the T_g of PLA of 70°C (as determined by the max tan δ of dynamic mechanical analysis scans) possesses a greater viscosity at the moment of deposition resulting in higher shear forces within the composite filament allowing in situ wire drawing of P-glass particles within the polymer matrix. Figure 4.6 is a schematic representation of the in situ wire drawing process of P-glass in the ABS:SEBS-g-MA matrix during deposition. PLA is usually 3D printed at temperatures ranging from 170°C to 220°C, and for this

experiment it was necessary that the print temperatures be above 220°C to avoid clogging of the print nozzle by the P-glass, which, at the same time, reduced the viscosity of PLA negating any shear forces which would elongate the P-glass particles.

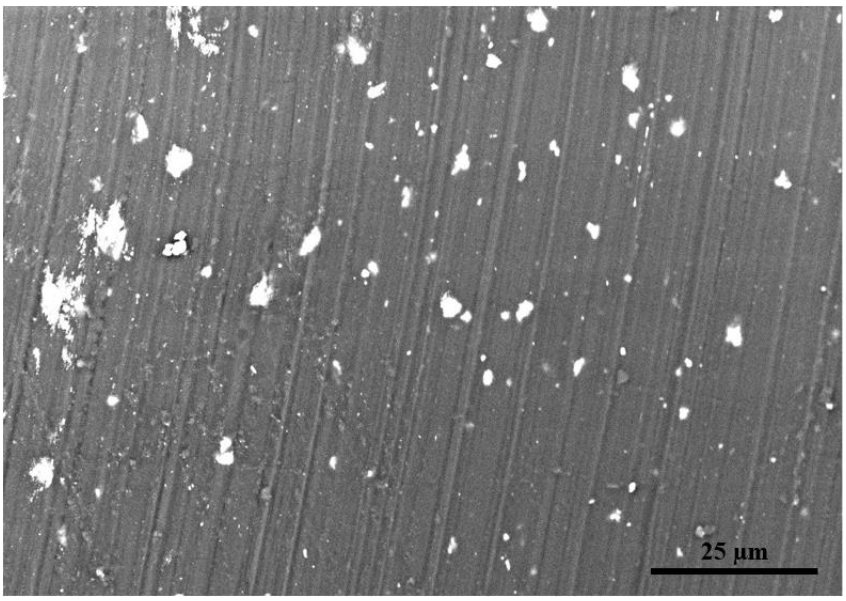

Figure 4. 5 Scanning electron micrograph of a filament specimen of PLA loaded with P-glass at a loading of 15% by weight

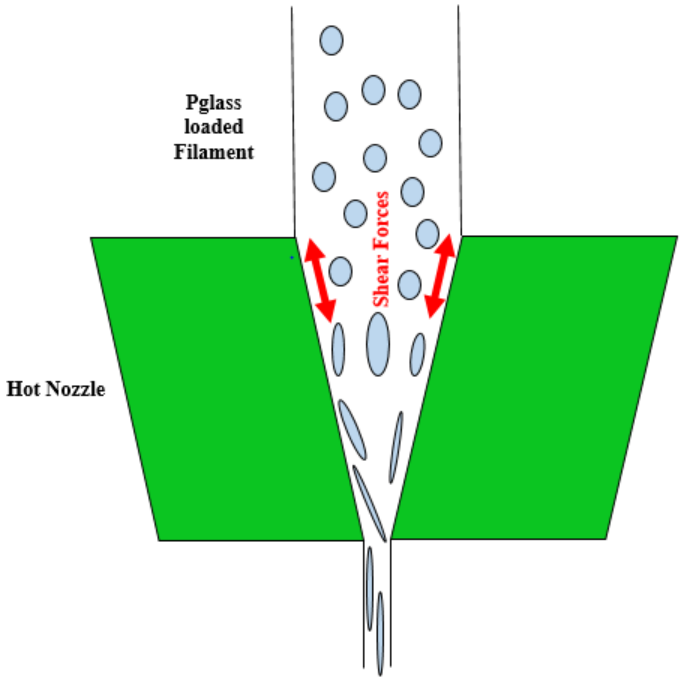

Figure 4. 6 Schematic depicting the in situ wire drawing of P-glass during the 3D printing process

When the loading of P-glass was increased to 10% by weight and above, agglomeration played a key role in reducing the mechanical properties, specifically the property of UTS. In the

case of ABS:SEBS-g-MA loaded at 10% and 20% P-glass, the SEM micrographs of the fracture surfaces revealed that there were more particles that did not elongate during deposition as indicated by white circles on Figure 4.7. The particle size of the undrawn P-glass particles ranged from 15 μm to 2.5 μm. The agglomeration between P-glass particles in the 20% P-glass ABS:SEBS-g-MA system (specified on Figure 4.7(b) by a rectangle) interfered with the proper in situ wire drawing of the P-glass and acted as a crack propagation site.

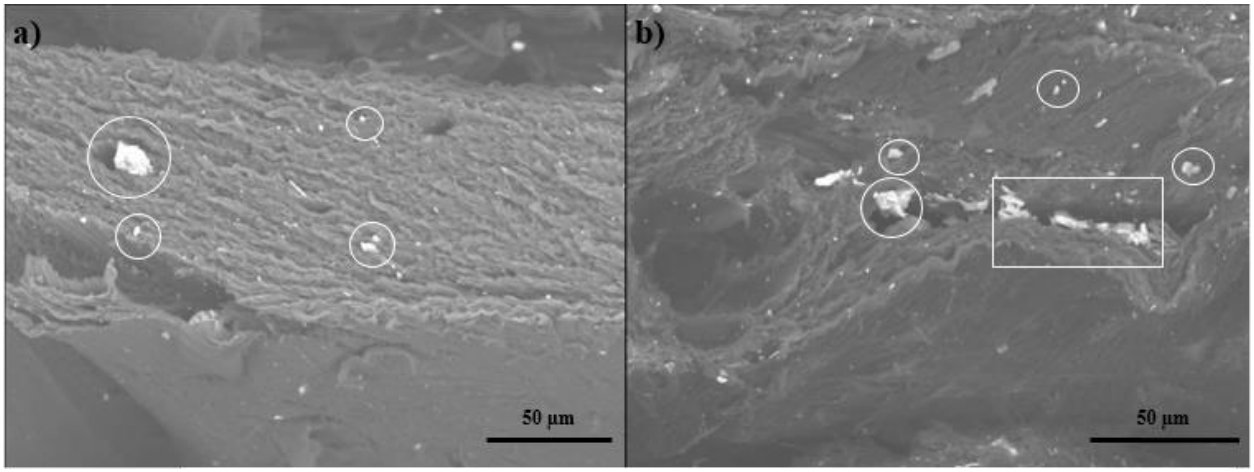

Figure 4. 7 Tensile test fracture surfaces of ABS:SEBS-g-MA loaded with a) 10% P-glass b) 20% P-glass

In order to investigate the effect of print temperature on the efficacy of the in situ wire drawing of P-glass particles in the ABS:SEBS-g-MA 10% P-glass system, two specific print temperatures were experimented with, 240°C and 280°C. Based on SEM images, there was not a clear difference between the two print temperatures in terms of the amount of P-glass particles that were in situ wire drawn as can be seen on the high magnification inset images representing the printing temperatures of 240°C and 280°C (Figure 4.8). The only clear difference between the print temperatures was observable when comparing the lower magnification SEM images where an overall more ductile fracture occurred, as indicated by a greater amount of plastic deformation on the fracture surface of the specimen printed at 280°C (Figure 4.8(b)).

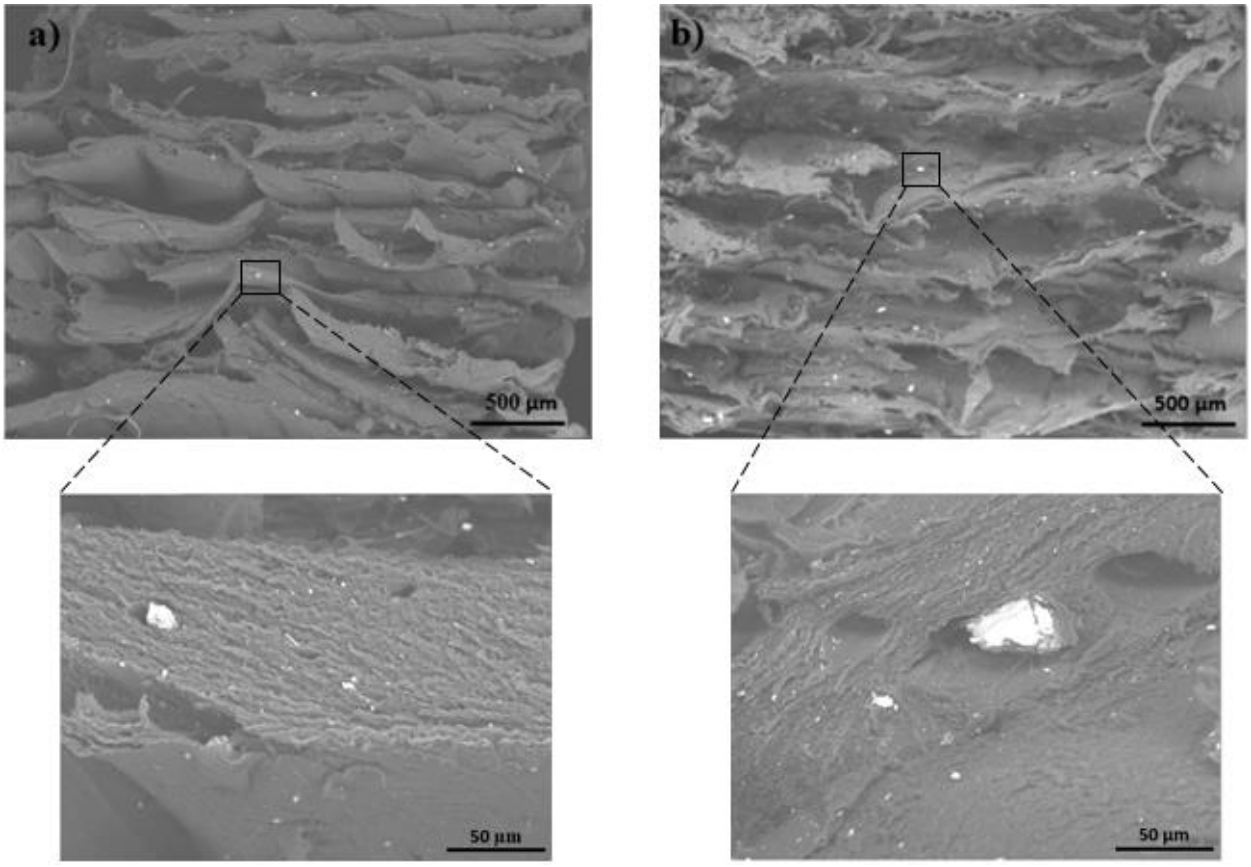

Figure 4. 8 SEM micrographs of tensile specimens fabricated from ABS:SEBS-g-MA loaded with P-glass 10% by weight and printed at a) 240°C b) 280°C

In the case of the PLA/P-glass system there was no observable evidence of in situ wire drawing of P-glass particles based on fractographic analysis. The SEM images in Figures 4.9(a) and 4.9(b) are representative images of PLA loaded at the 2.5% and 10% by weight P-glass. In these images and throughout the fracture surface there were no signs of wire drawn P-glass particles. A noteworthy observation while analyzing the fracture surface of this system was the robust attachment of the phosphate glass particles to the PLA matrix, a plausible reason behind the increase of UTS for the 2.5% and 5% loading as well as the incremental increase in strain on every P-glass loading in PLA.

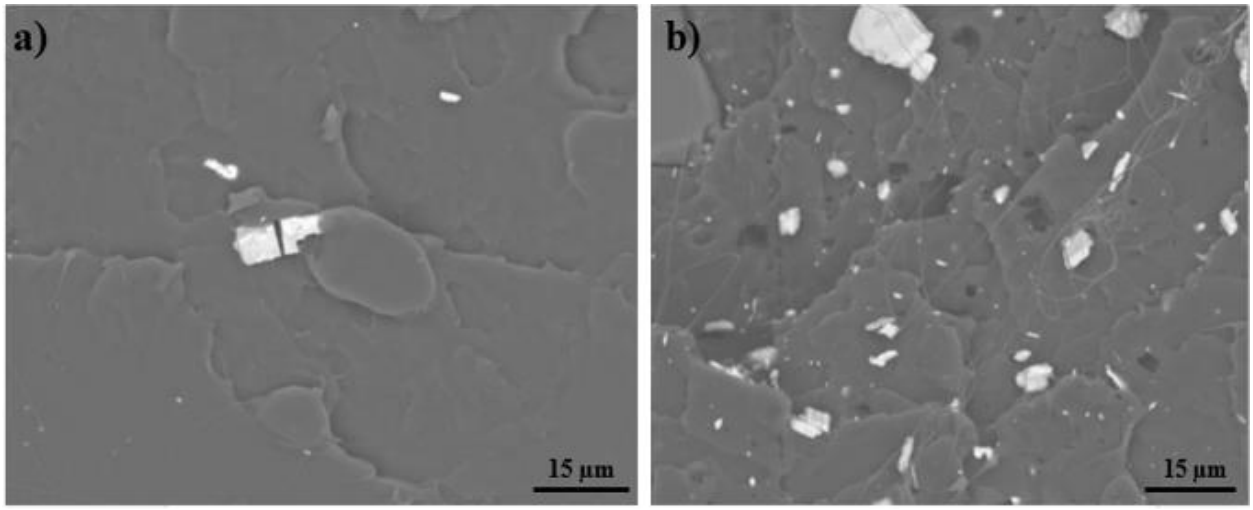

Figure 4. 9 SEM micrographs of fracture surfaces of PLA loaded with P-glass at a) 2.5% by weight and b) 10% by weight

Agglomeration also played a factor in the reduction of the UTS in the higher P-glass loadings in the case of the PLA systems. Figure 4.10 is a SEM micrograph of the fracture surface of PLA loaded with 10% P-glass and the agglomerate size of phosphate glass in unit sizes ranging from5 to 100μm.

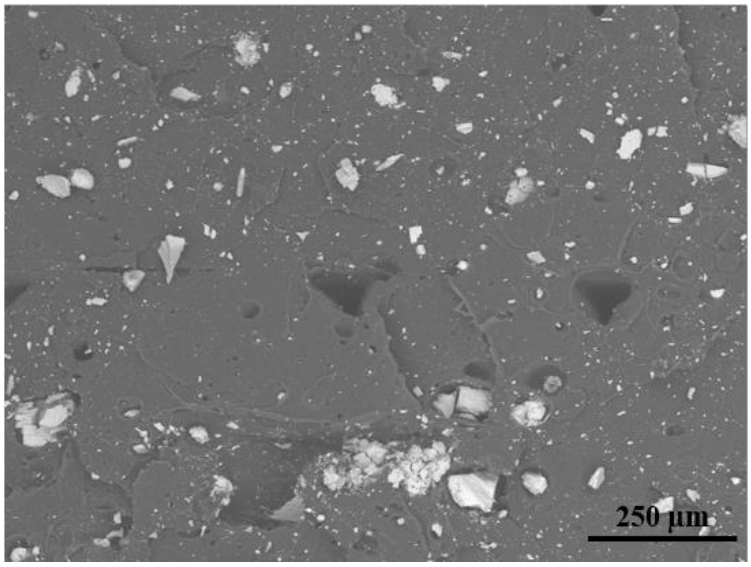

Figure 4. 10 SEM micrograph of a fracture surface of PLA loaded with P-glass at 10% by weight

4.3.2 Tensile Test Results.

The results of the tensile testing for the ABS:SEBS-g-MA loaded with P-glass systems are tabulated in Table 4.3 and graphically represented in Figures 4.11 and 4.12. The best performer out of the three systems was the 5% (by wt.) P-glass loading, which had a UTS value of 14.8 ± 0.2MPa as compared to the baseline value of 14.4 ± 0.2MPa. Though the UTS was not significantly increased, the lack of a negative result to the mechanical properties for the 5% P-glass loading confirms the theory behind this study that in situ wire drawing of an additive into a polymer matrix diminishes the detrimental effects of agglomeration and provides a more stable attachment to the polymer matrix. In the case of the material loaded at 10% by weight there was a minimal but not statistically significant reduction of UTS compared to the baseline. The fractographic evidence indicated some agglomeration and large P-glass particles could have been detrimental to the mechanical properties at this percent loading. The significant reduction of UTS for the material loaded with 20% by weight P-glass was most likely caused by voids within the material as observed on the fracture surface of the tensile specimens as well as particle agglomeration. Figure

4.13(a) is a SEM image of the 20% P-glass fracture surface where particle agglomeration and voids throughout the surface are observable. Further analysis of extruded filament corresponding to the 20% by weight loading also indicated particle agglomeration and voids as can be observed in Figure 4.13(b).

Table 4. 3 Tensile rest results for ABS:SEBS-g-MA loaded with P-glass at various weight percentages.

Material	**UTS (MPa)**	**ST. DEV**	**%EL at Break**	**ST. DEV**	**Sample size (n)**
ABS:SEBS-g-MA - P-glass 5% @240C	14.8	0.2	69	4	4
ABS:SEBS-g-MA - P-glass 10% @240C	14.1	1.3	49	8	5
ABS:SEBS-g-MA - P-glass 20% @240C	11.0	0.5	63	14	5
ABS:SEBS-g-MA - Baseline @240C	**14.4**	**0.2**	**54**	**14**	**3**

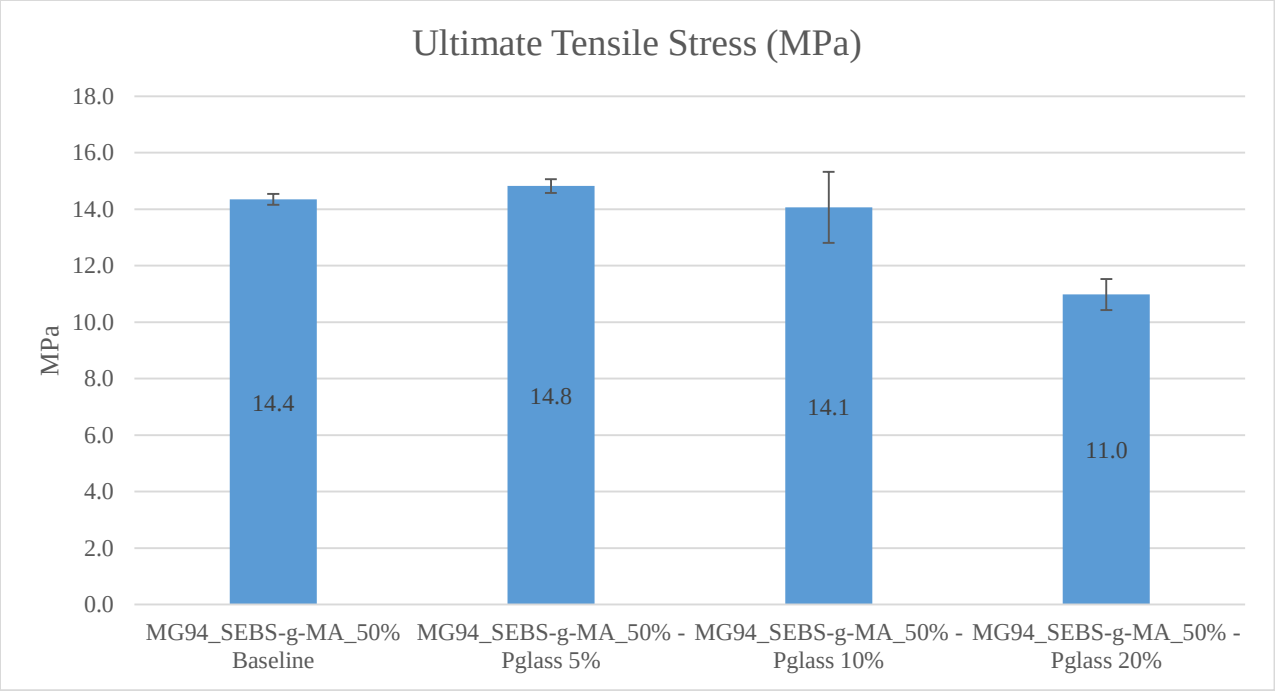

Figure 4. 11 UTS ABS SEBS-g-MA P-glass Systems

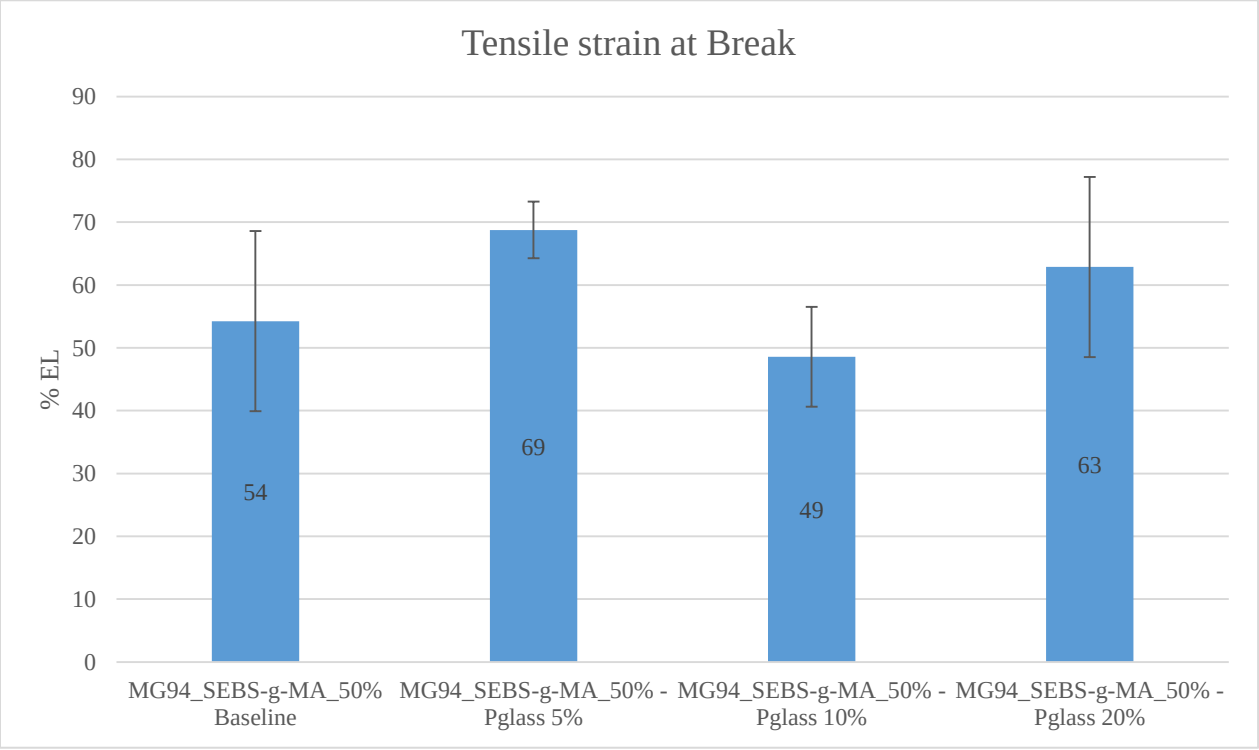

Figure 4. 12 %EL at break values for the ABS SEBS-g-MA P-glass Systems

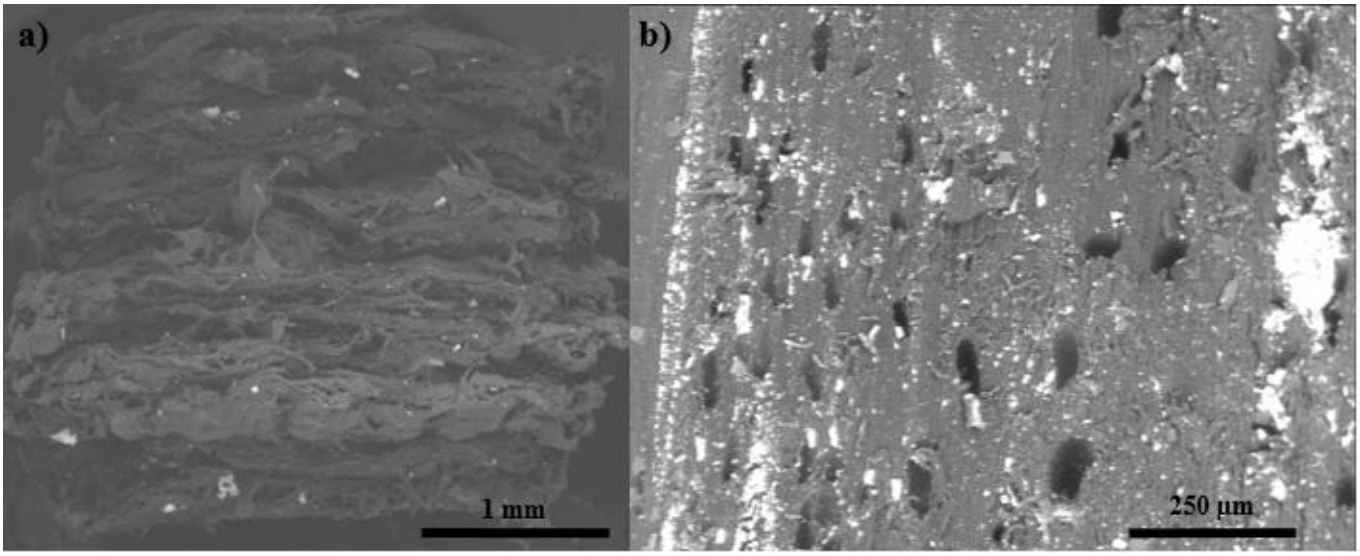

Figure 4. 13 SEM micrographs of ABS SEBS-g-MA loaded with P-glass at 20% by weight a) Fracture surface b) Filament (tangential view)

In terms of % EL at break, the best performer was also the 5% P-glass loading as the elongation at break increased from 54 ± 14% for the baseline specimens to 69% ± 4%. The only system which exhibited a reduction of % EL at break as compared to baseline ABS:SEBS-g-MA specimens was the 10% P-glass loading printed at 240°C. The reduction of percent elongation at break for this system occurred because of large P-glass agglomerates that acted as crack initiation sites as determined by the fractographic analysis in Figure 4.14 indicated by circles, where the longitude of middle right particle is around 34.5 μm and bottom left 22.5 microns. From SEM image analysis most elongated particles have a diameter ranging from 0.5 to 2 μm, whereas particles of the sizes shown in Figure 4.14 are too large to in situ wire draw within the polymer matrix and lead to detrimental effects on the mechanical properties of the printed part.

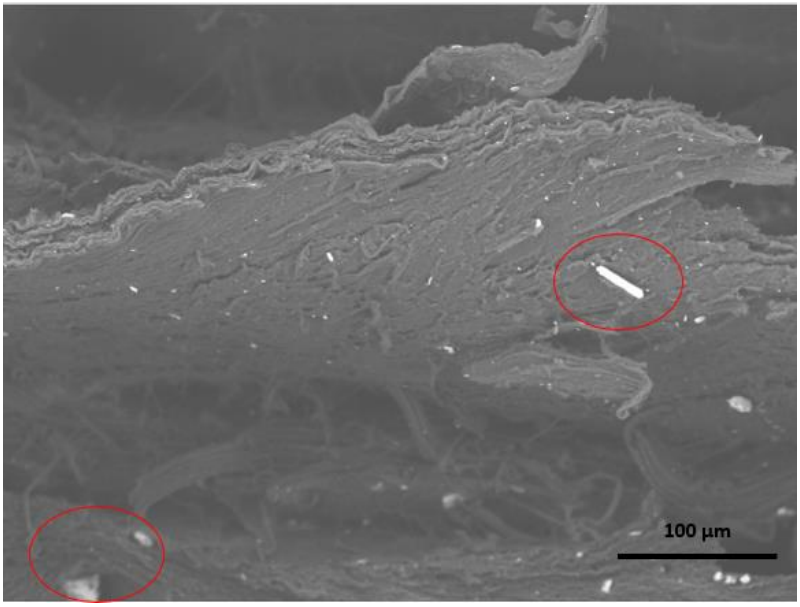

Figure 4. 14 SEM micrograph of the fracture surface of a specimen of ABS SEBS-g-MA loaded with P-glass at 10% by weight printed at 240 °C

As mentioned before, in the case of the ABS:SEBS-g-MA system loaded with 10% by weight P-glass, two different printing temperatures were studied in order to understand the effect of elevated process temperatures. Fractographic analysis on spent tensile specimens revealed that many P-glass particles were not wire drawn within the polymeric matrix. Therefore, a second set of tensile test specimens was printed at a higher temperature (280°C) to explore the relationship between temperature and the ability to draw P-glass particles. There was not a clear difference in the amount of wire drawn particles compared to the previous printing temperature of 240°C based on fractographic evidence, but there was a difference in the mechanical properties as can be noted in Table 4.4. There is a slight increase on the UTS in the system printed at 280°C and a noticeable increment in percent elongation at break (% EL) compared to the ABS:SEBS-g-MA baseline specimens printed at the same temperature. This could be an indication that the P-glass particles printed at higher temperature parameters have a positive effect on the tensile behavior of the system, but the loss in viscosity does not allow in situ wire drawing of the particles within the polymer matrix. Additionally, the higher temperature could have also led to an increase in fusion

between print rasters as the increased heat would allow for a greater degree of subdiffusion to occur while the latent heat would increase the duration of any diffusion processes [31].

Table 4. 4 SEBS-g-MA/ P-glass 10% Printed at Different Temperatures

Material	UTS (MPa)	ST. DEV	%EL	ST. DEV	Sample size (n)
ABS:SEBS-g-MA - P-glass 10% @240C	14.1	1.3	48	8	3
ABS:SEBS-g-MA - P-glass 10% @280C	12.0	0.3	62	16	3
ABS:SEBS-g-MA @240C	14.3	0.2	54	7	3
ABS:SEBS-g-MA @280C	11.6	0.2	54	14	3

The tensile test results of the PLA loaded with P-glass are tabulated in Table 4.5 and graphically represented in Figures 4.15 and 4.16. While there was a slight increase of UTS values for the 2.5% and 5% by weight loading of P-glass compared to the pure PLA baseline, the increase was not statistically significant. Once the % loading by weight increased to 10% and 15%, the UTS decreased by 13% in the case of the 10% P-glass loading and a reduction of 24% for the 15% P-glass loading. The % EL at break increased beyond error for the 2.5 and 15% by weight loadings of P-glass; the particles reduced the brittle nature of PLA indicated by an increase in the elongation at break. However, there was no evidence of in situ wire drawn particles of P-glass in the PLA matrix.

Table 4. 5 Mechanical testing results for PLA loaded with P-glass.

Material	UTS (MPa)	St. Dev	%EL	St. Dev	Sample size (n)
PLA/P-glass 2.5%	57.7	1.7	6.0	2.2	5
PLA/P-glass 5%	57.7	1.5	4.6	0.9	5
PLA/P-glass 10%	48.4	2.8	4.4	0.9	5
PLA/P-glass 15%	42.2	2.1	5.2	1.5	6
PLA - Baseline	**55.1**	**2.6**	**3.3**	**1.6**	**4**

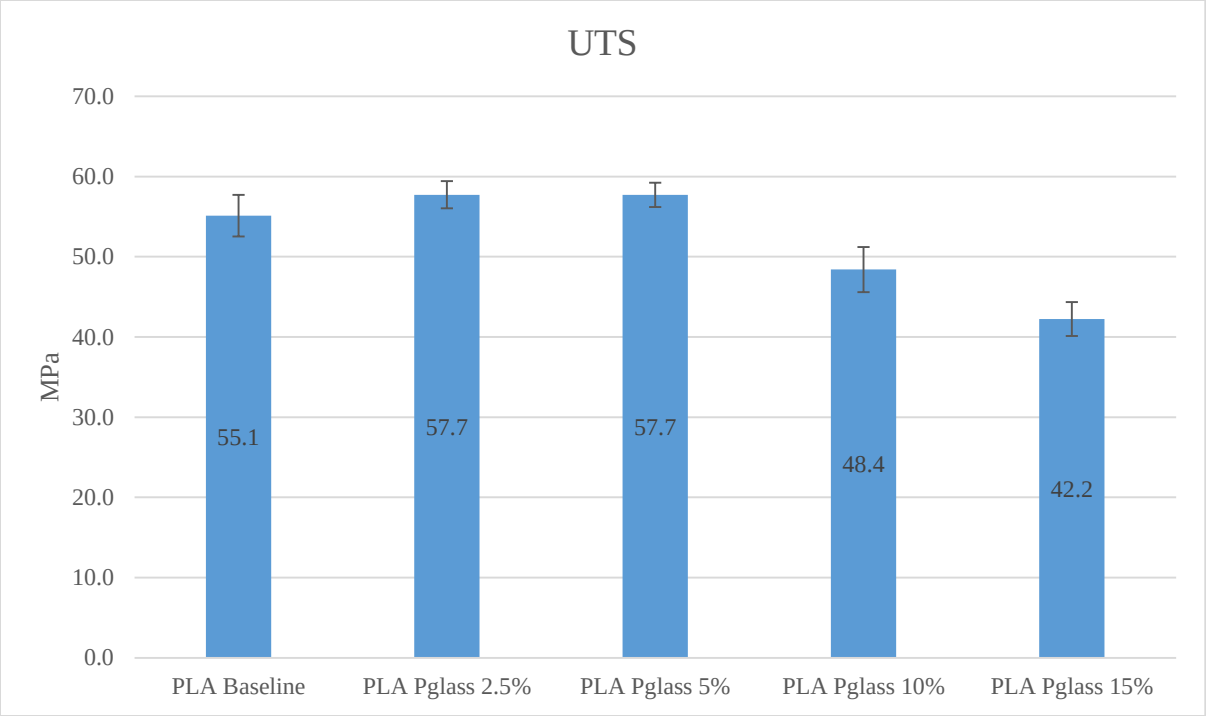

Figure 4. 15 UTS values for PLA loaded with P-glass at various weight percentages

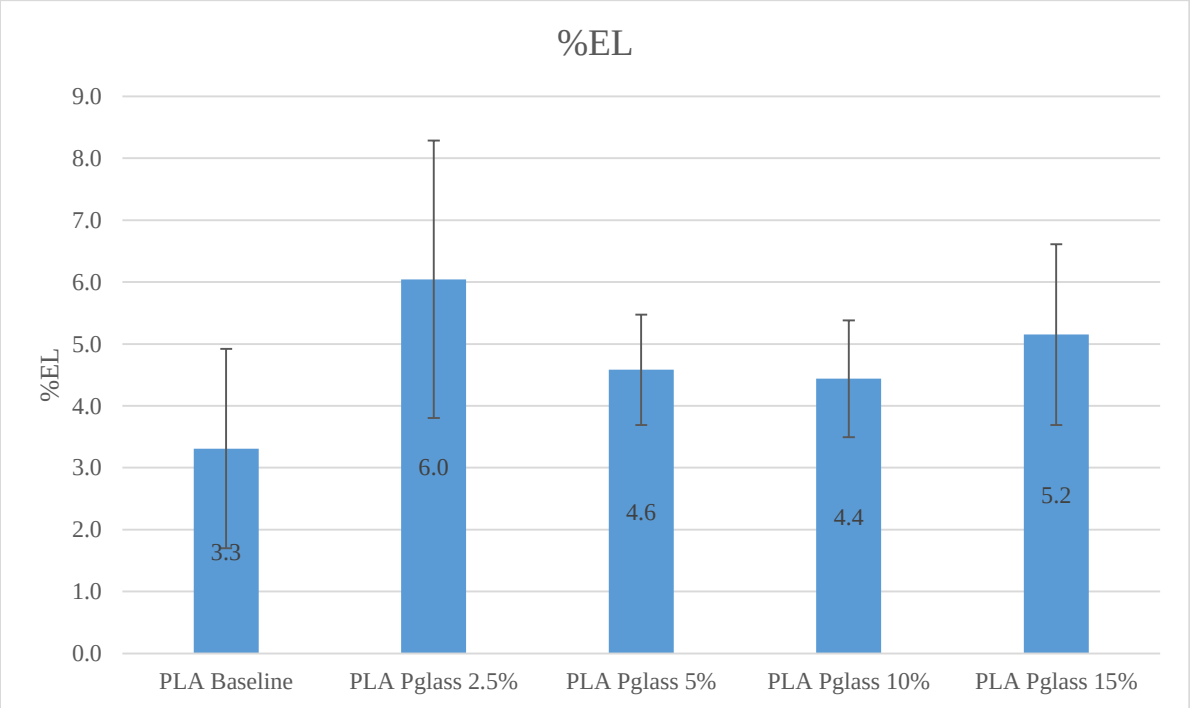

Figure 4. 16 Percent elongation values for PLA loaded with P-glass at various weight percentages

As was the case for the ABS:SEBS-g-MA system loaded with 20% P-glass, the PLA P-glass 15% system exhibited the highest decrease in strength. The decrease in tensile strength was unexpected, so further investigation as to the cause of the observed malefic was warranted. The SEM micrographs of the PLA P-glass system also exhibited a high amount of voids present similar to the 20% P-glass ABS:SEBS-g-MA system. The presence of voids is a key factor in the reduction of UTS and there was a trend of voids increasing proportionally with the percent loading of P-glass. In order to normalize the UTS values with 100% filled tensile specimens for every system, density measurements following guidelines from ASTM Standard D792-13 [32] were made. The measurements were then compared to the theoretical density of each material system to create a normalization factor, which was then applied to the UTS results for each material system. Our group has utilized this strategy to assess the effect of additives on mechanical properties in previous work [21]. The specimens used for the density test were the grip section of the mechanical test specimens (n = 5 for each sample pool). The test was performed with a Minerlab specific gravity kit (Minerlab LLC, Prescott, AZ, USA) and an analytical balance readable to 0.1mg Sartorius CP124S (H&C Weighing Systems, Columbia, MD, USA). The results for the density test along with the normalized UTS and percent infill calculations are shown in Tables 4.6 and 4.7 for the ABS:SEBSg-MA and PLA systems, respectively. Figures 4.17 and 4.18 are graphical representations of these tables. The infill percent is the percentage of the measured density over theoretical density. It is notable that, after the normalization process, an appreciable increase in mechanical strength was revealed for both PLA and the ABS-SEBS-g-MA material systems over the baseline specimen pools.

In the case of the ABS:SEBS-g-MA system, there was an incremental increase in strength for all the loadings when compared to the baseline values. The previously noted trend of an

increase in void content with an increase of P-glass loading was confirmed by the density measurements taken—meaning that the actual infill percentage decreases with the addition of P-glass. The maximum increase in UTS was no greater than 20% over the baseline values (17.8MPa compared to 14.7MPa) which is equal to the 10 and 20% by weight loading of P-glass. A similar trend was observed in the PLA system where the addition of P-glass led to an increase in strength with the exception of the 10% load where the UTS remained equal to the baseline. Further experiments with the PLA/10% by weight P-glass system were carried out as will be explained later.

Table 4. 6 Normalized UTS Data ABS:SEBS-g-MA System

Material	**Theoretical Density ($\frac{g}{cm^3}$)**	**Measured Density ($\frac{g}{cm^3}$)**	**ST DEV**	**% Infill**	**UTS (Mpa) Measured**	**ST DEV**	**UTS (Mpa) Normalized**	**ST DEV**
ABS:SEBS-g-MA - Baseline	0.98	0.96	0.0023	98%	14.4	0.2	14.7	0.2
ABS:SEBS-g-MA - P-glass 5%	1.11	0.98	0.0064	88%	14.8	0.2	16.8	0.3
ABS:SEBS-g-MA - P-glass 10%	1.25	0.99	0.0058	79%	14.1	1.3	17.8	1.6
ABS:SEBS-g-MA - P-glass 20%	1.51	0.94	0.0041	62%	11	0.5	17.8	0.9

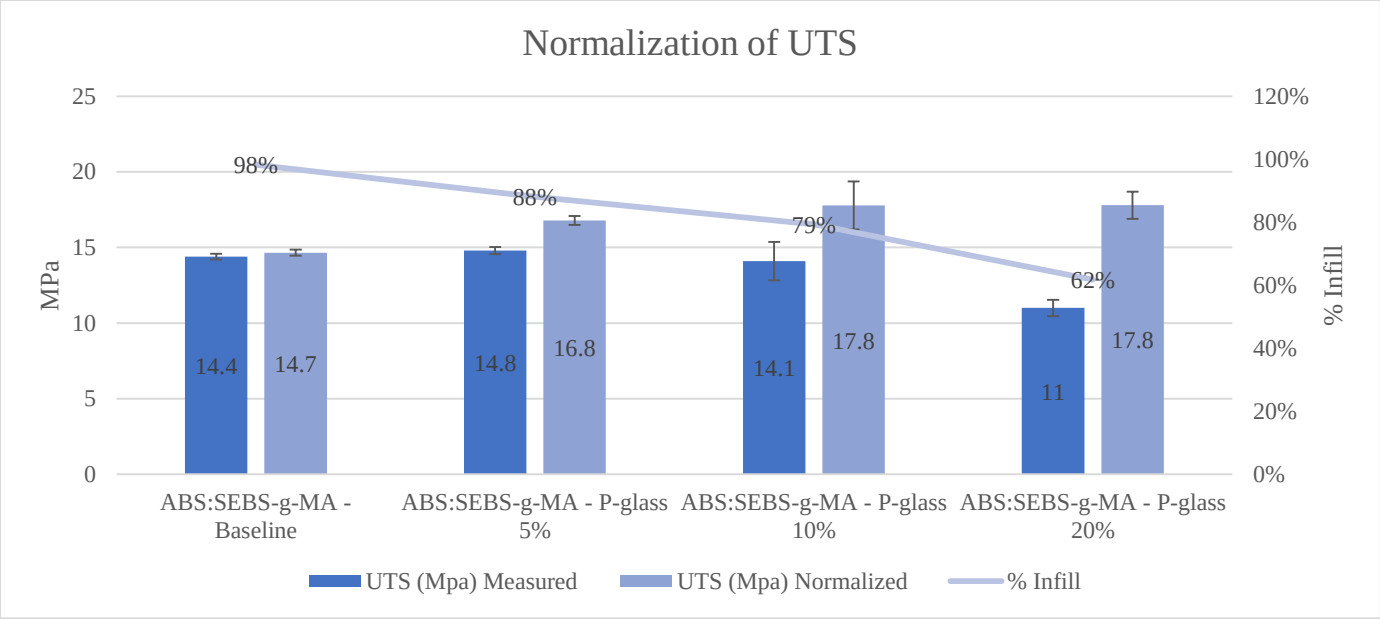

Figure 4. 17 Normalization of UTS for ABS:SEBS-g-MA system

Table 4. 7 Normalized UTS Data PLA System

Material	Theoretical Density ($\frac{g}{cm^3}$)	Measured Density ($\frac{g}{cm^3}$)	ST DEV	% Infill	UTS (Mpa) Measured	ST DEV	UTS (Mpa) Normalized	ST DEV
PLA Baseline	1.24	1.22	0.0017	98%	55.1	2.6	56.0	2.6
PLA - P-glass 2.5%	1.30	1.23	0.0031	95%	57.7	1.7	61.0	1.8
PLA - P-glass 5%	1.36	1.26	0.0027	93%	57.7	1.5	62.1	1.7
PLA - P-glass 10%	1.48	1.28	0.0059	86%	48.4	2.8	56.0	3.3
PLA - P-glass 15%	1.60	1.11	0.0019	70%	42.2	2.1	60.6	3.0

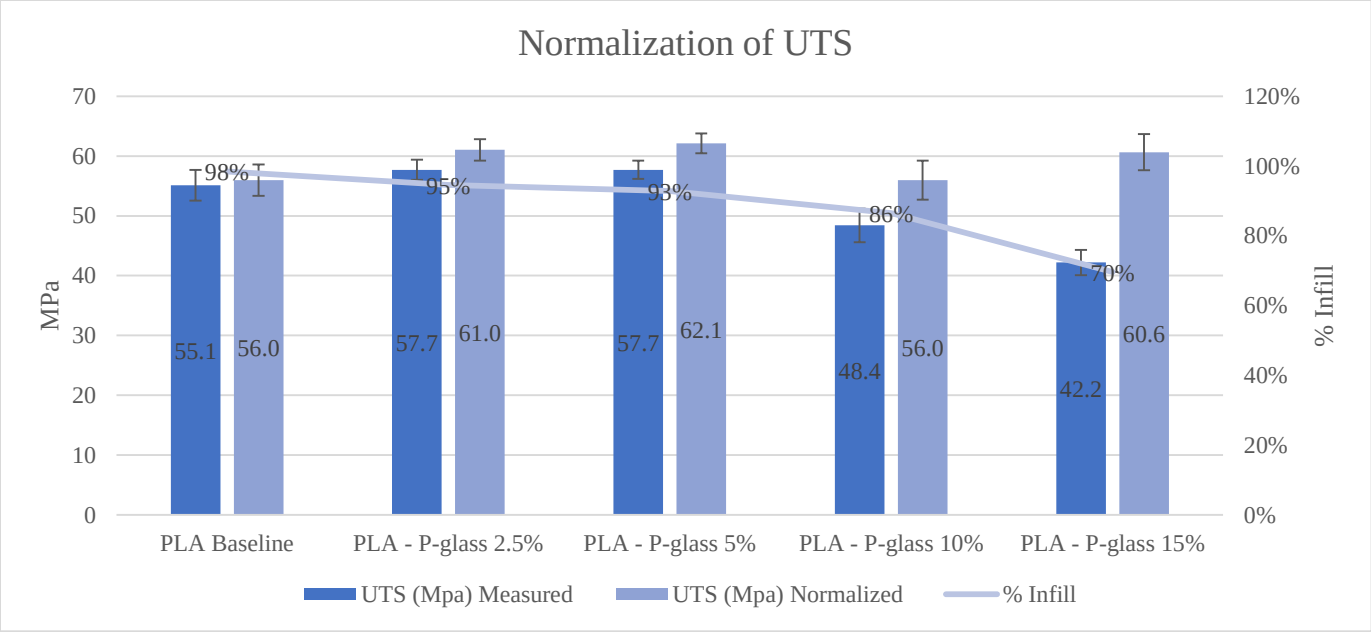

Figure 4. 18 Normalization of UTS for PLA system

4.3.3 Melt Flow Rate Analysis

Results of MFR measurements performed on the pelletized filament from all the systems are shown in Table 4.8. In the case of ABS:SEBS-g-MA, it was observed that increasing the loading percentage of the P-glass led to an incremental decrease in the MFR values (g/10 min) which is indicative of an increase in viscosity. In contrast, increasing the loading percentage of P-glass within PLA led to a decrease in the viscosity as the percent loading of filler increased. A potential reason for this occurrence is the hygroscopic nature of PLA which increased with the content of P-glass. It must be noted that before the tests were made, no prior drying treatments were performed.

Table 4. 8 Melt flow rate values for the materials tested in this study

Material	Melt Flow Rate (g/10min)	Test Load (kg)	Temperature ºC
ABS SEBS-g-MA	**33.72**	**3.8**	**230**
P-glass 5% - ABS SEBS-g-MA	32.38	3.8	230
P-glass 10% - ABS SEBS-g-MA	30.41	3.8	230
P-glass 20% - ABS SEBS-g-MA	29.48	3.8	230

PLA	**16.98**	**2.16**	**210**
PLA/P-glass 2.5%	34.36	2.16	210
PLA/P-glass 5%	74.8	2.16	210
PLA/P-glass 10%	85.56	2.16	210
PLA/P-glass 15%	60.52	2.16	210

4.4 Further PLA/P-Glass System Analysis

After observing the high MFR results along with the lack of wire drawing within the PLA system, it was evident that the viscosity was not adequate to create enough shear forces to elongate the P-glass particles. One of the steps during our filament fabrication process involves a cooling method where the filament is run through a water bath. Due to hygroscopic nature of PLA, it was theorized that the filament absorbed moisture from the water bath. The Nature Works technical data sheet indicates the MFR values for the 4043D grade of 6 g/10 min using a 2.16 kg load and a temperature of 210°C [33]. The initial MFR results from the pelletized PLA filament resulted in values of 16.98 g/10 min by using the same testing weight and temperature without performing any prior drying treatments. In an attempt to discombobulate the difference in results, a new MFR test was performed by drying the extruded PLA baseline filament for 4 hours at 80∘C before the test in a VWR horizontal forced air safety oven (Radnor, PA, USA). New MFR measurements of the dried PLA extruded filament resulted in a value of 5.86 g/10 min, which is closer to the published value of 6 g/10min. After interpreting the results of the dried PLA filament, a new set of test specimens of the PLA/P-glass 10% loaded system was printed. The reason behind choosing this loading percentage was that by selecting a higher loading composite there would be a better chance of observing P-glass particles wire drawing. The filament was dried for 4 hours at 80∘C before printing. As was the case when evaluating the ABS:SEBS-g-MA system, in order to identify if printing temperature played a factor in the wire drawing of the P-glass particles and overall mechanical properties, additional printing temperatures were experimented with (in this case,

four). Paired data pools (sets of two for composites and three for baseline specimens) were printed at the different temperatures as seen in Table 4.9 along with the corresponding mechanical test results. The mechanical testing was carried out following the same procedure explained earlier.

Table 4. 9 Mechanical testing data for the PLA/P-glass 10% system where the filament was dried before printing and printed at different temperatures

Material	Ultimate Tensile Stress (MPa)	ST. DEV	Tensile strain at Break (%)	ST. DEV	Sample Size (n)
PLA/P-glass 10% @ 220 °C	57.1	2.9	3.2	1.6	3
PLA/P-glass 10% @ 230 °C	56.8	0.7	2.9	0.2	3
PLA/P-glass 10% @ 240 °C	58.0	1.7	3.3	0.4	3
PLA/P-glass 10% @ 260 °C	57.5	0.9	4.7	0.6	3
PLA Baseline @ 220 °C	56.4	2.2	5.3	1.5	3
PLA Baseline @ 230 °C	56.2	2.2	3.0	0.6	3
PLA Baseline @ 240 °C	57.6	1.5	4	1.1	3
PLA Baseline @ 260 °C	59.5	2.6	4.4	0.9	3

Figure 4.19 compares the UTS results of the dried versus undried filament for the pure PLA baseline and PLA 10% P-glass system; in this graph it can be appreciated that the UTS slightly, though not significantly, increased, for the dried PLA baseline from 55.1 ± 2.6 to 57.6 ± 1.5MPa. In the case of the PLA/P-glass 10% system there was a significant increase in the UTS values when comparing it to the undried filament of the same load. The undried P-glass loaded filament data pool possessed an average UTS value of 48.4 ± 2.8MPa when printed at 240°C while the dried filament printed at the same temperature reported a UTS value of 58.0 ± 1.7MPa, an increase of almost 20%. The tensile strain at break for the PLA/P-glass 10% system was reduced from 4.4% for the undried filament printed at 240°C to 3.3% for the dried filament printed at the

same temperature. The tensile strain at break for the dried filament surpassed the undried filament when printed at 260°C with a value of 4.7% ± 0.6%. Though the % EL at break was slightly reduced for some of the print temperature increments, it can be said that the drying of the filament improved the mechanical properties of PLA and the PLA composites. Specifically, for the test specimens of PLA loaded with 10% by weight P-glass printed at 240°Cwhere the UTS improved from 48.4 ± 2.1MPa for the undried filament to 58.0±1.7MPa and still conserved similar strain elongation at break values from 4.4% (undried filament) to 4.7% (dried filament). Drying the filament gave the opportunity to be able to print at higher temperatures and still maintain the correct viscosity needed for a good quality ME3DP print. We were not able to print temperatures of 260°C without implementation of a filament drying cycle.

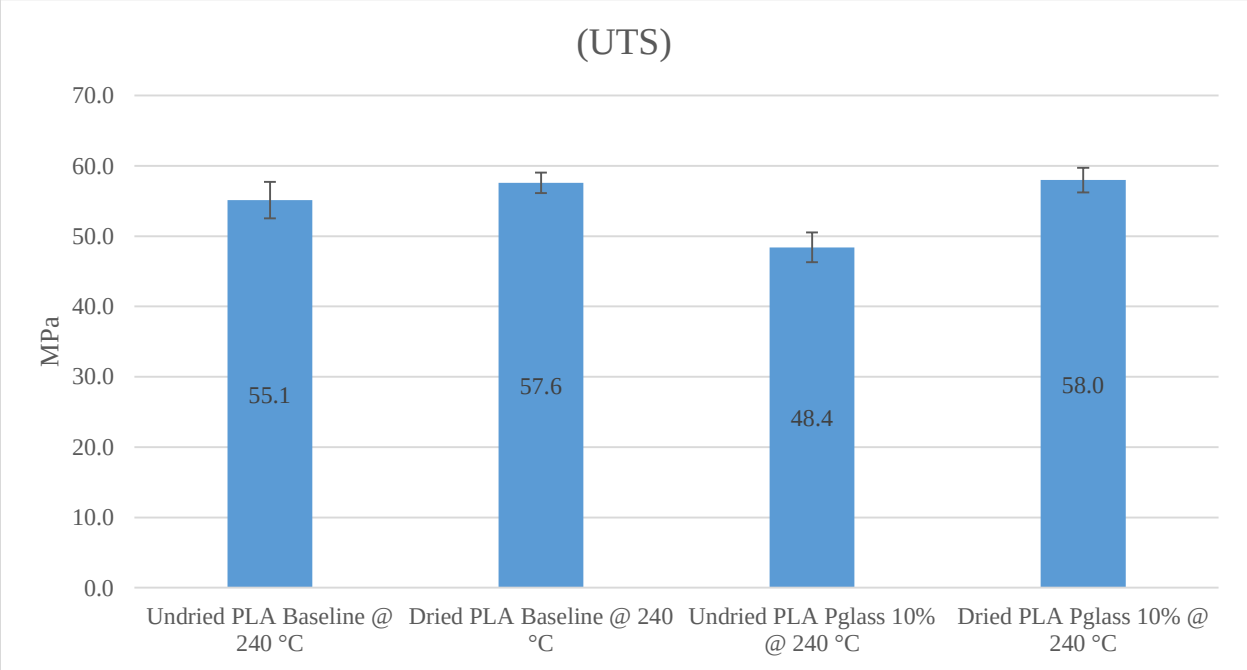

Figure 4. 19 UTS of undried vs dried neat and loaded with 10% by weight P-glass

After performing mechanical testing of the new set of PLA/P-glass 10% system, fracture surfaces of the test coupons were analyzed via SEM in order to determine if the drying cycle had an effect on the wire drawing process. Analysis of SEM micrographs revealed that specimens

printed at temperatures 220 and 230°C had similar fracture surface characteristics as the undried filament, some agglomeration, no in situ wire drawn particles, P-glass particle pullouts, and signs of well attached P-glass particles within the polymer matrix as it can be seen of Figure 4.20(a). Scanning electron microanalysis of the fracture surfaces of specimens from the 240°C and 260°C sample pool sets revealed many in situ wire drawn particles throughout the polymer matrix (Figure 4.20(b)). The drawn P-glass particles most likely played a role in the final mechanical properties of the specimens printed at 260°C as this sample pool exhibited the highest UTS values. The elongated P-glass particles seem to be longer than those found in the ABS:SEBS-g-MA polymer blend; however we were unable to approximate a length because they were still embedded within the polymer matrix. The shape of the in situ wire drawn particles of the PLA composite appears to be more cylindrical than the ones observed in the ABS:SEBS-g-MA composite where they exhibited a rougher cylindrical shape (Figure 4.4(a)). This could be due to the differences in the rheology of the material systems; the viscosity found in the dried PLA composite represented higher shear forces in the P-glass particles and created sharper micro-rods of phosphate glass within the polymer matrix.

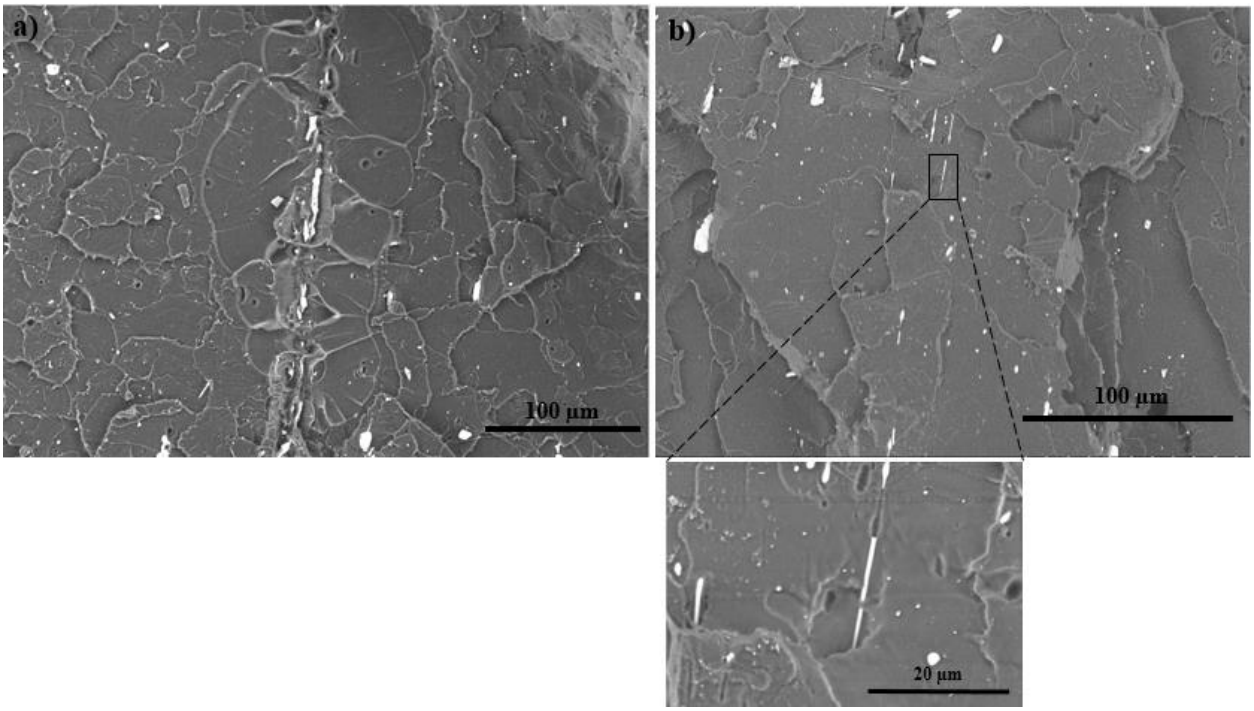

Figure 4. 20 SEM micrograph of the fracture surface of PLA loaded with P-glass at 10% by weight printed at a) 220°C b) 260°C

Again, we performed a normalization process of the UTS results for the dried versus undried PLA following the same experimental process explained above and the results are displayed in Table 4.10 and Figure 4.21. The trend of a decreased % infill with the increase in P-glass loading was maintained after drying the filament. As was the case with the undried filament, drying the filament resulted in 86% infill when loaded with 10% by weight P-glass meaning that the increase in UTS is attributed the drying process. Although the UTS is greater for the dried filament by 20%it leads to the conclusion that the different morphology of the P-glass present in this system had a profound effect on the mechanical properties as it was initially theorized.

Table 4. 10 Normalization of UTS values for Dried PLA printed at 240 °C

Material	**Theoretical Density** ($\frac{g}{cm^3}$)	**Measured Density** ($\frac{g}{cm^3}$)	**ST DEV**	**% Infill**	**UTS (Mpa) Measured**	**ST DEV**	**UTS (Mpa) Normalized**	**ST DEV**
PLA - Dried	1.24	1.24	0.0019	100%	56.4	2.2	56.5	2.2

PLA -P-glass 10% - Dried	1.48	1.27	0.0023	86%	58	1.7	67.7	2.0

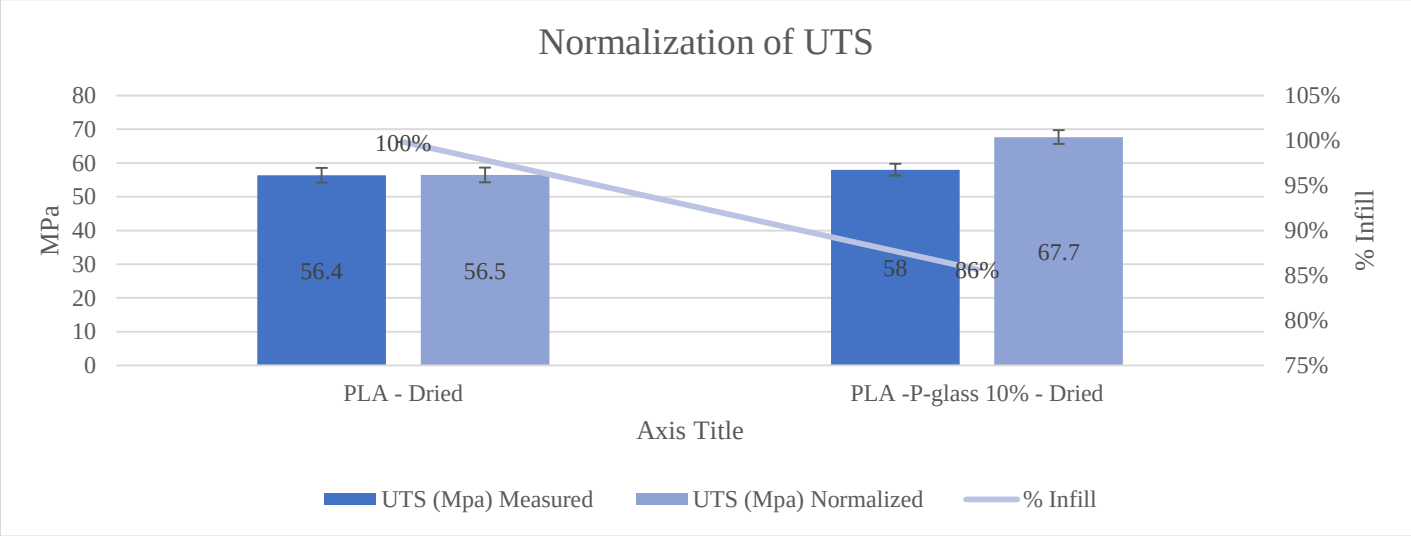

Figure 4. 21 Normalization of UTS of Dried vs Undried PLA system

4.5 Conclusions

We have demonstrated the creation of 3D printable thermoplastic composites loaded with low melting temperature phosphate glass. Combining this low melting temperature filler material with 3D printable thermoplastics, in this case PLA and a rubberized blend (50:50 by weight ratio of ABS and SEBS-g-MA) in some cases, led to wire drawing of the particles. When wire drawing was successful, there was a reduction in particle agglomeration. The ability to draw low melting temperature phosphate glass depends on many factors including polymer viscosity, particle filler size, and, particularly in the case of PLA, print temperature.

Initial results involving PLA revealed that the addition of P-glass at a 5% by weight loading increased the UTS by 4.5%; however, no wire drawing was observed. The drying of extruded PLA filament had a profound effect on the melt flow rate and later proved to be a key enabler for the

achievement of wire drawing within PLA. Drying the PLA also enabled printing at higher temperatures, while maintaining a viscosity great enough to initiate wire drawing.

Normalization of tensile test data was paramount in understanding the result of the addition of P-glass on the mechanical strength of the material systems explored here. The process of 3D printing imparts voids in between the print rasters which effectively diminishes the cross-sectional area of a tensile specimen and, thus, the UTS values. Specific gravity measurements allowed for the development of normalization factors for each of the material systems to give an idea of the bulk material properties.

The work presented here demonstrates the 3D printing of a hybrid material system where the matrix and filler material possessed similar thermal properties. The similarity in properties allow, in some cases, the drawing of phosphate glass filler material into a wire-like morphology. The 3D printing process played more of a role in the wire drawing process than the filament fabrication process. The potential to create hybrid material-based 3D-printed structures from this and similar material systems will expand the frontiers of FDM-type 3D printing.

4.6 References

[1] B. H. Stuart, Polymer Analysis, John Wiley Sons, 2008.

[2] A. A. Collyer, Rubber Toughened Engineering Plastics, Springer Science Business Media, 2012.

[3] J. Z. Liang andR. K. Y. Li, “Rubber toughening in polypropylene: a review,” Journal of Applied Polymer Science, vol. 77, no. 2, pp. 409–417, 2000.

[4] J. G. Siqueiros, K. Schnittker, and D. A. Roberson, “ABS maleated SEBS blend as a 3D printable material,” Virtual and Physical Prototyping, vol. 11, no. 2, pp. 123–131, 2016.

[5] Y. Xu, D. D. L. Chung, and C. Mroz, “Thermally conducting aluminum nitride polymer-matrix composites,” Composites - Part A: Applied Science and Manufacturing, vol. 32, no. 12, pp. 1749–1757, 2001.

[6] P. R. Hornsby, “Fire retardant fillers for polymers,” International Materials Reviews, vol. 46, no. 4, pp. 199–210, 2001.

[7] G. Mittal, V. Dhand, K. Y. Rhee, S.-J. Park, and W. R. Lee, “A review on carbon nanotubes and graphene as fillers in reinforced polymer nanocomposites,” Journal of Industrial and Engineering Chemistry, vol. 21, pp. 11–25, 2015.

[8] G. Koronis, A. Silva, and M. Fontul, “Green composites: a review of adequate materials for automotive applications,” Composites Part B: Engineering, vol. 44, no. 1, pp. 120–127, 2013.

[9] S. Kumar and J.-P. Kruth, “Composites by rapid prototyping technology,” Materials and Design, vol. 31, no. 2, pp. 850–856, 2010.

[10] M. L. Shofner, K. Lozano, F. J. Rodriguez-Macias, and E. V. Barrera, “Nanofiber-reinforced polymers prepared by fused deposition modeling,” Journal of Applied Polymer Science, vol. 89, no. 11, pp. 3081–3090, 2003.

[11] S. J. Leigh, R. J. Bradley, C. P. Purssell, D. R. Billson, and D. A. Hutchins, “A Simple, Low-Cost Conductive Composite Material for 3D Printing of Electronic Sensors,” PLoS ONE, vol. 7, no. 11, Article ID e49365, 2012.

[12] O. Ivanova, C. Williams, and T. Campbell, “Additive manufacturing (AM) and nanotechnology: promises and challenges,” Rapid Prototyping Journal, vol. 19, no. 5, pp. 353–364, 2013.

[13] N. M. A. Isa, M. I. Ibrahim, N. Sa’ude, and M. Ibrahim, “Characterization of copper filled in ABS material for freeform fabrication,” ARPN Journal of Engineering and Applied Sciences, vol. 11, no. 9, pp. 6531–6535, 2016.

[14] S. Masood and W. Song, “Development of new metal/polymer materials for rapid tooling using fused deposition modelling,” Materials & Design, vol. 25, no. 7, pp. 587–594, 2004.

[15] M. Nikzad, S. H. Masood, and I. Sbarski, “Thermo-mechanical properties of a highly filled polymeric composites for Fused Deposition Modeling,” Materials and Design, vol. 32, no. 6, pp. 3448–3456, 2011.

[16] G. Wu, N. A. Langrana, R. Sadanji, and S. Danforth, “Solid freeform fabrication of metal components using fused deposition of metals,” Materials and Design, vol. 23, no. 1, pp. 97–105, 2002.

[17] L. J. Love, V. Kunc, O. Rios et al., “The importance of carbon fiber to polymer additive manufacturing,” Journal of Materials Research, vol. 29, no. 17, pp. 1893–1898, 2014.

[18] H. L. Tekinalp, V. Kunc, G. M. Velez-Garcia et al., “Highly oriented carbon fiber-polymer composites via additive manufacturing,” Composites Science and Technology, vol. 105, pp. 144–150, 2014.

[19] S. Hwang, E. Reyes, K.-S. Moon, R. Rumpf, and N. Kim, “Thermo-mechanical characterization of metal/polymer composite filaments and printing parameter study for fused deposition modeling in the 3D printing process,” Journal of Electronic Materials, vol. 44, no. 3, pp. 771–777, 2014.

[20] D. Roberson, C. M. Shemelya, E. MacDonald, and R. Wicker, “Expanding the applicability of FDM-type technologies through materials development,” Rapid Prototyping Journal, vol. 21, no. 2, pp. 137–143, 2015.

[21] C. M. Shemelya, A. Rivera, A. T. Perez et al., “Mechanical, electromagnetic, and X-ray shielding characterization of a 3D printable tungsten–polycarbonate polymer matrix composite for space-based applications,” Journal of Electronic Materials, vol. 44, no. 8, pp. 2598–2607, 2015.

[22] A. R. Torrado, C. M. Shemelya, J. D. English, Y. Lin, R. B. Wicker, and D. A. Roberson, “Characterizing the effect of additives to ABS on the mechanical property anisotropy of specimens fabricated by material extrusion 3D printing,” Additive Manufacturing, vol. 6, pp. 16–29, 2015.

[23] H. Ku, H. Wang, N. Pattarachaiyakoop, and M. Trada, “A review on the tensile properties of natural fiber reinforced polymer composites,” Composites Part B: Engineering, vol. 42, no. 4, pp.
856–873, 2011.

[24] M. Gupta, Y. Lin, T. Deans et al., “Biaxially oriented poly (propylene-g-maleic anhydride)/ phosphate glass composite films for high gas barrier applications,” Polymer, vol. 50, no. 2, pp. 598–604, 2009.

[25] A. M. Papadopoulos, “State of the art in thermal insulation materials and aims for future developments,” Energy and Buildings, vol. 37, no. 1, pp. 77–86, 2005.

[26] X. Xu, F. L. Harding, and M. A. Albers, Glass compositions for high thermal insulation efficiency glass fibers, US5932499 A, 1999. http://www.google.com/patents/US5932499.

[27] C. J. Kief, J. Aarestad, E. MacDonald et al., “Printing multi functionality: additive manufacturing for cubesats,” in Proceedings of the AIAA SPACE 2014 Conference and Exposition, August 2014.

[28] E. MacDonald, R. Salas, D. Espalin et al., “3D printing for the rapid prototyping of structural electronics,” IEEE Access, vol. 2, pp. 234–242, 2014.

[29] Standard Test Method for Tensile Properties of Plastics, ASTM International, 2014.

[30] Standard Test Method for Melt Flow Rates of Thermoplastics by Extrusion Plastometer, ASTM International, 2013.

[31] B. N. Turner, R. Strong, and S. A. Gold, “A review of melt extrusion additive manufacturing processes: I. Process design and modeling,” Rapid Prototyping Journal, vol. 20, no. 3, Article ID 17111231, pp. 192–204, 2014.

[32] Standard Test Method for Density and Specific Gravity of Plastics by Displacement, ASTM International, 2013.

[33] A. A. NatureWorks, R. Kean, T. Schechinger, S. Birrell, and J. Euken, “Final Technical Report,” Tech. Rep. DOE/ID/14216-1, 2007.

CHAPTER 5: PHASE CHARACTERIZATION OF ABS SEBS-g-MA POLYMER BLEND

5.1 Introduction

Scanning transmission electron microscopy (STEM) is a type of transmission electron microscope. STEM works similarly to scanning electron microscopes (SEM) where an electron gun generates a beam of electrons that is focused by a series of lenses to recreate an image from the electron source directed to a specimen. The probe can be scanned over the sample in raster pattern by exciting scanning deflection coils, in order to detect scattered electrons with their intensity to be plotted as a function of probe position to reproduce an image [1]. Contrary to the bulk material specimens used in SEM, STEM requires electron transparent specimens [1] and detectors are placed below the sample. Figure 5.1 is a schematic representation of some of the elemental components that can be found in STEM instruments.

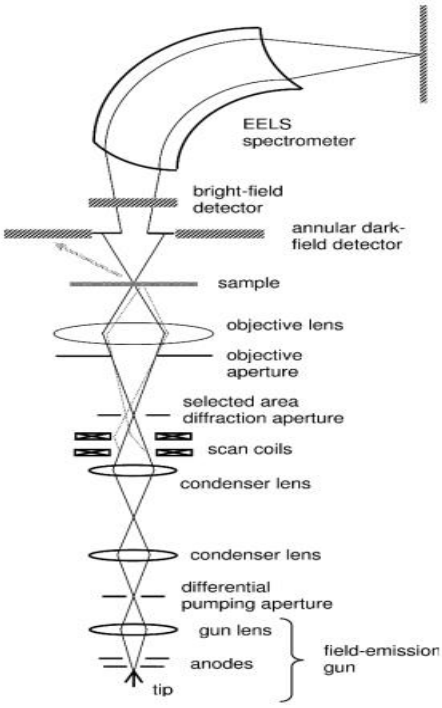

Figure 5. 1 Essential elements in STEM instruments [1]

STEM is an important tool for polymer characterization as they can provide useful information within the processing-structure-property paradigm [2]. STEM importance relies in the ability to explore morphologies in polymer synthesis and processing which can lead to advances in functionality and application [2]. In this Chapter, phase morphology of the ABS SEBS-g-MA polymer blend system through STEM will be explored along with dynamic mechanical analysis (DMA) and infrared spectroscopy by attenuated total reflection (ATR).

5.2 Experimental Procedure

Sample preparation for STEM were prepared by cryo-ultramicrotomy using a RMC Boeckeler PT-X ultramicrotome (RMC Boeckeler Instruments, Tucson, AZ, USA) outfitted with a CR-X cryosectioning unit and diamond knife. Sample thickness were in the range of 70 to 90 nanometers. A solution of dimethyl sulfoxide (DMSO) with 40% water was used in the knife boat for sample collection. Because of the elastic behavior of the polymer blend, the collected samples were placed under hot water (around 80°C) to reduce wrinkling prior grid mounting. STEM imaging was carried out through the use of a Hitachi SU3500 scanning electron microscope (SEM) operating with an accelerating voltage of 30kV equipped with a Deben STEM detector (Deben UK Limited, London, England). Optimal contrast occurred during brightfield and darkfield mixed mode signal processing was used.

DMA was performed using a TA Systems 2980 DMA (TA Instruments, New Castle, DE, USA). DMA samples were material extrusion 3D printed using a Lulzbot Taz 4 (Aelph Objects Inc, Loveland, Colorado, USA) outfitted with a 0.6 mm nozzle diameter with the following dimensions: 17.5mm x 12.5mm x 1.3mm. ATR was performed using a Nicolet IS5 FTIR spectrometer equipped with an iD7 ATR accessory (Thermo Fisher Scientific, Waltham, MA, USA).

5.3 Results

5.3.1 Microstructural Characterization of the Polymer Phases

The scanning transmission electron micrographs of the extruded filament cross sections for all the ABS MG94 SEBS-g-MA system are represented from Figure 5.2 to 5.5. Unfortunately, due to the softness of the SEBS-g-MA material problems during microtoming surfaced along radiation damage from the beam impeded the capture of worthy images for the ABS SEBS-g-MA 90 wt% and pure SEBS-g-MA. The pure ABS micrograph presented in Figure 5.2 shows the typical two phase morphology consisting of a continuous poly(styrene-co-acrylonitrile) phase in which a rubber phase of polybutadiene is dispersed into the poly(styrene-co-acrylonitrile) phase in form of spherical particles.

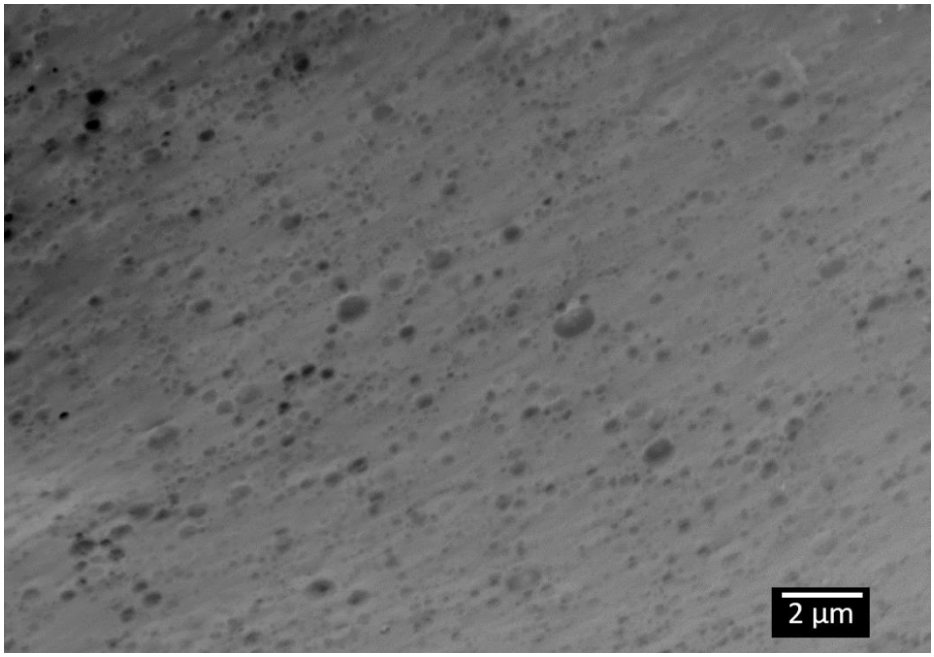

Figure 5. 2 STEM micrograph of ABS

Figures 5.3 to 5.5 represent the filament cross sectional area for the 25, 50, and 75 percent by weight SEBS-g-MA material systems in ABS. In Figure 5.3 (25 wt%) we can appreciate similarities to the pure ABS morphology with the inclusion of elongated globules that represent

the ethylene butylene from the SEBS. It must be noted that the distinction between the ABS and SEBS-g-MA phases indicates immiscibility between the two polymers. Higher than its constituent MFI results from this polymer blend on Chapter 3 was an indication that alloying might have occurred. This assumption can be discarded due to the clear morphology distinction that is more evident in Figures 5.4 and 5.5 that represent the 50 and 75 wt%. In these two figures globules of ABS are distributed within the ethylene butylene matrix along spheroids of polystyrene which are native of the SEBS microstructure. The content of ABS globules is less evident in the 75 than the 50 SEBS-g-MA wt% which further confirms the absence of polymer alloying.

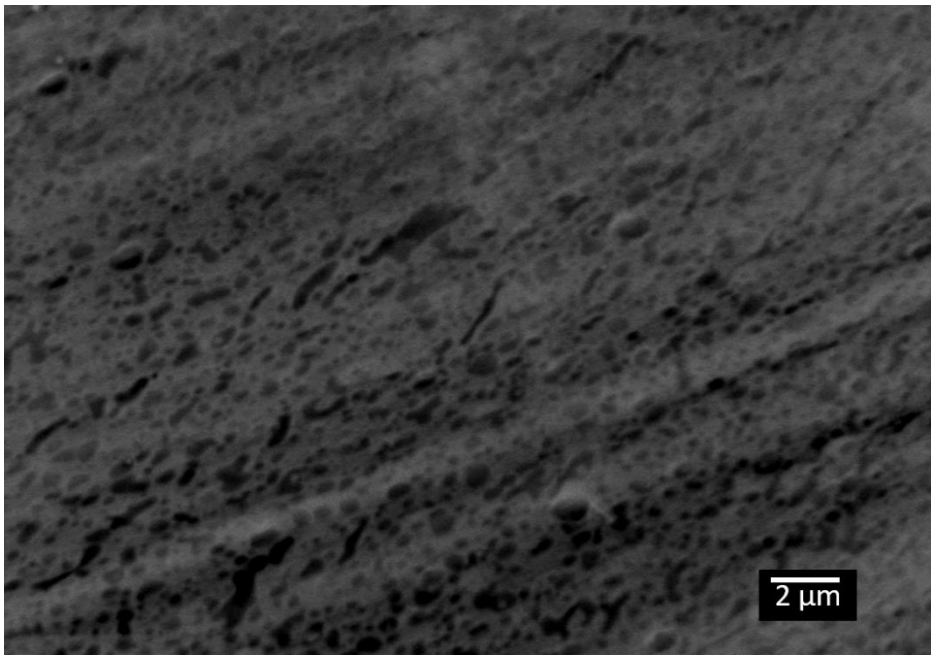

Figure 5. 3 STEM micrograph of ABS SEBS-g-MA 25%

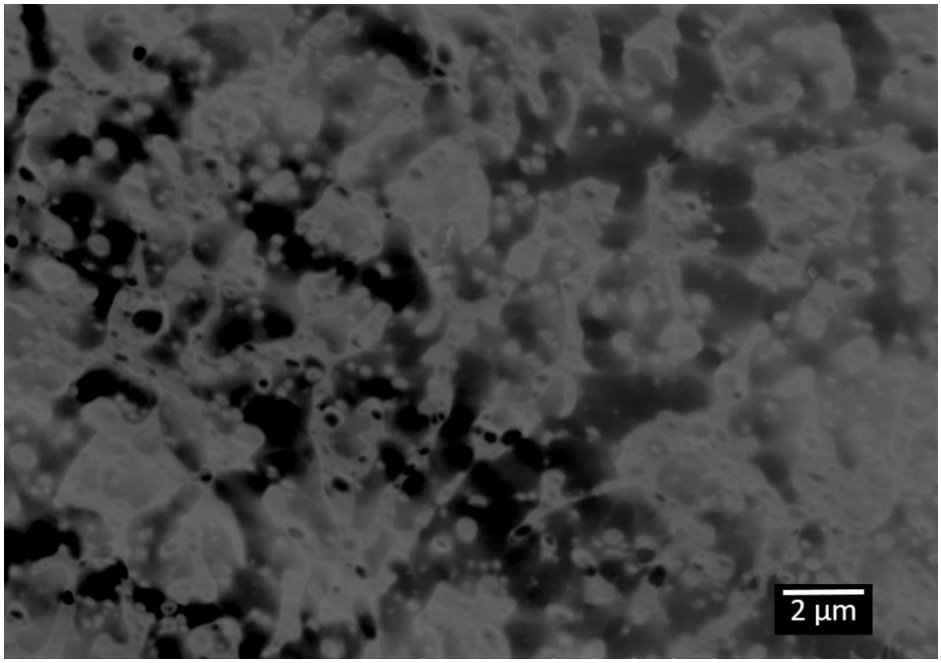

Figure 5. 4 STEM micrograph of ABS SEBS-g-MA 50%

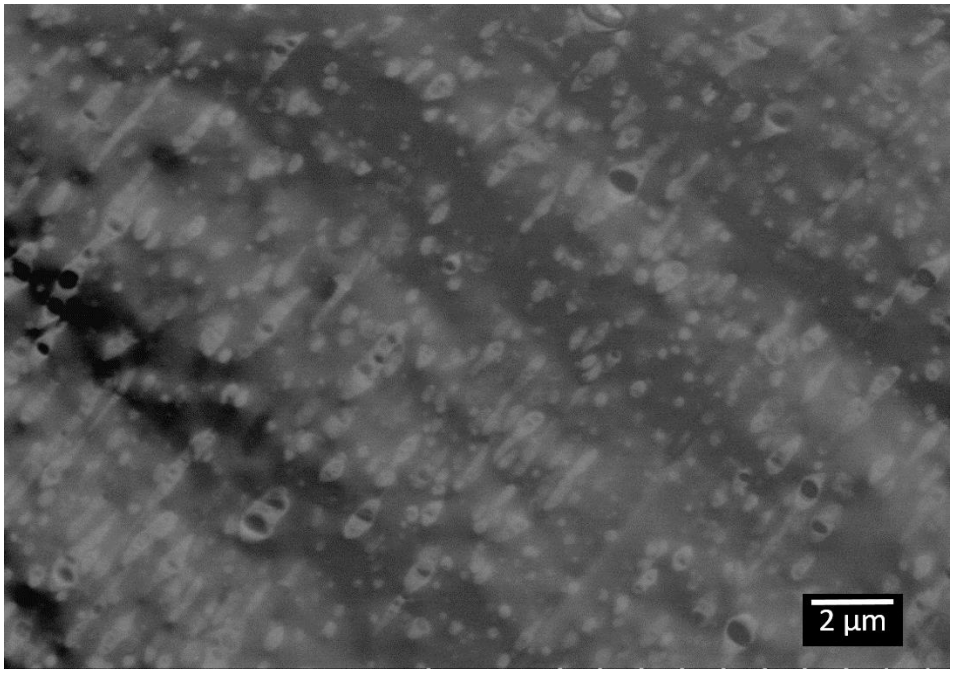

Figure 5. 5 STEM micrograph of ABS SEBS-g-MA 75%

5.3.2 Dynamic Mechanical Analysis

Results of the DMA test are represented in Figures 5.6 to 5.9. DMA analysis was performed to determine the glass transition temperature ($T_{g)}$ of the different weight ratios of SEBS-g-MA in

the ABS blend system. Glass transition temperatures were taken from the tan δ peak compared against temperature. The DMA results show a similar glass transition for pure ABS and the 25 and 50 wt% SEBS-g-MA of around 120 °C. The 75 wt% SEBS-g-MA tan δ peak was reduced by a few degrees to 115 °C and experienced another tan δ peak in the -31 °C which indicates multiple T_g values.

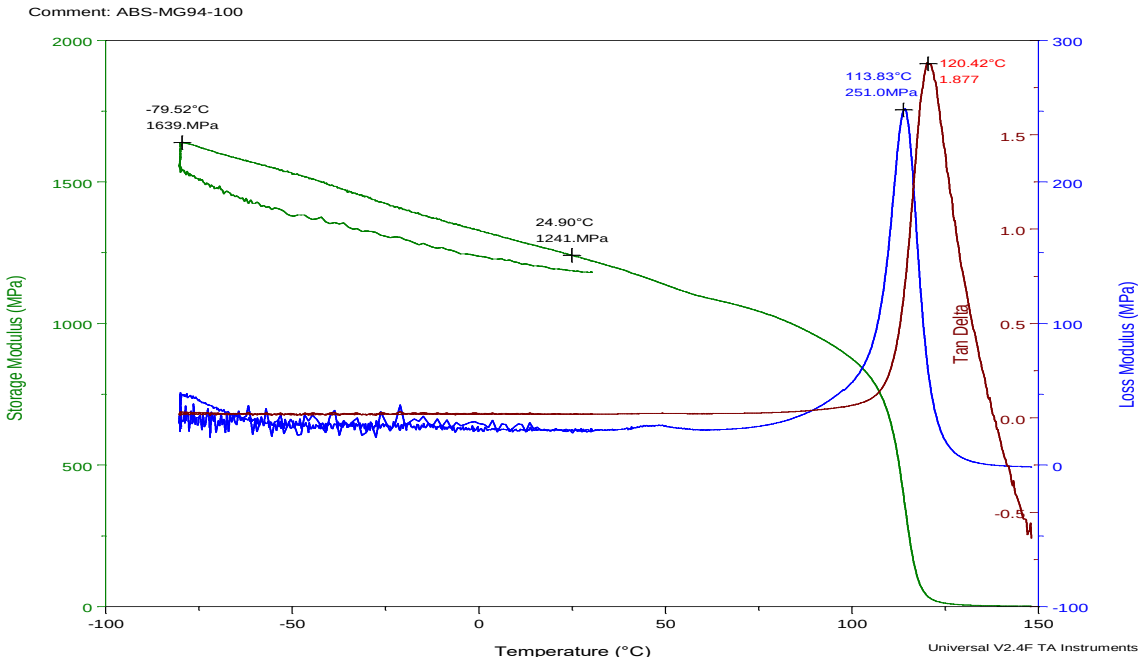

Figure 5. 6 DMA results of pure ABS

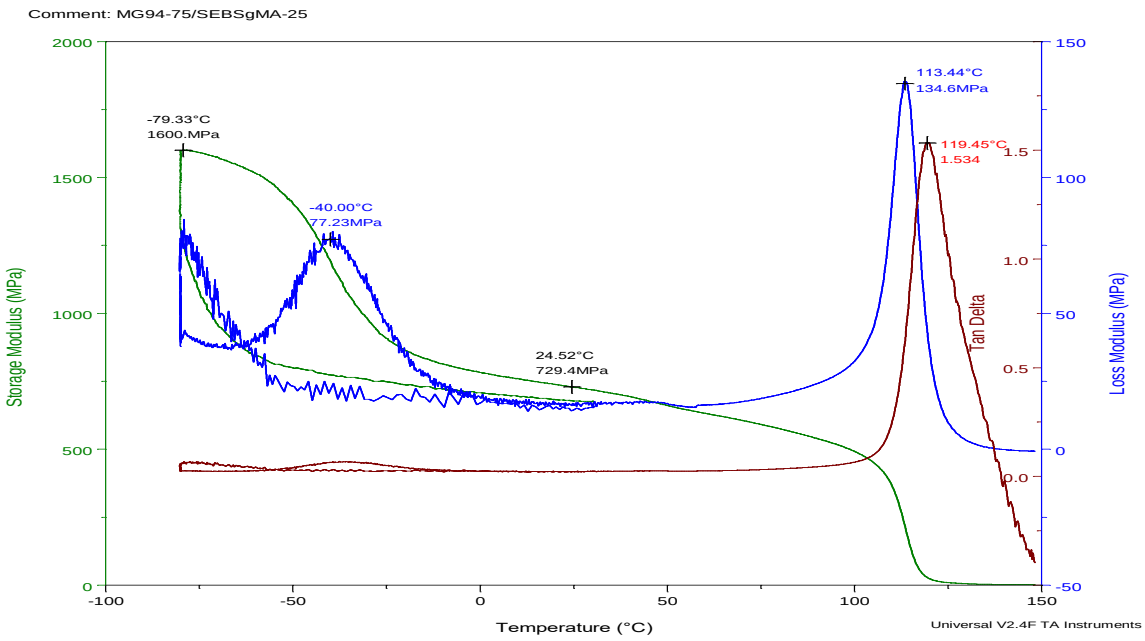

Figure 5. 7 DMA results of ABS SEBS-g-MA 25 wt%

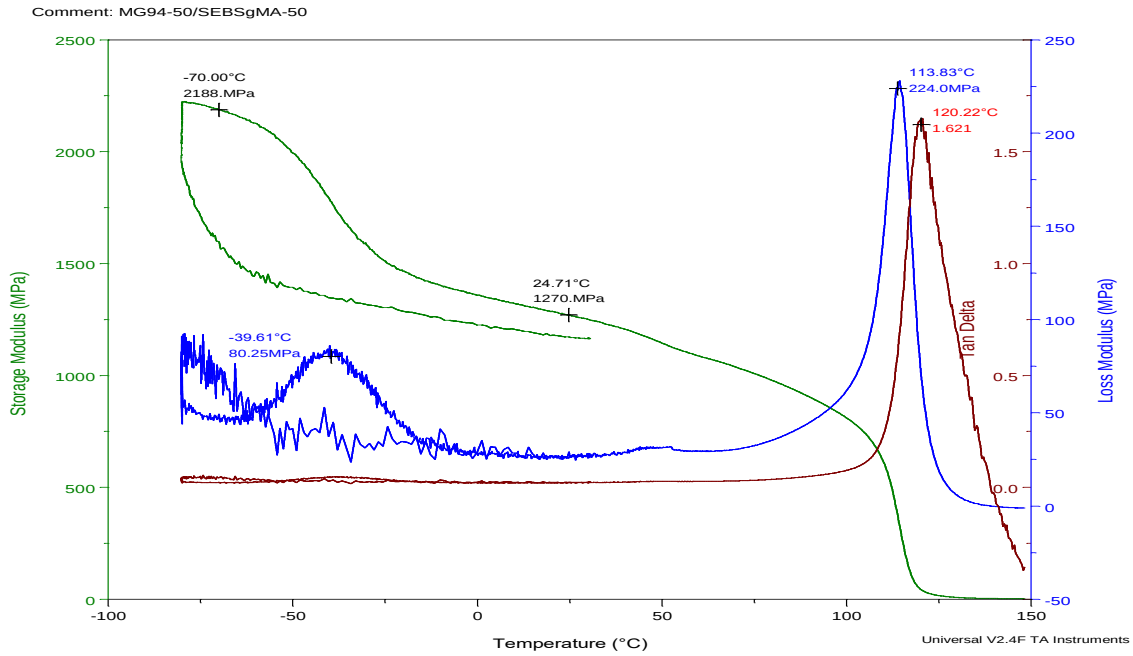

Figure 5. 8 DMA results of ABS SEBS-g-MA 50 wt%

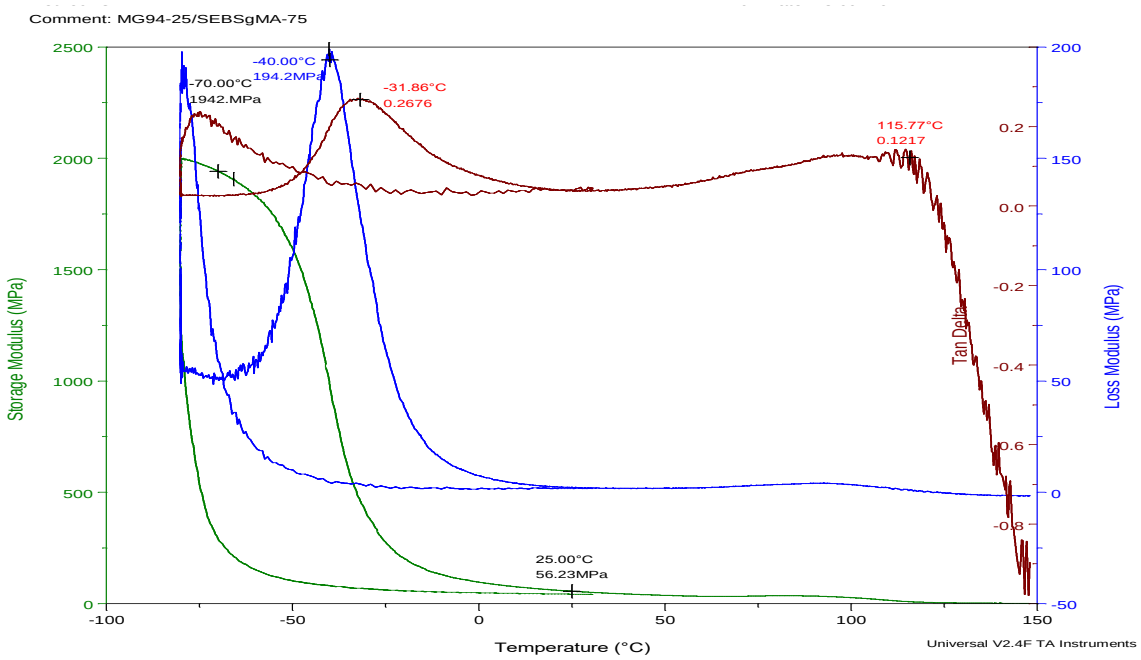

Figure 5. 9 DMA results of ABS SEBS-g-MA 75 wt%

5.3.3 Infrared Spectroscopy by Attenuated Total Reflectance

The collected ATR spectra for all the blends is represented in Figure 5.10. The spectra is very similar for all the blends and seem to follow the same characteristics of the pure ABS spectra with some increments of absorbance in the aromatic and alphatic region (C=H stretch modes). These spectra further confirms the absence of alloying occurring in the ABS SEBS-g-MA material system.

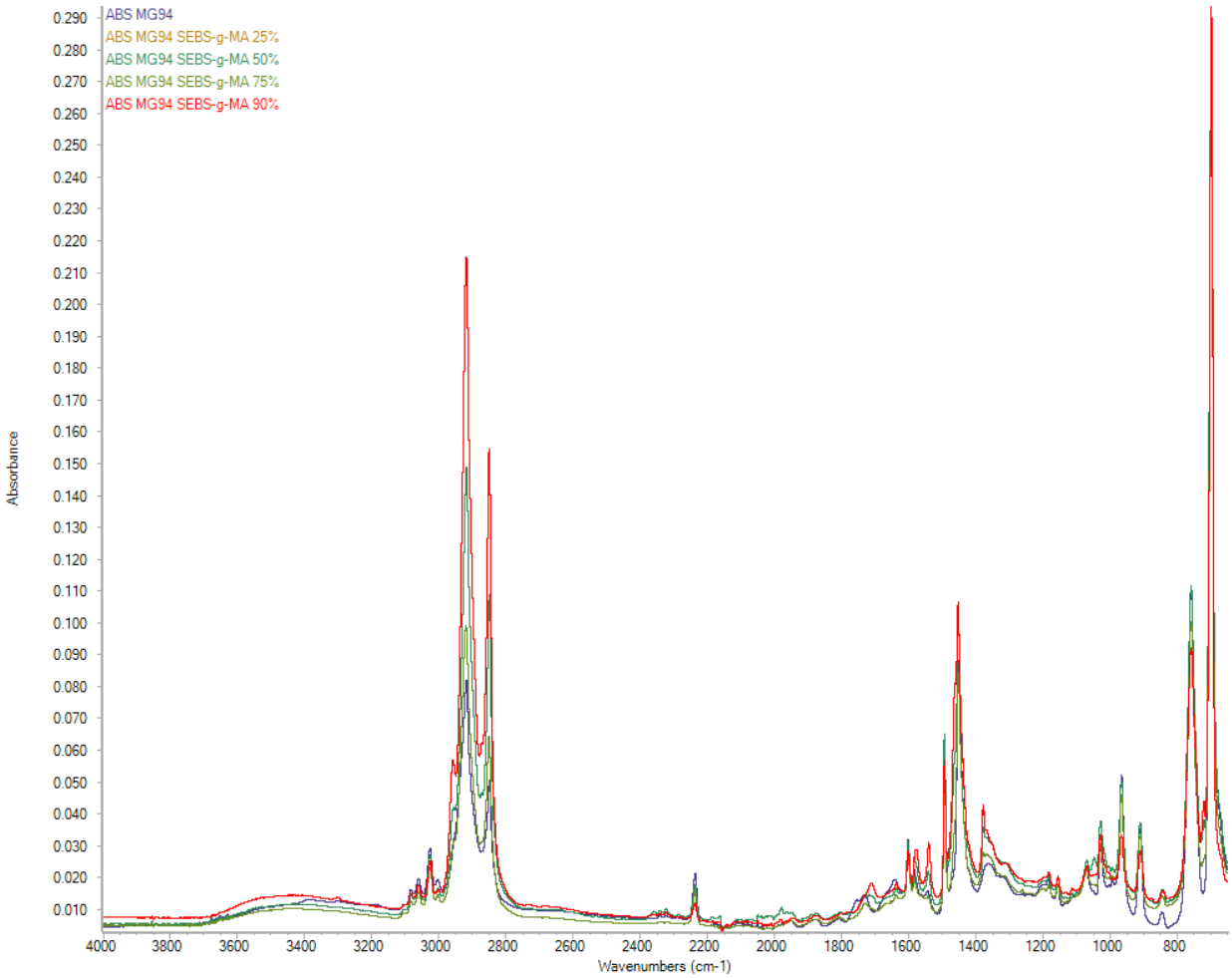

Figure 5. 10 ATR Spectra of ABS SEBS-g-MA system

5.4 References

[1] P.D. Nellist, Scanning Transmission Electron Microscopy, in: Science of Microscopy, Springer, New York, NY, 2007: pp. 65–132. doi:10.1007/978-0-387-49762-4_2.

[2] M.R. Libera, R.F. Egerton, Advances in the Transmission Electron Microscopy of Polymers, Polymer Reviews. 50 (2010) 321–339. doi:10.1080/15583724.2010.493256.

[3] Y. Aoki, A. Hatano, T. Tanaka, H. Watanabe, Nonlinear Stress Relaxation of ABS Polymers in the Molten State, Macromolecules. 34 (2001) 3100–3107. doi:10.1021/ma002076l.

APENDIX A: PERMISSION TO INCLUDE MATERIAL FROM JOURNAL OF *VIRTUAL AND PHYSICAL PROTOTYPING*

RE: Request for using a published article in Dissertation
Ma, Grace <Grace.Ma@tandf.com.sg>
Yesterday, 9:48 PM
Siqueiros, Jose G;An Jia (Dr) <AnJia@ntu.edu.sg>;Yeong Wai Yee (Asst Prof) <WYYeong@ntu.edu.sg>;Ng, Jenny <Jenny.Ng@tandf.com.sg>
Dear Gilberto,

Good day to you and thank you for your query.

Taylor & Francis is pleased to offer reuses of its content for a thesis or dissertation free of charge contingent on resubmission of permission request if work is published.

We would advise that a link to the final published version of record is included in your dissertation so that interested readers may be able to read your paper as well.

I hope this information is helpful.

Regards,

Grace

Grace Ma

Managing Editor, STM APAC | Taylor & Francis Asia Pacific

cid:image001.jpg@01D1C2F9.186EE0E0

an Informa business

Level 5| 28 Hennessy Road, Admiralty | Hong Kong

Direct line: +852 2234 2963
e-mail: Grace.Ma@tandf.com.sg

Web: www.taylorandfrancisgroup.com

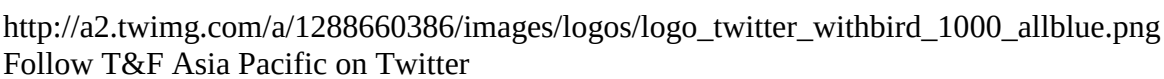

From: Siqueiros, Jose G [mailto:jgsiqueiros@miners.utep.edu]
Sent: Wednesday, 28 March 2018 1:41 AM
To: Ma, Grace <Grace.Ma@tandf.com.sg>
Cc: An Jia (Dr) <AnJia@ntu.edu.sg>; Yeong Wai Yee (Asst Prof) <WYYeong@ntu.edu.sg>
Subject: Re: Request for using a published article in Dissertation

Dear Grace,

I am a PhD candidate from the University of Texas at El Paso, in 2016 I published an article on the Virtual and Physical Prototyping Journal and I would like to include it on my dissertation. The article is cited below:

J.G. Siqueiros, K. Schnittker, D.A. Roberson, ABS-maleated SEBS blend as a 3D printable material, Virtual and Physical Prototyping. 11 (2016) 123–131. doi:10.1080/17452759.2016.1175045.

My University would grant me permission to use the cited article on my dissertation if approved by a reply to this email.

Thank you for your time and assistance,

Best Regards

Gilberto Siqueiros

From: Yeong Wai Yee (Asst Prof) <WYYeong@ntu.edu.sg>
Sent: Monday, March 26, 2018 8:07 PM
To: Siqueiros, Jose G
Cc: Ma, Grace; An Jia (Dr)
Subject: RE: Request for using a published article in Dissertation

Dear Gilberto,

The copyright ownership of the published journal papers belong to the publisher.

Please kindly liaise with the publisher, Ms Grace Ma here.

Dear Grace,

Appreciate your assistance and time on this request.

Thanks,

Wai yee

From: Siqueiros, Jose G [mailto:jgsiqueiros@miners.utep.edu]
Sent: Tuesday, 27 March 2018 5:53 AM
To: Yeong Wai Yee (Asst Prof)
Subject: Request for using a published article in Dissertation

Dear Dr Yeong,

I am a Ph.D. candidate at the University of Texas at El Paso, TX, USA. An article I have written was published in the journal of Virtual and Physical Prototyping cited below:

J.G. Siqueiros, K. Schnittker, D.A. Roberson, ABS-maleated SEBS blend as a 3D printable material, Virtual and Physical Prototyping. 11 (2016) 123–131. doi:10.1080/17452759.2016.1175045.

I would like to request permission for the use of this article in my dissertation. The University of Texas at El Paso would grant permission to use if agreed in a form of reply to this email.

I appreciate your time and look forward to a reply to this message.

Thank you

Best Regards,

Gilberto Siqueiros

APENDIX B: PERMISSION TO USE MATERIAL FROM *INTERNATIONAL JOURNAL OF POLYMER SCIENCE*

Re: Request to use a published article in dissertation
Huda Qabeel <huda.qabeel@hindawi.com>
Yesterday, 1:11 AM
Siqueiros, Jose G
Dear Dr. Siqueiros,

Thank you for your email. Authors retain the copyright of their manuscripts, and all Open Access articles are distributed under the terms of the Creative Commons Attribution License, which permits unrestricted use, distribution, and reproduction in any medium, provided that the original work is properly cited.

Best regards,

Huda

--
****
Huda Qabeel
Editorial Office
Hindawi
****

On 3/26/2018 9:59:43 PM Siqueiros, Jose G wrote:
> Dear Dr Qabeel,
>
>
>
> I am a Ph.D. candidate at the University of Texas at El Paso, TX, USA. An article I have written was published in the International Journal of Polymer science cited below:
>
>
>
> J. Gilberto Siqueiros, "In Situ Wire Drawing of Phosphate Glass in Polymer Matrices for Material Extrusion 3D Printing," International Journal of Polymer Science, vol. 2017, Article ID 1954903, 14 pages, 2017. doi:10.1155/2017/1954903.
>
>
>
>
> I would like to request permission for the use of this article in my dissertation. The University of Texas at El Paso would grant permission to use if agreed in a form of reply to this email.
>
>

>
> I appreciate your time and look forward to a reply to this message.
>
>
>
> Thank you
>
> Best Regards,
>
> Gilberto Siqueiros

CURRICULUM VITA

Jose Gilberto Siqueiros, was born February 16th, 1987 in Chihuahua, Chihuahua, Mexico in to Jose Gilberto Siqueiros and Veronica Estrada. Gilberto holds a B.S. in Mechanical Engineering from the University of Texas at El Paso. After finishing his B.S., Gilberto worked in the manufacturing industry for 3 years before embarking in the pursue of a graduate degree at his Alma matter the University of Texas at El Paso.

Selected Publications:

J.G. Siqueiros, K. Schnittker, D.A. Roberson, ABS-maleated SEBS blend as a 3D printable material, Virtual and Physical Prototyping. 11 (2016) 123–131. doi:10.1080/17452759.2016.1175045.

J.G. Siqueiros, D.A. Roberson, In Situ Wire Drawing of Phosphate Glass in Polymer Matrices for Material Extrusion 3D Printing, International Journal of Polymer Science. (2017). doi:10.1155/2017/1954903.

F. Andrade, **J.G. Siqueiros**, I. Delgado, D.A. Roberson, Exploring the Influence of Phase Content and Raster Pattern on the Shape Memory Properties of Additively Manufactured Specimens Deformed at Different Temperatures. Additive Manufacturing. (2017). In Revision.

D.A. Roberson. **J.G. Siqueiros**, Novel Polycarbonate/SEBS-g-MA Blend for FDM-Type 3D Printing. ANTEC, (2016) 10-14.

Permanent address: 1336 Desert Jewel St,
El Paso, TX 79912
jgsiqueiros@miners.utep.edu

This dissertation was typed by Jose Gilberto Siqueiros.